Role of the cGMP-dependent protein kinase type I in the regulation of stress response and thermogenesis

Dissertation

der Mathematisch-Naturwissenschaftlichen Fakultät

der Eberhard Karls Universität Tübingen

zur Erlangung des Grades eines

Doktors der Naturwissenschaften

(Dr. rer. nat.)

vorgelegt von

Andrea Gerling

aus Heidelberg

Tübingen

2012

Die vorliegende Arbeit wurde unter der Leitung von Prof. Dr. R. Feil in der Zeit von Juli 2007 bis August 2012 am Interfakultären Institut für Biochemie der Eberhard Karls Universität Tübingen, Abteilung Signaltransduktion - Transgene Modelle angefertigt.

Tag der mündlichen Prüfung:	26.09.2012
Dekan:	Prof. Dr. Wolfgang Rosenstiel
1. Berichterstatter:	Prof. Dr. Robert Feil
2. Berichterstatter:	Prof. Dr. Peter Ruth

Acknowledgements

Many thanks to my supervisor Prof. Dr. Robert Feil for giving me the opportunity to work on this interesting and challenging project in his lab. Thank you for your permanent support during the last years.

I am very grateful to Prof. Dr. Peter Ruth, Prof. Dr. Gabi Dodt and Prof. Dr. Cora Weigert for their interest in my work.

I thank Prof. Michael J. Shipston for a very interesting collaboration and helpful discussions.

A big thank you to Sylvia Kasparek for their help with the preparation of adrenal tissue slices and to Prof. Dr. Olga Garaschuk for access to her lab and equipment.

I would like to thank Elisabeth Metzinger and S. Hasanovic for their technical support with RIA and HPLC.

All my colleagues from the Feil lab I thank for the stimulating working environment. Special thanks to Dr. Susi Feil for the mouse supply, to Barbara Birk for her daily support and technical help and especially to Martin Thunemann for helpful discussions, advices and hands.

Many thanks to my former colleagues and now friends, Nadja and Matthias. Thank you for your encouraging words and for moving to such a nice city to spent the weekends in.

Thanks also to Eva who replaced Nadja as my sparring partner.

Thanks a lot to my friends Ina, Steffi, Ivi, Nicole and Leo for always cheering me up and standing by me.

Most of all I would like to thank my parents and my sister for their invaluable help and support not only during the last years. I know I can always count on you.

Sebastian, thank you for always being there for me.

Table of contents

Abbreviations

8-Br-cGMP	8-Bromo-cGMP
11β- HSD	11β- hydroxysteroid dehydrogenase
^{18}F-FDG	18-Fluorodeoxyglucose
ACh	acetylcholine
ACTH	adrenocorticotropic hormone
AngII	angiotensin II
ANP	atrial natriuretic peptide
ATP	adenosine triphosphate
AVP	arginine vasopressin
BAT	brown adipose tissue
bp	base pair
BK channel	large-conductance calcium- and voltage- activated potassium channel
BNP	B-type natriuretic peptide
BSA	bovine serum albumin
BW	body weight
Ca^{2+}	calcium
cAMP	cyclic adenosine monophosphate
CBG	corticosteroid-binding globulin
cGK	cGMP-dependent protein kinase
cGMP	cyclic guanosine monophosphate
CFTR	cystic fibrosis transmembrane conductance regulator
CIT	cold-induced thermogenesis
CNG channel	cyclic nucleotide-gated channel
CNP	C-type natriuretic peptide
CNS	central nervous system
CO_2	carbon dioxide
CORT	corticosterone
Cre	cyclization recombination
Cyp11A1	cholesterol side-chain cleavage enzyme
Cyp11B1	11β-hydroxylase
Cyp11B2	aldosterone synthase
Cyp17	17α-hydroxylase
Cyp21A2	21α-hydroxylase
DIT	diet-induced thermogenesis
DMEM	dulbecco’s modified eagle medium
DMH	dorsomedial hypothalamus
DNA	deoxyribonucleic acid
eNOS	endothelial nitric oxide synthase
EtOH	ethanol
FACS	fluorescence-activated cell sorting

FCS	fetal calf serum
FDG	fluorodeoxyglucose
FSP-1	fibroblast specific protein 1
FST	forced swim test
GABA	γ-aminobutyric acid
GAPDH	glyceraldehyde 3-phosphate dehydrogenase
GR	glucocorticoid receptor
GTP	guanosine triphosphate
HDL	high density lipoprotein
HPA	hypothalamic-pituitary-adrenal
HPT	hypothalamic-pituitary-thyroid
IL-1β	interleukin-1β
IL-6	interleukin-6
i.p.	intraperitoneal
iNOS	inducible nitric oxide synthase
IRAG	inositol 1,4,5- triphosphate receptor-associated cGMP kinase substrate
PET	positron emission tomography
PCR	polymerase chain reaction
pGC	particulate guanylyl cyclase
KO	knock-out
LD	light/ dark cycle
LDL	low density lipoprotein
loxP	locus of crossing-over [X]-over of P1
LPS	lipopolysaccharides
LTD	long-term depression
LTP	long-term potentiation
MACS	magnetic activated cell sorting
MC2R	type 2 melanocortin receptor
MEFs	mouse embryonic fibroblasts
MLC	myosin light chain
MLCK	myosin light chain kinase
MLCP	myosin light chain phosphatase
mRNA	messenger RNA
MYPT1	myosin-binding subunit of MLCP
NE	norepinephrine
Nes	Nestin
NO	nitric oxide
NOS	nitric oxide synthase
nNOS	neuronal nitric oxide synthase
NP	natriuretic peptide
NTS	nucleus tractus solitarii
OD	optical density

PAGE	polyacrylamide gel electrophoresis
PBS	phosphate buffered saline
PDE	phosphodiesterase
Pen/Strep	penicillin/streptomycin
PET	positron emission tomography
PG	pituitary gland
PGC-1α	PPARγ coactivator-1α
PI3K	phosphoinositide-3-kinase
PNMT	phenylethanolamine N-methyltransferase
POMC	proopiomelanocortin
PPARγ	peroxisome proliferator activated receptor γ
PKA	proteinkinase A
PVDF	polyvinylidene difluoride
PVN	paraventricular nucleus
RGS2	regulator of G protein signalling 2
RT	room temperature
RT-PCR	reverse transcription-PCR
SAS	sympathoadrenal system
s.c.	subcutaneous
SCN	suprachiasmatic nucleus
SDS	sodium dodecyl sulfate
SEM	standard error of the mean
SFA	fibroblast surface antigen
SMCs	smooth muscle cells
SNS	sympathetic nervous system
SOCS3	suppressor of cytokine signalling 3
SR-BI	class B, type I scavenger receptor
StAR	steroidogenic acute regulatory protein
TBE	Tris/Borate/ EDTA buffer
TBS(-T)	Tris buffered saline (with Tween)
TRH	thyrotrophin-releasing hormone
UCP-1	uncoupling protein-1
VSMCs	vascular smooth muscle cells
WAT	white adipose tissue
X-gal	5-bromo-4-chloro-3-indolyl-β-D-galactopyranoside
ZF	zona fasciculata
ZG	zona glomerulosa
ZR	zona reticularis
ZT	Zeitgeber time

Figures

Tables

A Introduction

A.1. cGMP signalling

The intracellular signalling molecule cyclic guanosine monophosphate (cGMP) acts as a second messenger in a variety of physiological processes such as cardiovascular homeostasis, inflammation, neuronal plasticity, and learning (Kemp-Harper and Feil, 2008). It is generated from guanosine triphosphate (GTP) by two classes of guanylyl cyclases, which differ in their cellular localisation and activators (**Figure 1**). The first class, the membrane-bound particulate guanylyl cyclase (pGC), can be activated by atrial (ANP), B-type (BNP) and C-type (CNP) natriuretic peptides (Lucas et al., 2000). So far, only the ligands for GC-A to GC-D, out of the seven pGC-receptors (GC-A to GC-G), have been identified. GC-A binds ANP and BNP and is among others expressed in vascular smooth muscle cells, endothelium, heart, central and peripheral nervous system as well as in the adrenal gland. GC-B can also be found in vascular smooth muscle cells, endothelium, heart, and additionally in bone. CNP is the molecule activating this receptor (Kuhn, 2003). In accordance with their distribution, natriuretic peptides (NPs) play a prominent role in the regulation of cardiovascular functions.

The second class of cGMP-generating enzymes are the soluble guanylyl cyclases, which are localised in the cytosol (**Figure 1**). They are activated via the conformational change induced by binding of the gaseous signalling molecule nitric oxide (NO) to their heme group (Friebe and Koesling, 2003). NO in turn is synthesised by three isoforms of NO synthases. Those NO synthases (NOS) convert L-arginine in the presence of oxygen into NO and citrulline (Bryan et al., 2009). Neuronal NOS (nNOS; NOS-1) and endothelial NOS (eNOS; NOS-3) are constitutively expressed, whereas inducible NOS (iNOS; NOS-2) is expressed upon stimulation with, for instance, lipopolysaccharides (LPS) and cytokines (Forstermann et al., 1994). In the CNS, nNOS-generated NO has been linked to synaptic plasticity and learning (Feil et al., 2005a). Besides its function as a neurotransmitter in the CNS, NO can also act as a paracrine agent. For example, endothelial cells in the cardiovascular system release large amounts of NO resulting in vasodilation of smooth muscle cells (Ignarro, 2002).

Downstream, the physiological effects of cGMP are mediated by three different cellular effector molecules. These are cyclic nucleotide-gated (CNG) channels, cGMP-regulated phoshodiesterases (PDEs) and cGMP-dependent protein kinases (cGKs) (**Figure 1**) (Beavo and Brunton, 2002). CNG channels play an important role in the signal transduction pathway in the visual and olfactory system and are opened by binding of cyclic nucleotides, cGMP and cyclic adenosine monophosphate (cAMP) (Biel et al., 1999; Kaupp and Seifert, 2002). PDEs hydrolytically degrade cGMP and therewith contribute to the regulation of intracellular cGMP levels (Sonnenburg and Beavo, 1994). Conversely, PDE activity can also be modulated by cGMP, either directly by binding to a regulatory domain or indirectly through phosphorylation (Omori and Kotera, 2007). In total, there are 11 families of PDEs present in mammals. They are

derived from 21 genes (Bender and Beavo, 2006) and vary in their specificity and affinity for cGMP and cAMP (Conti and Beavo, 2007). Only few are cGMP-specific, such as the cGMP-binding and cGMP-hydrolysing PDE5. In smooth muscle cells, PDE5 is under conditions of low calcium the main cGMP-hydrolysing PDE, whereas under higher calcium conditions PDE1 variants become more important. The physiological importance of PDE5 is well known from the PDE5 inhibitor sildenafil (Viagra®, *Pfizer*) that is used for the treatment of erectile dysfunction (Rybalkin et al., 2003). The third cGMP effector molecules, the cGMP-dependent protein kinases, mediate most of the physiological functions of cGMP and their various cellular functions are discussed in more detail in A.1.1.

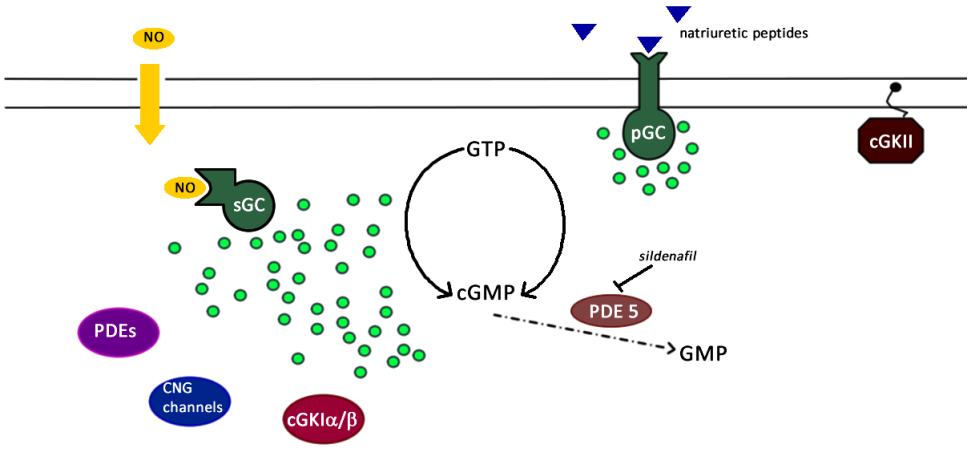

Figure 1: Overview on cGMP signalling. Membrane-bound particulate and cytosolic soluble guanylyl cyclases (pGCs and sGCs) are thought to generate local and global pools of cGMP (green dots) from GTP, respectively. cGMP is degraded by the cGMP-specific phosphodiesterase 5 (PDE5). Besides other cGMP effector molecules, cGKI mediates the physiological functions of cGMP.

A.1.1. cGMP-dependent protein kinases

cGMP-dependent protein kinases (cGKs) belong to the serine/threonine kinases and are present in a variety of eukaryotes (Francis and Corbin, 1999; Pfeifer et al., 1999). In mammals, two genes -*prkg1* and *prkg2*- encode cGKI and cGKII, respectively (Hofmann et al., 2009). Structure, function and expression of cGKI will be described in A.1.1.1. cGKII is membrane-bound by myristoylation of the N-terminus and has a molecular weight of 87 kDa. Even though, the structures of cGKII and cGKI are very similar (**Figure 2**) and both form homodimers, they differ in their tissue distribution and function (Hofmann et al., 2009; Vaandrager et al., 2005). CFTR (cystic fibrosis transmembrane conductance regulator) has been identified as an *in vivo* substrate for cGKII based on its localisation in the apical membrane of enterocytes (Vaandrager et al., 1998). Additional cGKII expression can be found in the intestinal mucosa, chondrocytes, lung, kidney, several brain nuclei and the adrenal cortex (Hofmann et al., 2009). Besides regulating the intestinal fluid secretion by the phosphorylation of CFTR, cGKII has been suggested to be

involved in endochondral ossification (Miyazawa et al., 2002; Pfeifer et al., 1996), the synchronization of the circadian clock after induced phase-shifts (Oster et al., 2003), modulation of anxiety-like behaviour (Werner et al., 2004) and aldosterone secretion (Gambaryan et al., 2003; Spiessberger et al., 2009).

A.1.1.1. Structure, expression and function of cGKI

Due to alternative promoter usage, two isoforms of the cGMP-dependent protein kinase I (cGKI) exist in mammals. The isozymes cGKIα and cGKIβ differ only in their N-terminal ~100 amino acids (Wernet et al., 1989) and, as mentioned above, form homodimers in the cytosol (Hofmann et al., 2009). Each monomer is composed of two functional domains: a catalytic and a regulatory domain (**Figure 2**). The catalytic domain contains the MgATP- and substrate binding pockets. The regulatory domain is further subdivided in an N-terminal region and a cGMP-binding site with a high and low affinity binding pocket. If both binding sites are occupied with cGMP, conformational changes in the secondary structure lead to a more elongated activated molecule (Landgraf et al., 1990). The N-terminal region contains a leucine-zipper motif responsible for dimerization and subcellular localisation, as well as an autoinhibitory/pseudosubstrate site inhibiting the catalytic centre in the absence of cGMP. Binding of cGMP to the low affinity binding pocket of the regulatory domain induces autophosphorylation of the amino-terminal autophosphorylation site and precedes substrate phosphorylation after binding of cGMP to the high affinity binding pocket (Hofmann et al., 2006). The N-terminal differences between the two cGKI isoforms result in different affinities for cGMP with cGKIα (K_a ~0.1 µM) having a ten-fold higher affintiy than cGKIβ (K_a ~0.5-1 µM) *in vitro* (Ruth et al., 1991). Besides the classical activation pathway, another cGMP-independent mechanism has been suggested for cGKIα activation involving oxidative processes. This process involves a hydrogen peroxide-induced disulfide cross-link between the cysteine residues (Cys42) in the leucine-zipper region of cGKIα. Thereby cGKIα can be activated cGMP-independently without an increase in the catalytic rate (Burgoyne et al., 2007).

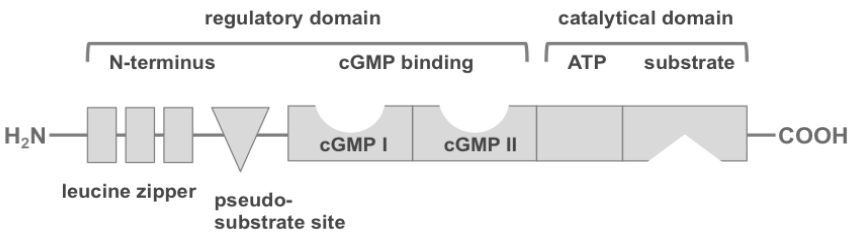

Figure 2: Structure of cGKI. cGKIα and cGKIβ only differ in their N-terminal region. (Figure adapted from Hofmann et al., 2006).

cGKI is expressed in a variety of tissues. High concentrations (>0.1 µM) of cGKI can be found in smooth muscle cells (Iα and Iβ), platelets (Iβ), and dorsal root ganglia (Iα) (Hofmann et al., 2006;

Schmidt et al., 2002; Weber et al., 2007). In the brain, cGKI is expressed at high levels in the hippocampus (Iβ), cerebellar Purkinje cells (Iα) and the dorsomedial hypothalamus, while lower levels can be detected in the suprachiasmatic nucleus, paraventricular nucleus, amygdala, olfactory bulb, and cerebral cortex (Feil et al., 2005a; Feil and Kleppisch, 2008). In the periphery, low levels of cGKI have been identified in cardiac muscle, granulocytes, chrondrocytes, and osteoclasts (Keilbach et al., 1992).

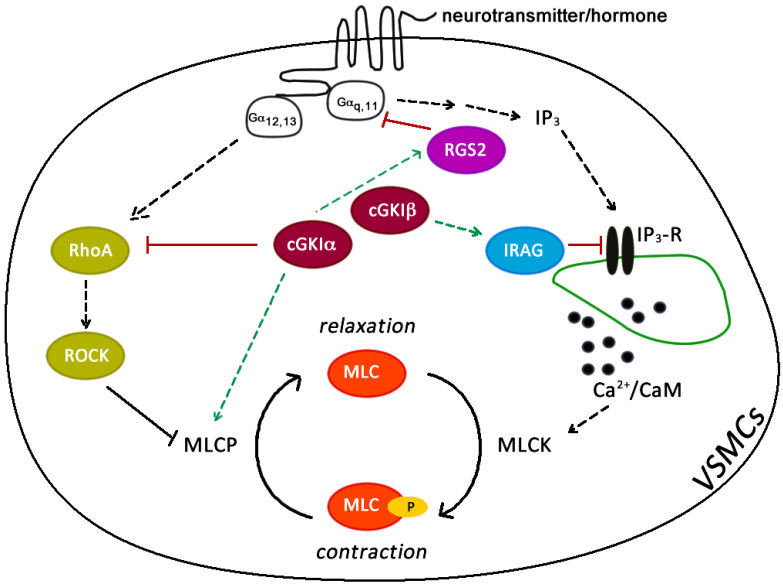

Figure 3: Model of the isoform-specific contributions of cGKIα and cGKIβ to the relaxation of smooth muscle cells. For a detailed explanation see text. (Figure adapted from Surks et al., 2007).

Due to its broad expression, cGKI is involved in numerous physiological functions like the inhibition of platelet aggregation, functions of the nervous system and smooth muscle relaxation in the cardiovascular system (Feil et al., 2005a; Massberg et al., 1999; Pfeifer et al., 1998; Sausbier et al., 2000). The latter is the most intensely studied function of cGKI and might influence blood pressure and tissue perfusion by contributing to the control of the vascular tone. Shear stress in the vasculature leads in endothelial cells to the production of NO through eNOS. The released NO diffuses to the underlying smooth muscle cells, activates the NO/sGC/cGKI pathway and finally leads to the relaxation of smooth muscle cells (Munzel et al., 2003). The positive effects of nitroglycerine and other NO-releasing substances, that are used to treat angina pectoris, are based upon this mechanism (Ignarro, 2002). The molecular mechanism of smooth muscle relaxation is tightly coupled to the phosphorylation state of the regulatory myosin light chain (MLC) (**Figure 3**). MLC is phosphorylated by the myosin light chain kinase (MLCK) and dephosphorylated by the myosin light chain phosphatase (MLCP) causing contraction and relaxation, respectively. Both cGKI isoforms are expressed in smooth muscle cells (Geiselhöringer et al., 2004; Keilbach et al., 1992) and interfere with the regulation of the phosphorylation status of MLC. cGKIα does so by interacting with the myosin-binding subunit of

MLCP (MYPT1) and with the regulator of G protein signaling 2 (RGS2) (Surks, 2007; Surks et al., 2003). cGKIβ inhibits calcium release from the sarcoplasmic reticulum through the phosphorylation of inositol 1,4,5-triphosphate receptor-associated cGMP kinase substrate (IRAG) (Schlossmann et al., 2000). Despite these suggested isoform-specific functions of cGKI in smooth muscle cells, SM-Iα and SM-Iβ rescue mice (A.1.1.2), which express only one or the other isoform specifically in smooth muscle cells, showed no differences in smooth muscle relaxation (Weber et al., 2007). Therefore, the topic of isoform-specific functions of cGKI *in vivo* remains an open question.

In addition to its role in smooth muscle relaxation, cGKI is involved in the phenotypic modulation of smooth muscle cells. Under physiological conditions smooth muscle cells are contractile due to their highly expressed contractile proteins (SMα-actin, SM myosin heavy chain). In contrast, under pathophysiological conditions or in culture SMCs can switch from the differentiated state to a dedifferentiated synthetic phenotype losing contractile properties and producing large amounts of extracellular matrix and increasing proliferation rates (Owens et al., 2004). This plasticity of SMCs plays an important role in vasculoproliferative diseases such as restenosis and atherosclerosis (Ferns and Avades, 2000; Gomez and Owens, 2012). The exact role of cGKI in this process is still a topic of ongoing research. In primary VSMCs isolated from cGKI-deficient mice the growth-promoting effect of cGMP, which can be seen in wild-type VSMCs, was absent suggesting an involvement of cGKI (Wolfsgruber et al., 2003). *In vivo* studies with smooth muscle- specific cGKI KO mice imply a pro-atherogenic role for cGKI, whereas in a carotid ligation model for restenosis no differences were observed between the mutant and control mice (Lukowski et al., 2008; Wolfsgruber et al., 2003). Therefore, the role of cGKI in vascular remodelling is probably context specific and differs between atherosclerosis and restenosis (Hofmann et al., 2006).

As mentioned above, an involvement of cGKI in many functions of the nervous system has been suggested including memory formation and learning. The cellular mechanism underlying learning and memory is believed to be based on changes in synaptic plasticity (Martin and Morris, 2002). For example, weakening of synaptic connections, called long-term depression (LTD), is associated with motor learning in the cerebellum (Boyden et al., 2004). Since cGKI is highly expressed in Purkinje cells (Feil et al., 2005b; Lohmann et al., 1981), it would stand to reason that it also plays a role in LTD and LTD-associated learning. Indeed, studies in Purkinje cell-specific cGKI KO mice showed that LTD is almost completely lost in these mice, but only some motor learning abilities were affected (Feil et al., 2003). Strengthening of synaptic connections, termed long-term potentiation (LTP), has been suggested to be crucial for spatial learning in the hippocampus (Chen and Tonegawa, 1997). In hippocampal slices, cGKI has been demonstrated to be involved in the induction of LTP (Zhuo et al., 1994), and in cell culture it was shown that cGKI acts thereby presynaptically (Arancio et al., 2001). However, synaptic transmission in LTP in *in vivo* studies with cGKI KO mice was unchanged (Kleppisch et al., 1999), whereas adult (12-14 weeks old), but not juvenile (3-4 weeks old) hippocampus-specific cGKI KO mice

displayed impaired hippocampal LTP after repetitive episodes of theta burst stimulation (Kleppisch et al., 2003). Besides the role of cGKI in LTD and LTP, more recent studies with mouse mutants lacking cGKI in the whole nervous system showed its contribution to complex behaviours. These behaviours include the formation of fear memory (Paul et al., 2008), social and object recognition (Feil et al., 2009), and the regulation of the sleep-wake activity (Langmesser et al., 2009).

A.1.1.2. Mouse models for the *in vivo* analysis of cGKI function

Studies in cGKI-deficient mouse models provide convincing evidence for a range of *in vivo* functions of cGKI. However, cGKI KO mice with a global deletion of cGKI (Pfeifer et al., 1998; Wegener et al., 2002) are not a suitable model for most *in vivo* studies given that they die at around 6 weeks of age. This is very limiting, especially in behavioural studies, which are usually performed in mature animals. The reason for the early lethality of cGKI KO mice is most likely their smooth muscle dysfunction and the resulting severe gastrointestinal problems (Pfeifer et al., 1998; Weber et al., 2007).

To circumvent the limitations of the chronic cGKI KO mouse, a “floxed” cGKI mouse line was created that allows generation of tissue-specific (conditional) cGKI KO mouse lines using the Cre/*loxP* technology (Wegener et al., 2002). This technology is based upon the features of the P1 bacteriophages’ Cre recombinase (**c**yclization **re**combination). This site-specific recombinase recognises *loxP* (**l**ocus **o**f crossing-over [**X**]**-**over of **P**1) sites, specific 34-bp DNA sequences, and catalyses recombination of them. If the two *loxP* sites are equally oriented, Cre recombination results in excision of the intervening DNA including one *loxP* site (Feil, 2007). Tissue-specific KO mice can be generated by crossing a “floxed” mouse, in which the target gene is flanked by two *loxP* sites, to a tissue-specific Cre mouse, in which expression of Cre recombinase is driven by a tissue-specific promoter. Even more advanced is the use of ligand-inducible Cre recombinases, in which the KO is additionally controlled in a time-specific manner (Metzger and Feil, 1999). With the Cre/*loxP* technology, cGKI can be inactivated in any tissue of interest enabling the analysis of physiological functions or pathophysiological consequences in adult animals. In this study, two different Cre mouse lines were used to obtain tissue-specific cGKI KO mice. The Nes-Cre mouse line expresses Cre recombinase under the control of the rat Nestin (Nes) promoter and enhancer resulting in Cre mediated recombination events in neuronal and glial precursor cells (Zimmerman et al., 1994). By breeding Nes-Cre mice (Tronche et al., 1999) to “floxed” cGKI mice, we obtained a mouse line, which is designated in the following as cGKI brain-KO, but lacks cGKI also in the peripheral nervous system.

Despite the multiple advantages of conditional upon conventional KO mice, there are also some drawbacks to this method. Leaky or mosaic expression of the Cre transgene can occur leading on the one hand to transient expression in unwanted or unanticipated cell types and on the other hand to an incomplete deletion. In the latter case, the possible remaining activity of the gene in a

fraction of target cells can sometimes be sufficient to preserve the physiological function of the protein masking a potential phenotype (Feil, 2007).
Thus, another cGKI-deficient mouse line was generated. One allele of the SM22α gene, which is only expressed in smooth muscle cells, was replaced by the bovine cGKIα and cGKIβ encoding sequence in these transgenic mice. Subsequently, they were crossed onto a cGKI KO background and the resulting offspring expressed one or the other isoform selectively in smooth muscle cells, therefore depicting a cGKI KO for non-smooth muscle tissues (Weber et al., 2007). In the following these mice are termed SM-Iα and SM-Iβ rescue mice. Originally these mice have been designed to decipher *in vivo* the isoform-specific role of cGKI in smooth muscle cells, but additionally they represent a suitable model for behavioural studies since they display almost normal life expectancy in contrast to global cGKI KO mice. Nevertheless, one should keep in mind that the cGKI isoforms are overexpressed in the smooth muscle tissues of this mouse model with the overexpression being more pronounced in case of cGKIα (Weber et al., 2007). The reason for the reduced life expectancy of SM-Iα/β rescues is also still unclear (Weber et al., 2007), and recently deficits in duodenal bicarbonate secretion resulting in bleeding ulcerations have been suggested as underlying pathology (Singh et al., 2012).

A.2. Stress

Despite the common usage of the word “stress”, the scientific definition of the phenomenon stress is less clear. In 1950, Hans Selye first introduced the term “stress” and defined it as a state resulting in a non-specific adaptive response of the organism to sustain its homeostatic equilibrium (Selye, 1950). His concept of non-specificity implied a general response mechanism that is independent of the causative external or internal stimulus (“stressor”). This was later refined by Johnson et al. (1992), who suggested that specific stressors cause specific responses with different brain regions involved. However, above a certain threshold intensity any stressor causes a common non-specific stress response pattern (Goldstein and Kopin, 2007; Pacak and Palkovits, 2001). Some of the differences evoked by distinct stressors, especially of stressors applied during this project, will be discussed in A.2.4.
Selye considered the hypothalamic-pituitary-adrenal (HPA) axis to be the key effector of the non-specific stress response. On the other hand, Cannon, who created the term “homeostasis” some years before Selyes’ stress concept, emphasised the activation of the sympathoadrenal system during the “fight-or-flight response”, as he named the general reaction of the organism when homeostasis is threatened (Goldstein and Kopin, 2007). Somehow they both ended up being right, since both pathways are activated by stressors (Kyrou and Tsigos, 2009). The main focus of this project is on the HPA axis, but, since this system closely interacts with the sympathetic nervous system (SNS) in mediating the stress response, the latter is also briefly introduced (Kvetnansky et al., 1995).

A.2.1. Sympathetic nervous system (SNS)

In response to a stressor, the activation of the SNS provides a mechanism for the rapid adaptation of vital functions such as cardiovascular, gastrointestinal and endocrine functions (Kyrou and Tsigos, 2009). The released catecholamines mediate this adaptation process and two sources for catecholamines can be distinguished. The first source is the sympathoadrenal system (SAS), which releases stored adrenaline and to a lesser extent noradrenaline from the chromaffin cells of the adrenal medulla. The chromaffin cells, which are modified postganglionic neurons, are stimulated via acetylcholine (ACh) released by preganglionic sympathetic neurons in the splanchnic nerves (Perlman and Chalfie, 1977). The second source for catecholamines is the sympathoneuronal system (SNS) (Kvetnansky et al., 2009). About 70% of the circulating noradrenaline in the plasma are released from widely distributed sympathetic nerves. The integration of incoming and outgoing signals of SNS activation takes place in neurons of the paraventricular nucleus (PVN) that project to autonomic targets in brain stem and spinal cord such as the intermediolateral column (Swanson and Sawchenko, 1980; Ulrich-Lai and Herman, 2009). Both pathways of the sympathetic system contribute to the rapid effects after stressor exposure, but they are not always activated in parallel or to the same extent (Goldstein and Kopin, 2007).

A.2.2. Hypothalamic-pituitary-adrenal (HPA) axis

While the SNS is primarily linked to the fast alarm reactions of the fight-or-flight response, the slower changes including behavioural adaptations after stressor exposure are mainly associated with the HPA axis (Engelmann et al., 2004) (**Figure 4**). As in SNS activation, also for this endocrine axis the hypothalamic PVN is the main integration site for inhibitory and excitatory stimuli threatening homeostasis (Ulrich-Lai and Herman, 2009). Excitatory stimuli reach the PVN via afferents from brain stem neurons, e.g. the nucleus tractus solitarii (NTS), as well as from other hypothalamic nuclei like the dorsomedial hypothalamus (DMH) and the arcuate nucleus. Inhibition of PVN neuronal activity is ensured by GABAergic input. Via this route, information from the limbic system, for example, is communicated to the HPA axis (Herman and Cullinan, 1997; Herman et al., 2002; Ulrich-Lai and Herman, 2009). Upon activation, a subpopulation of parvocellular neurons in the PVN synthesises and secretes corticotrophin-releasing hormone (CRH) and arginine vasospressin (AVP), whereas another subpopulation secretes AVP only (Charmandari et al., 2005). Both neuron types project to the median eminence where they terminate at capillaries releasing their hormones directly into the blood circulation via the hypothalamic-hypophyseal portal system (Whitnall, 1993). Both, CRH and AVP, are able to stimulate adrenocorticotropic hormone (ACTH) secretion by binding to corticotrophs in the anterior pituitary gland. They potentiate their actions synergistically, while AVP alone has only little stimulatory action (Antoni, 1993).

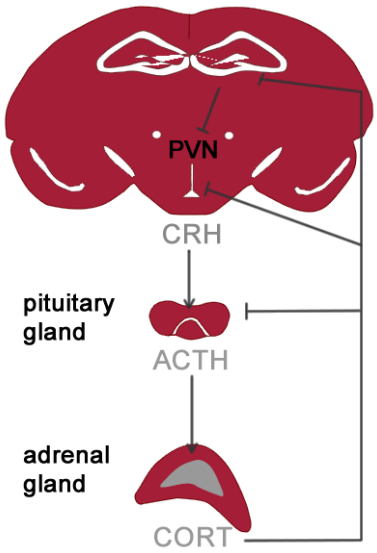

Figure 4: Scheme of hypothalamic-pituitary-adrenal (HPA) axis activation and negative feedback regulation. In response to external and internal stimuli, the parvocellular neurons of the hypothalamic paraventricular nucleus (PVN) produce corticotrophin releasing hormone (CRH), which stimulates corticotrophs in the anterior pituitary gland. In turn, corticotrophes secrete adrenocorticotropic hormone (ACTH) that reaches via the blood stream the adrenal gland cortex. Upon binding of ACTH to its specific receptors, corticosterone (CORT) is synthesised and secreted. CORT inhibits its own secretion at the level of the brain (PVN and hippocampus) and the pituitary gland via negative feedback signalling.

The released ACTH is a 39 amino acid peptide, but only the first 24 amino acids are important for the biological activity. It is processed by tissue-specific proteolytic cleavage from the precursor pro-opiomelanocortin (POMC), a 267 amino acid protein, which is synthesised in melanotrophs and corticotrophs of the pars intermedia and distalis of the anterior pituitary gland (Bicknell, 2008; Imura et al., 1965; Papadimitriou and Priftis, 2009). In addition to the main stimulation route via brain-derived factors, ACTH secretion is modulated by a variety of other factors in a paracrine manner (Denef, 2008; Schwartz, 1990). For example, cytokines act on and are released by the pituitary gland. Best investigated among them is IL-6 that is produced by folliculo-stellate cells and can stimulate ACTH secretion (Renner et al., 1998; Vankelecom et al., 1989). In the basal state ACTH is secreted in an ultradian pulsatile pattern following a circadian rhythm. In rodents, ACTH secretion peaks at the beginning of the night corresponding to their activity onset (Papadimitriou and Priftis, 2009). The ACTH secretion pattern follows the circadian rhythm in CRH secretion, which is coordinated by input of the suprachiasmatic nucleus (SCN) to the PVN (Walker et al., 2010), and in turn causes then the pulsatile circadian secretion of glucocorticoids from the adrenal cortex (Dickmeis, 2009).

Glucocorticoids are the final output of the stress-induced HPA axis activation. In contrast to catecholamines, glucocorticoids are not stored, but synthesised on demand (Thomson, 1998). ACTH is the most potent stimulus for their synthesis and secretion and influences this process

both acutely and chronically (Gallo-Payet and Payet, 2003). Its action is primarily mediated by binding to its receptor, the type 2 melanocortin receptor (MC2R). Stimulation of this transmembrane G protein coupled receptor leads to activation of adenylyl cyclase, an increase in cAMP and subsequent protein kinase A (PKA) activation (Sewer and Waterman, 2003). The acute effects of ACTH include the phosphorylation of cholesterol ester hydroxylase, which converts cholesterol esters to free cholesterol and therefore increases the substrate availability for steroidogenesis (Jefcoate, 2002). Additionally, ACTH influences the synthesis of steroidogenic acute regulatory protein (StAR), which regulates the transport of cholesterol from the outer to the inner mitochondrial membrane (Stocco, 2001). Chronic effects of ACTH include an increase in the synthesis of steroidogenic enzymes such as the cytochrome P450 monooxygenases Cyp11A1, CYP17, CYP21A2, and Cyp11B1 at the transcriptional level (Papadimitriou and Priftis, 2009). Similarly, expression levels of LDL receptors, the receptors for plasma low density lipoproteins, and SR-BI receptors, class B, type I scavenger receptors that bind high density lipoprotein (HDL), are upregulated by ACTH (Kovanen et al., 1980; Rigotti et al., 1996). Thus, ACTH stimulates glucocorticoid synthesis in diverse ways, but vice versa ACTH secretion is also controlled by glucocorticoids since the HPA axis underlies a classical negative feedback mechanism primarily to prevent an excess in glucocorticoid production. This feedback mechanism is not only controlled by glucocorticoids acting on ACTH synthesis in the pituitary, but also by glucocorticoid control of CRH synthesis in the PVN (Andrews et al., 2012). Three distinct time domains can be distinguished in feedback control. Fast feedback occurs within seconds to minutes, intermediate (early delayed) feedback happens within two hours and slow (late delayed) feedback takes place within several hours (Hinz and Hirschelmann, 2000). Delayed feedback inhibiton is mediated by the classical way of steroid hormone receptors acting as transcription factors. Thus, CRH, AVP and ACTH mRNA and protein levels are downregulated (Keller-Wood and Dallman, 1984; Papadimitriou and Priftis, 2009). This termination of the HPA axis activation is mainly mediated via the intracellular glucocorticoid receptor (GR) and its density in the brain is highest in the PVN (de Kloet et al., 2005). However, it is also expressed in other tissues of the HPA axis and different expression levels of GRs in pituitary and adrenocortical cells have been associated with inter-indiviual differences in HPA axis responsiveness (Briassoulis et al., 2011). The fast feedback regulation is attributed to the rapid, non-genomic effects of glucocorticoids by binding to membrane-associated G protein coupled receptors and subsequent activation of downstream signalling cascades (Tasker et al., 2006). But also the intracellular receptors probably play a role in the rapid effects of glucocorticoids (Falkenstein et al., 2000). Besides the regulation of their own secretion, the biological action of glucocorticoids in physiological processes ranges from suppression of immune reactions to the modulation of metabolic processes (Gross and Cidlowski, 2008).

Only the free fraction of glucocorticoids is biologically active and these are in the plasma about 5% of the circulating glucocorticoids. The remaining 95% are bound to the plasma proteins transcortin and albumin. Transcortin (corticosteroid-binding protein, CBG) has a high affinity but

low capacity for glucocorticoids, whereas albumin has a low affinity but high capacity (Henley and Lightman, 2011). Following stressor exposure, CBG synthesis can be down-regulated to increase free glucocorticoid levels (Spencer et al., 1996) and CBG has been suggested to regulate plasma glucocorticoid concentrations by influencing the clearance rate (Bright, 1995; Bright and Darmaun, 1995). Activity of glucocorticoids is additionally modulated at the tissue level by the two isozymes of 11β-hydroxysteroid dehydrogenase (11β-HSD), which catalyse the interconversion of inactive 11-dehydrocortisone and active corticosterone. Although, 11β-HSD1 has been shown to act bidirectionally, *in vivo* it primarily acts as a reductase increasing intracellular levels of active corticosterone (Tomlinson et al., 2004).

How important the complex control of HPA axis activation and glucocorticoid levels is, becomes obvious when looking at the severe effects of HPA axis disturbances. An excess of glucocorticoids, either due to an overproduction of endogenous glucocorticoids or by medication with glucocorticoids, leads to Cushing's syndrome with central obesity manifested in "moon faces" and "buffalo humps" (Hatipoglu, 2012). Just the opposite, a lack of glucocorticoids, occurs in Addison's disease, which is characterised by various symptoms such as weight loss, muscle weakness, fatigue, low blood pressure and hyperpigmentation. Untreated the disease can result in an adrenal crisis (severe adrenocortical insufficiency) that is life-threatening. Therefore, it is usually treated with a corticosteroid replacement therapy (Ten et al., 2001). Apart from over- or underproduction of glucocorticoids, also less severe dysregulations of the HPA axis can cause diseases. Especially psychiatric diseases like depression have been associated with a disturbed HPA axis regulation (Chrousos, 2009; Maletic et al., 2007).

A.2.3. Adrenal glands – special role at the interface of SNS and HPA axis

The two main stress response routes (SNS and HPA axis) are not only simultaneously activated after stressor exposure, but additionally interact with each other in the brain (PVN) and the periphery (adrenal glands) (Kvetnansky et al., 1995). The adrenal glands as the tissue, where the "effector hormones" of the stress response - catecholamines and glucocorticoids- are produced (Schinner and Bornstein, 2005), are fundamental for this interaction and thus the anatomical and functional details of this tissue are briefly introduced.

Anatomically, the adrenal glands are paired organs located above the kidneys. In the mouse, the weight of both adrenal glands is between 3 to 7.5 mg, and female mice have in general heavier adrenal glands than males (Bielohuby, 2007). The adrenal gland contains two structures with different embryological origin: the catecholamine-secreting medulla and the corticosteroid-producing cortex. Both structures have long been thought to act completely independent of each other, but recent studies have revealed a close intra-adrenal interaction (Ehrhart-Bornstein et al., 1998). Also the spatial separation of the two layers seems not to be as strict as formerly believed and chromaffin cells can be found in the cortical layer in some species (Bornstein et al., 1999). The cortical layer can be further subdivided in three concentric zones, which can be distinguished

by their morphology and by the expression of different enzymes. In the outermost zona glomerulosa (ZG) the mineralocorticoid aldosterone is produced due to the zone-specific expression of aldosterone synthase (Cyp11B2). The adjoining zona fasciculata (ZF) expresses 11β-hydroxylase (Cyp11B1), and thus catalyses the synthesis of corticosterone, the main glucocorticoid in rodents (cortisol in humans). In contrast to humans, mice do not have a functionally distinct zona reticularis (ZR), because they lack 17α-hydroxylase expression and thus adrenal androgen synthesis (Rainey et al., 2004). However, mice have another morphological feature: the so-called X-zone that is located at the transition from cortex to medulla and regresses at puberty in males and during the first pregnancy in females (Keegan and Hammer, 2002). ZG and ZF share the enzymes that are required for the first steps in steroidogenesis, and also the substrate, cholesterol, is identical for mineralo- and glucocorticoid synthesis. Determination of the final corticosteroid synthesised in each zone is consequently only achieved by the zone-specific enzymes catalyzing the final steps (Cyp11B1, Cyp11B2) (Rainey et al., 2004).

The adrenal gland is an extremely well vascularised organ with small cortical arteries entering the adrenal capsule, dividing into arterioles and capillaries that cross the cortex to the medulla. At the corticomedullary junction, the cortical capillaries come together with the medullary capillaries. Additionally, medullary arteries traverse through the cortex to the medulla without branching. Both types of arteries, cortical and medullary, finally drain into the central medullary vein. The dense vascularisation ensures that each steroidogenic cell is in direct contact with a sinusoidal capillary. This facilitates the transport of oxygen and cholesterol to the steroidogenic cells as well as the export of corticosteroid products (Bassett and West, 1997; Breslow, 1992; Gomez-Sanchez, 2007; Thomas et al., 2003). Due to the anatomy of the adrenal vascularisation, most of the blood reaching the medulla is enriched with corticosteroids that are able to increase adrenaline synthesis by upregulation of phenylethanolamine N-methyltransferase (PNMT), the enzyme that catalyses the conversion of noradrenaline to adrenaline (Wurtman, 2002).

Similarly complex as the vascularisation is the innervation of the adrenal gland. Two different types of neurons exist in the medulla. The chromaffin cells represent modified postganglionic neurons and are innervated by sympathetic fibers in the splanchnic nerve. The medullary ganglion cells are assumed to form an intrinsic network innervating chromaffin cells as well as cortical cells (Holgert et al., 1998). The intrinsic innervation of the adrenal cortex is complemented by the extrinsic neurons, which mainly contact blood vessels and adrenocortical cells in the subcapsular region (Delarue et al., 2001; Vinson et al., 1994; Whitworth et al., 2003).

Even though, ACTH is considered to be the main and most potent stimulator of steroidogenesis, there is often a marked discrepancy between ACTH levels and secreted steroids, especially under conditions of chronic stress (Bornstein, 2000; Bornstein and Chrousos, 1999). Both, changes in adrenal blood flow and nervous inhibition and stimulation, have been demonstrated to affect steroidogenesis and might explain at least partially this discrepancy (Breslow, 1992; Edwards et al., 1986; Gomez-Sanchez, 2007; Vinson et al., 1994). Especially the sensitivity of adrenal cells to ACTH that changes in the course of the diurnal rhythm of plasma CORT levels,

has been attributed to splanchnic innervation (Ulrich-Lai et al., 2006b). Apart from nervous stimulation and blood flow, numerous other factors such as cytokines have been implicated in the regulation of adrenal steroidogenesis mostly by acting in a paracrine manner (Bornstein et al., 2004; Ehrhart-Bornstein et al., 1998; Pignatelli et al., 1998).
Taken together, the adrenal glands are not only important sites of stress hormone production, but also represent a crucial interface between SNS and HPA axis stimulation and thus a location for the fine-tuning of the stress response.

A.2.4. Stressor-specific responses

As mentioned above (A.2), there are non-specific components of the stress response, which are shared between all types of stressors, but there are also specific patterns of neuroendocrine activation for each stressor type (Pacak and Palkovits, 2001). The specific patterns differ in the level of SNS, sympathoadrenal and HPA axis activation (Goldstein and Kopin, 2007). Four main categories of stressors can be distinguished: physical, psychological, and social stressors as well as stressors that challenge the cardiovascular and metabolic homeostasis. Duration of stress (acute or chronic) and intensity might also play a role in the activation of specific patterns (Kvetnansky et al., 2009). Physical stressors include cold and heat stress. Psychological stressors mainly affect emotional processes and thus often result in behavioural changes like fear and anxiety. Most of the stressors that are used in animal experiments can not be assigned to just one stressor type and are consequently mixed stressor types (Pacak and Palkovits, 2001).
During cold stress, the activation of the sympathetic nervous system predominates and leads to adaptive mechanisms like sympathetically mediated cutaneous vasoconstriction and shivering (Goldstein and Kopin, 2007). The parvocellular neurons of the PVN that are involved in HPA axis activation are not significantly activated, but thyrotrophin-releasing hormone (TRH) protein levels in the magnocellular neurons are two-fold increased, and hence the hypothalamic-pituitary-thyroid (HPT) axis has been suggested to contribute to the cold stress response pattern (Fiedler et al., 2006; Pacak and Palkovits, 2001; Zoeller et al., 1990).
Restraint stress can be considered as a mixture of physical and psychological stress. A maximal response in the activated stress effector systems can be seen within the first 30 minutes after the start of the immobilisation (Pacak and Palkovits, 2001). Repetitive restraint stress leads to a rapid decrease in the activation of the stress systems. This habituation or desensitisation process applies to all repetitive stressors of the same type (homotypic), whereas repetitive stress with different stressor types (heterotypic) leads to a sensitisation (Armario et al., 2004; Girotti et al., 2006). SNS and HPA axis are both strongly activated in response to restraint stress (Goldstein, 2010).
Systemic administration of interleukin-1β (IL-1β), an immune challenge, belongs to the physical stressor types and exemplifies the bidirectional relationship between the immune and stress system (Kvetnansky et al., 2009; Turnbull and Rivier, 1999). It strongly activates the HPA axis by

increasing CRH, ACTH and CORT levels (Turnbull and Rivier, 1999). Systemically administered IL-1β induces prostaglandin production via binding to IL-1β receptors in the endothelium of the blood-brain-barrier. The released prostaglandin then excites nucleus tractus solitarii (NTS) neurons that give input to the PVN (Ericsson et al., 1995; Zhang and Rivest, 1999).
When interpreting the results of animal experiments using these different types of stressors, one should keep in mind, that although the common underlying stress response is the same, stress hormone levels might vary in composition and quantity due to stressor-specific effects.

A.2.5. cGMP signalling and HPA axis regulation

NO/cGMP signalling and NP-stimulated cGMP production have been implicated in HPA axis modulation and steroidogenesis for quite some time (Brann et al., 1997; Ducsay and Myers, 2011; McCann et al., 1998). For instance, in rat hypothalamic explants, NO has been shown to inhibt IL-1β stimulated CRH release (Costa et al., 1993). Inhibitory effects of NO have also been demonstrated at the level of the adrenal gland *in vitro* and *in vivo*. In bovine zona glomerulosa cells, NO donors are able to stimulate cGMP production and inhibit basal, ACTH- and AngII-stimulated aldosterone release (Sainz et al., 2004). In rat zona fasciculata cells, NO donors also decrease basal and ACTH-stimulated CORT production dose-dependently (Cymeryng et al., 1998). In line with the *in vitro* experiments, NOS inhibition *in vivo* increases glucocorticoid secretion in rats (Adams et al., 1992). On the other hand, NO donors were suggested to enhance the rapid CORT release in ACTH-stimulated adrenal gland quarters *in vitro* via activation of cyclooxygenases and prostaglandin production (Mohn et al., 2005).
The published effects of NPs on HPA axis stimulation and steroidogenesis are also mainly inhibitory. For example in humans, intranasally applied ANP is able to suppress HPA axis response to insulin-induced hypoglycemia (Perras et al., 2004). *In vitro* NPs inhibit CRH-stimulated, but not basal ACTH secretion in hemi-pituitary preparations (Guild and Cramb, 1999). At the level of the adrenal gland, NPs also inhibit steroidogenesis. BNP and ANP decrease steroidogenesis in human adrenocortical cells and in the mouse adrenocortical tumor cell line Y1, respectively. Concurrently, both types of NPs stimulate cGMP production in the according cells (Heisler et al., 1989; Liang et al., 2007), whereas ACTH decreases cGMP levels time-and dose-depently in rat zona glomerulosa cells (Gallo-Payet et al., 1999).
Whether the inhibitory effects of NO and NPs are primarily depending on cGMP or whether these effects are mediated by cGKs is not yet clear. At least the inhibitory effect of ANP on ACTH-stimulated aldosterone secretion in bovine zona glomerulosa cells has been shown to be rather mediated by changes in cAMP levels that are regulated by the cGMP-stimulated PDE2 than by direct effects of cGMP on steroidogenesis (MacFarland et al., 1991; Nikolaev et al., 2005; Tsai and Beavo, 2011). On the other hand, a stimulatory effect of cGMP on steroidogenesis is supported by a study showing that 8-Br-cGMP, a cGMP analogon that does not activate PDE2, increases aldosterone production in rat zona glomerulosa cells. This effect was attributed to

cGKII, which is expressed in zona glomerulosa cells of rats (Gambaryan et al., 2003). In contrast to this, but in line with the inhibitory effect of NPs *in vitro*, injection of ANP in wild-type mice decreased ACTH-stimulated aldosterone secretion. This effect was absent in cGKII KO mice suggesting that cGKII influences ACTH-stimulated aldosterone secretion (Spiessberger et al., 2009).

An involvement of cGKs in HPA axis modulation and steroidogenesis is also supported by their expression profile. Especially cGKI is expressed in many tissues of HPA axis regulation such as hippocampus, hypothalamus, pituitary and adrenal gland (Feil et al., 2005b; Gambaryan et al., 2003; Kleppisch et al., 2003). Furthermore, in Leydig cells, the other steroidogenic tissue besides adrenal glands, cGKI has been shown to phosphorylate StAR and thus to modulate basal steroidogenesis (Andric et al., 2007). Additionally, the PDE5-specific inhibitor sildenafil increases testosterone production in Leydig cells after application for several days (Andric et al., 2010). Hence, steroidogenesis in Leydig cells seems to be cGMP dependent.

Another indication for an involvement of cGKI in steroidogenesis comes from studies in mice genetically deficient for the pore-forming subunits of the large-conductance calcium-and voltage-activated potassium (BK) channel (Sausbier et al., 2004). The BK channel was suggested to be a cGKI substrate (Sausbier et al., 2000) and BK KO mice show a diminished response to restraint stress primarily due to a reduced activation of PVN neurons and therefore decreased CRH secretion (Brunton et al., 2007).

A.3. Thermogenesis

A.3.1. Thermogenesis in brown adipose tissue (BAT)

Rodents and humans are mammals and accordingly homeotherms that defend their body temperature against environmental temperature fluctuations. Efficient thermoregulation becomes particularly important when mammals are exposed to low environmental temperatures, for example rodents to 4 °C. To produce heat, the first thermogenic mechanism being activated is the shivering thermogenesis resulting in skeletal muscle contractions (Morrison et al., 2008; Nakamura, 2011). However, during prolonged cold exposure non-shivering thermogenesis becomes more and more important. This thermogenic mechanism is almost completely depending on BAT (Foster and Frydman, 1979). Actually, mice kept at a room temperature of ~20 °C can be considered to be under constant cold stress and thus constant recruitment of BAT-dependent non-shivering thermogenesis, because the zone of thermoneutrality, a range of ambient temperatures, in which minimal metabolic energy is required for the maintenance of a constant body temperature, is around 30 °C in mice (Karp, 2012). Compared to white adipose tissue (WAT) that stores energy, the energy in BAT is completely used for heat-production. BAT

is characterised by a high number of mitochondria, high vascularisation and innervation by the SNS. In rodents, the highest amount of BAT can be found between the shoulder blades, in the so called interscapular region, but smaller portions are located around the aorta and the hilus of the kidneys (Cinti, 2007). The ability of BAT to generate heat is linked to the expression of uncoupling protein-1 (UCP-1, thermogenin), a protein at the inner mitochondrial membrane acting as a facultative proton transporter thereby uncoupling substrate oxidation from ATP production (Rousset et al., 2004). BAT thermogenesis is induced by the activation of β-adrenergic receptors through noradrenaline, which is released from sympathetic nerve terminals (Cannon and Nedergaard, 2004). For instance, cold exposure (in humans ≤ 23 °C, in mice ≤ 30°C) is an effective stimulator of the SNS and the resulting thermogenic process is called cold-induced thermogenesis (CIT) (Klingenspor, 2003; Lowell and Spiegelman, 2000; Silva, 2006). Furthermore, BAT has also been implicated in the regulation of body weight and the thermogenic process in response to over-eating (“cafeteria diet”) is referred to as diet-induced thermogenesis (DIT) (Ravussin and Galgani, 2011; Rothwell and Stock, 1987). Additionally, thyroid hormones have also been shown to exhibit thermogenic properties (Silva, 2006). It was long believed that only infants and hibernating animals have relevant amounts of BAT, but recently new interest in this tissue awakened due to the discovery of active BAT in adult humans and its potential in treating obesity is much discussed (Ravussin and Galgani, 2011).

A.3.2. cGKI - a potential role in thermogenesis

NO has long been known to be involved in BAT regulation. NO inhibits brown adipocyte proliferation, while concurrently promoting the differentiation and expression of BAT-specific genes (Nisoli et al., 1998). These effects of NO on mitochondrial biogenesis are mediated through cGMP-dependent mechanisms (Nisoli et al., 2003). An involvement of cGKI in adipogenesis was recently also shown in a study with 3T3L1 preadipocytes. In these cells, PDE5 inhibition with sildenafil and subsequent cGKI activation increased the differentiation process (Zhang et al., 2010). Furthermore, it was suggested that cGKI mediates the NO/cGMP effects in brown adipocytes and plays a crucial role in BAT differentiation and mitochondrial biogenesis (Haas et al., 2009).

A.4. Aim of this thesis

The aim of the current project was to investigate the potential role of cGKI in the stress response and in thermogenesis.

To address the question of cGKI function in HPA axis regulation *in vivo*, two cGKI-deficient mouse models lacking cGKI either in the nervous system (cGKI brain-KO) or in all tissues except smooth muscle cells (SM-Iβ rescue mice) were compared to litter-matched controls with respect to plasma stress hormone levels (ACTH, CORT) under basal conditions and after injection of IL-1β. SM-Iβ rescue mice showed differential responses after the immune challenge and were additionally exposed to another stressor type, restraint stress. To further investigate the underlying mechanism of the observed phenotype, adrenal glands and primary adrenal cell cultures of SM-Iβ rescue mice and controls were examined in more detail.

To analyse cGKI function in thermogenesis, the two cGKI-deficient mouse models were exposed to cold and fasting stress and changes in core body temperature were monitored using telemetry.

B Materials and Methods

B.1. Materials

B.1.1. Reagents and equipment

All chemicals and reagents were purchased from Carl Roth (Karlsruhe, Germany), if not otherwise specified. A list of reagents purchased from other companies can be found in the appendix (I.1). Surgical instruments and suture material were purchased from Fine Science Tools (Heidelberg, Germany) and Ethicon (Norderstedt, Germany), respectively. Anaesthetics for surgeries were kindly provided by the veterinary facility of the University of Tuebingen. A list of the equipment used in this project is attached in the appendix (I.1).

B.1.2. Solutions and buffers

All solutions and buffers were prepared with de-ionized ultrapure filtered water, if not otherwise mentioned. Percent concentrations for liquid reagents are based upon volume per volume (v/v). For solid reagents, they are expressed as weight percentage (w/v) based upon mass per volume (with x g/100 ml solution = x percent concentration). For pH adjustment 1 N NaOH or 1 N HCl was used. Recipes and storage conditions for general solutions and buffers are listed below. Method-specific solutions and buffers used in this project can be found in the appendix (I.2).

10x TBE buffer (store at RT)

Tris	0.5 M	108 g
Boric acid	0.5 M	55 g
EDTA pH 8.0 (0.5 M)	10 mM	20 ml
ddH_2O		ad 1 l

Phophate buffered saline (PBS), pH 7.4 (store at RT)

NaCl	135 mM	4 g
KCl	3 mM	100 mg
$Na_2HPO \bullet 2\ H_2O$	8 mM	710 mg
KH_2PO_4	2 mM	120 mg
ddH_2O		ad 500 ml
→ autoclave		

Tris-HCl, pH 8.0 (store at RT)

Tris	1 M	121.14 g
ddH_2O		ad 1 l
→ adjust pH to 8.0 with HCl		

10x TBS, pH 8.0 (store at RT)

Tris	100 mM	12.11 g
NaCl	1.5 M	87.66 g
ddH_2O		ad 1 l
→ adjust pH to 8.0 with HCl		

TBS-T (store at RT)

10x TBS	1x	100 ml
Tween-20	0.1%	1 ml
ddH_2O		ad 1 l

B.2. Mice, cell culture and *in vitro* organ culture

B.2.1. Maintenance and breeding of investigated mouse lines

Animals were maintained and bred in the animal facility of the Interfaculty Institute of Biochemistry (IFIB, Tuebingen, Germany) under standard conditions (LD 12:12, lights on at 0500 h, 19-21 °C) in Makrolon® cages type II (up to 4 mice) or type III (up to 10 mice). Regular chow (Altromin 1314, Altromin Spezialfutter GmbH & Co. KG, Lage, Germany) and tap water was provided *ad libitum*. For breeding, one or two adult females (at least 8 weeks old) were mated with one reproductive male (at least 6 weeks old). The offspring was ear punched at an age of 3 weeks and tissue processed for genotyping (see B.2.2). Approximately one week later, mice were separated from the mother and grouped by gender. The *in vitro* and *in vivo* experiments were performed in various cGKI mutant mouse lines (**Table 1**). If not otherwise stated, female mice were used in all experiments. In experiments with SM-Iβ rescue mice, two different groups of control mice (control I and II) were used (see **Table 1**). Analysis revealed no differences between the two groups in all experiments performed in this project. Therefore, they are not shown separately, but combined as one group and referred to as control.

Table 1: Overview on cGKI mutant mouse lines used in this project

transgenic mouse line	genetic background	genotype	cGKI expression	referred to as	reference
L1	129/Sv C57BL/6	L1/L1	global cGKI deletion	cGKI KO	(Wegener et al., 2002)
		+/L1	comparable to wild type	control	
SM-Iβ x cGKI	129/Sv	+/- L1/L1	global cGKI deletion cGKIβ expression from SM22α-gene locus	SM-I β rescue	(Weber et al., 2007)
		+/- +/L1	endogenous cGKI expression cGKIβ expression from SM22α-gene locus	control I	
		+/+ +/L1	comparable to wild type	control II	(Wegener et al., 2002)
Nes-Cre x cGKI	C57BL/6	tg/+ L1/L2	cGKI deletion in central and peripheral nervous system	cGKI brain-KO	(Langmesser et al., 2009)
		tg/+ +/L2	comparable to wild type control for Cre transgene	control	

B.2.2. PCR-based genotyping of mouse lines

To receive DNA for genotyping via polymerase chain reaction (PCR), ear biopsies were lysed overnight. For DNA lysis buffer composition see appendix (I.2.(a)).

DNA isolation from ear biopsies:

- Incubate samples overnight at 55 °C (50 µl DNA lysis buffer/ear biopsy)
- Centrifuge for 4 min. at 14,000 x g
- Transfer supernatant into new PCR cup
- Heat at 95 °C for 15 min. to inactivate proteinase K
- Obtained DNA can be stored at −20 °C or directly processed for genotyping

PCR is used for the amplification of DNA fragments from templates such as genomic or plasmid DNA. Two synthesised oligonucleotides (primers) serve as starting point for the enzymatic synthesis of the desired fragment by a heat-stable DNA polymerase (e.g. Taq polymerase). Requiring dNTPs in the reaction mix, the DNA polymerase is able to amplify the target DNA in a cyclic procedure consisting of three repeated steps (1. denaturation at 94 °C to receive single stranded DNA, 2. annealing of primers at 50-65 °C depending on the primer pair, 3. elongation at 72 °C). PCR used for genotyping identifies wild type and mutant mice by the presence or absence of an amplicon. Here, usually three primers instead of two primers are used. The additional amplification of a wild type DNA fragment prevents false negative results.

PCR for genotyping:

- Pipette 2 µl of DNA obtained from ear biopsies in a sterile PCR cup
- Heat PCR machine to 95 °C
- Pipette mastermix for PCR reaction

Standard PCR reaction mix:

10x PCR buffer (see I.2.(a))		2.5 µl
Primer A (25 µM)	0.3 µM	0.3 µl
Primer B (25 µM)	0.3 µM	0.3 µl
Primer C (25 µM)	0.3 µM	0.3 µl
Taq Polymerase (5 U/µl)	1 U	0.2 µl
ddH_2O		ad 25 µl

- Add 23 µl of the mastermix to each sample
- Mix by tapping PCR cups to the bench (make sure reaction mixture is localized to the bottom of the cup!) and run the appropriate PCR programme
- Mix PCR products with 5 µl of 6x DNA loading dye (see I.2.(a))
- Load 12 µl onto a 2% agarose gel and separate bands by gel electrophoresis (120 V, ~40 min.)
- Visualise and document results with an UV-transilluminator

Standard PCR protocol:

Initial denaturation	94 °C	5 min.	
Denaturation	94 °C	15 s	35 x
Annealing	55 °C	30 s	
Elongation	72 °C	30 s	
Final elongation	72 °C	5 min.	

The standard protocol needs to be optimised depending on the primer pairs and length of the amplified fragment. Primer sequences for the relevant transgenic mouse lines are attached in the appendix (I.3.1).

B.2.3. Cell culture of primary adrenal gland cells

Primary cell cultures are a better model than continuous cell lines to investigate cellular mechanisms underlying complex *in vivo* functions. Established cell lines have typically undergone a variety of changes to gain immortality, and primary cell cultures are therefore closer to the *in vivo* situation. Primary cell cultures were prepared from whole adrenal glands to examine the function of cGKI in CORT synthesis by comparing cells from control and SM-Iβ rescue mice. Freshly isolated cells were used for acute stimulations. DMEM, FCS and Pen/Strep were purchased from LifeTechnologies. Photos of cells were taken under a light microscope (Zeiss, Axiovert 40C) with a SONY Cyber-shot VX DSC-W17 using an ocular adaptor.

B.2.3.1. Isolation of primary cells

Mice sacrificed for cell culture experiments were rapidly killed by decapitation to avoid stress effects. Hereby steroidogenic cells are kept in a basic state, and depletion of cellular cholesterol stores is prevented. Removal of adrenal glands and processing of the tissue until enzymatic digestion was performed as fast as possible. PBS was kept at 4 °C, and removal of surrounding fat pads from the adrenal glands was done on ice under a binocular microscope. Solutions and media for enzymatic digestion (see I.2.(b)) were pre-warmed in a water bath to 37 °C.

Isolation of primary adrenal cells:

- Decapitate mice with large, curved scissors
- Remove adrenal glands and store in ice-cold PBS
- Free adrenal glands of surrounding fat pads under a binocular microscope
- Prepare enzyme working solutions A and B (see I.2) freshly in Ca^{2+}-free medium and warm to 37 °C
- Mince adrenal glands with a scalpel and transfer into pre-warmed enzyme working solution A (1 ml for 1-6 adrenal glands; 1.5 ml for 7-11 adrenal glands; 2 ml for 12-15 adrenal glands)
- Digest tissue fragments for 20 min. at 37 °C (water bath) and invert every 5 min
- Centrifuge for 5 min. at room temperature at 2,000 x g
- Remove supernatant carefully with a 1 ml pipette and replace with pre-warmed enzyme working solution B
- Digest for 20 min. at 37 °C. Invert every 5 min. During the last 5 min. resuspend with a 1 ml pipette until no tissue fragments, that are visible to the unaided eye, are left.
- Transfer cell suspension into a 15 ml falcon with 9 ml cell culture medium (see I.2)
- Centrifuge 5-10 min. at room temperature at 2,000 x g
- Discard supernatant and resuspend cell pellet in 1 ml cell culture medium
- Per adrenal gland approximately 100,000 to 200,000 cells can be obtained, depending on the age and gender of the mice
- Take 45 µl of the cell suspension and mix with 5 µl trypan blue (stains dead cells) for cell counting and determination of cell viability
- Count cells in a Neubauer counting chamber
- Count 4 large corner squares (V = 0.1 µl) consisting of 16 small squares each and calculate the mean of the 4 large squares.
  Total cell number = mean x 10^4 x volume of cell suspension (in ml)
- Seed cells in cell culture medium (see I.2.(b)) at:
  - a density of 50,000 cells/2.3 cm^2 (equal to 1 well of a 24-well plate, see also **Table 2**) for acute ACTH stimulation
  - a density of 100,000 cells/3.5 cm^2 (equal to 1 well of a 12-well plate, see also **Table 2**) for immunofluorescent staining

Table 2: Surface areas and medium/trypsin volumes of cell culture vessels

cell culture vessels	area	medium volume	trypsin volume
6-well plate	54 cm^2 (6 x 9 cm^2)	3 ml/well	0.7 ml/well
12-well plate	42 cm^2 (12 x 3.5 cm^2)	1.5 ml/well	0.5 ml/well
24-well plate	55 cm^2 (24 x 2.3 cm^2)	1 ml/well	0.3 ml/well
48-well plate	34 cm^2 (48 x 0.7 cm^2)	0.5 ml/well	0.2 ml/well
96-well plate	29 cm^2 (96 x 0.32 cm^2)	0.2 ml/well	0.03 ml/well
cell culture flask	25 cm^2	5 ml	2 ml
cell culture flask	75 cm^2	15 ml	3 ml
cell culture flask	175 cm^2	20 ml	5 ml

B.2.3.2. Stimulation of primary cells

ACTH stimulation

Acute stimulation of primary cells with increasing ACTH concentrations was performed to investigate, if CORT synthesis and release are affected in steroidogenic cells of SM-Iβ rescues *in vitro*. Only female mice (5-9 months old) were used in acute stimulation studies. Stimulation was performed in triplicates. Incubation medium was prepared by making a serial dilution of ACTH in cell culture medium according to the following scheme (**Figure 5**):

Preparation of ACTH incubation medium:

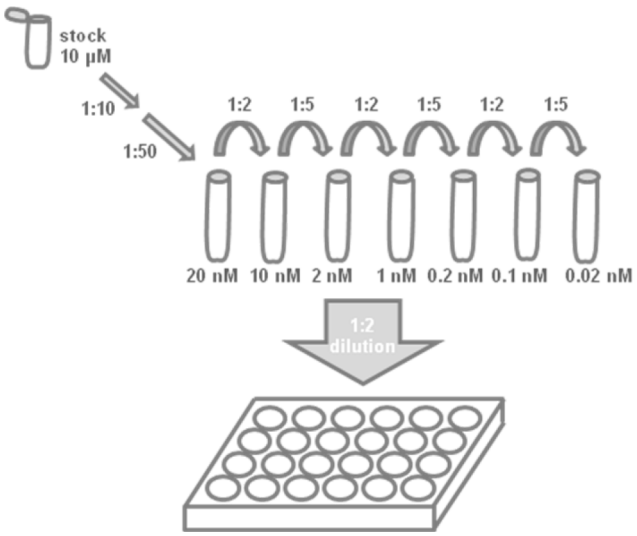

Figure 5: Dilution scheme for the acute ACTH stimulation in primary adrenal gland cell cultures. The ACTH stock dilution (see I.2.(b)) was pre-diluted 1:10 and 1:50 in cell culture medium. Dilution series was prepared twice as concentrated as required and diluted once more (1:2) by adding to an equal volume of cell culture media, which was already present in the wells.

ACTH stimulation of freshly isolated adrenal cells:

- Incubate cell suspension before counting in a 50 ml Falcon (make sure that the lid is not completely closed) for 1 h at 37 °C and 6% CO_2 to allow cells to recover from isolation procedure
- Centrifuge at room temperature at 600 x g for 10 min.
- Discard supernatant and resuspend cell pellet in 1-3 ml cell culture medium
- Count cells and adjust cell suspension to 100,000 cells/ml
- Distribute 500 µl cell suspension/well in 24-well cell culture plates
- Keep 6 ml of diluted cell suspension for protein determination (see B.5.1.2)
- Add 500 µl of respective ACTH incubation medium to the well
- Stimulate for 1 h at 37 °C and 6% CO_2
- Take supernatants and transfer into 1.5 ml Eppendorf reaction tube
- Centrifuge at room temperature at 600 x g for 10 min. (to remove cell debris)
- Transfer 800 µl in a new 1.5 ml Eppendorf reaction tube
- Store at −80 °C until CORT measurement

Processing of cell suspension for protein determination:

- Centrifuge at 600 x g for 10 min.
- Discard supernatant and wash cell pellet with PBS
- Centrifuge at 600 x g for 10 min.
- Repeat washing step
- Add freshly prepared SDS lysis buffer (~25 µl/100,000 cells; see also B.5.1.1) and resuspend vigorously
- Denaturate at 95 °C for 10 min.
- Centrifuge at 14,000 x g for 4 min. and perform protein determination (B.5.1.2) with an aliquot
- Store cell lysate at −20 °C

B.2.4. *In vitro* stimulation of adrenal gland slices

Compared to dispersed cell cultures in which cell-cell contacts are lost, organ slice cultures have the advantage that they preserve the microenvironment. Therefore experiments with slice cultures reflect the *in vivo* situation even better than primary cell cultures and allow an investigation of direct and indirect cell-cell interactions. In our experiment, one female SM-Iβ rescue mouse and one litter- and gender-matched control mouse were euthanised with CO_2. Adrenal glands were rapidly excised, stored in ice-cold PBS and freed from surrounding fat tissue. A complete removal of the sticky fat is absolutely necessary to enable proper cutting of the

glands. While one adrenal gland was immediately embedded in 4% low melting agarose (temperature ~42-45 °C), the other gland was kept in ice-cold PBS oxygenated with carbogen (5% CO_2, 95% O_2) and later sectioned. Adrenals were arranged with the craniocaudal axis perpendicular to the sectioning plane and cut into 200 µm-thick sections with a vibratome (Microm type HM 650 V, *MicromInternational*; frequency: 52; amplitude: 0.9; velocity: 3). Sectioning was performed in pre-cooled PBS, oxygenated with carbogen and temperature of PBS was controlled not to exceed 12 °C. Until ACTH stimulation slices were placed in organ culture medium in a 24-well plate within one hour after excision and kept for recovery at 37 °C, 6% CO_2. Adrenal gland slices were performed in the laboratory of Prof. Olga Garaschuk at the Institute of Physiology II in Tuebingen. Before stimulation 24-well plates were transported in pre-warmed Styrofoam boxes with warming pads into the cell culture rooms at the IFIB. Transportation time was not longer than 20 min. After transportation, slices were allowed to recover for approximately 1 h. For each stimulation condition (+/- 20 nM ACTH combined with +/- 100 µM 8-Br-cGMP), slices from the first and second adrenal gland of each animal were used and measured in triplicates.

ACTH stimulation of adrenal gland slices:

- Wash slices with organ culture medium (see I.2.(b))
- Add 1,000 µl of stimulation medium (+/- 20 nM ACTH, +/- 100 µm 8-Br-cGMP)
- Incubate at 37 °C and 6% CO_2
- Take 50 µl of supernatant at 0, 15, 30, 60, 120, 240 min. and 19 h
- Shake wells gently before taking the supernatant to ensure a homogenous mixture
- Store supernatants at −80 °C until CORT measurement

B.3. *In vivo* analysis

For the *in vivo* behavioural experiments, each experimental group consisted of randomly assigned either litter- or age-matched adult female mice. At least two weeks before the start of the experiments animals were caged in groups of two to four and transferred to the experimental room to allow adaptation to the new environment. Cage change was done not later than 5 days prior to the experiments. Two days before the experiments, the mice were left completely undisturbed with no researcher or animal technician entering the room, except for the circadian blood sampling experiment, in which the mice were handled daily before the experiment. All experiments were performed in accordance with the German animal protection law and were approved by the committee on animal care and welfare of the local government.

B.3.1. Circadian blood sampling

Basal stress hormone levels undergo diurnal variation and peak in nocturnal rodents around the end of the day, shortly before or right at activity onset (Malisch et al., 2008). Taking blood samples in the morning, when CORT levels are at their nadir and in the evening, when CORT levels reach their maximum, reveals changes in basal CORT levels and discloses, if the circadian rhythm of steroidogenesis is disturbed.

Blood samples from 5-7-month-old female SM-Iβ rescue mice and litter-matched controls were collected by tail nick 2 h after lights on (morning level) and 1 h before lights off (evening level). Tail nick was done with a sharp razor blade in the region of the central tail artery midway up the tail. The cutting was performed very fast and care was taken that the nick was not too deep to ensure that bleeding could be stopped quickly after blood sampling. Mice were adapted to this procedure by daily handling for 1 week prior to the blood collection. During these training sessions all steps of the blood sampling (taking animals from the home cage, placing them on a grid, fixing the tail) except for the tail nick were performed. The whole procedure including removal from the home cage to completion of blood sampling did not exceed 4 min. On the first experimental day, blood for the morning levels was collected. After a short recovery period of 2 days, blood for evening levels was collected from the same group of mice. Blood was collected with a Na-heparin capillary (minicaps®, end-to-end, 44.7 µl, #9000244, *Hirschmann Laborgeräte*) and transferred to a 1.5 ml Eppendorf reaction tube. Samples were centrifuged at 600 x g for 10 min. Heparin-plasma (~10 µl) was transferred to a new Eppendorf reaction tube and stored at −80 °C until CORT measurements.

To exclude that the results were influenced by the applied blood sampling method, another group of mice (7-12-month-old female SM-Iβ rescue mice and litter-matched controls) was sacrificed by decapitation in the morning, 2 h after lights on (for trunk blood collection see B.3.2). Again CORT and additionally ACTH concentrations were determined in those samples. Trunk blood was additionally collected from total cGKI-KO mice in the morning hours. Basal plasma CORT levels were determined as described (B.5.3.1).

B.3.2. IL-1β and ACTH injections

An important issue for the measurement of stress hormone levels in rodents, especially for basal levels, is the avoidance of interfering stressful influences caused by the handling or killing method. The use of anaesthesia or CO_2 is therefore not recommended since both substances have been shown to affect stress hormone levels (Vahl et al., 2005; van Herck et al., 1991). Nowadays, the method, which is most widely accepted to provide good results, is the decapitation of unanaesthetised mice by an experienced researcher. Therefore, this method was used for all *in vivo* experiments, in which blood for the measurement of stress hormone levels was collected, except for the circadian blood sampling. The whole procedure was performed rapidly and calmly.

Mice were taken from their home cage and decapitated instantaneously with very sharp scissors. Trunk blood was collected with the help of a second experimenter.

Trunk blood collection:

- Remove mice from the home cage as fast and gently as possible
- Decapitate with large, curved scissors
- Collect trunk blood in 50 µl 5 % EDTA-PBS (in 1.5 ml Eppendorf reaction tubes)
- Place immediately on ice
- Centrifuge at 600 x g at 4 °C for 10 min
- Transfer plasma to a fresh 1.5 ml Eppendorf reaction tube
- Store at –80 °C until CORT and ACTH measurements
- ~200-400 µl trunk blood can be expected from one mouse (20-30g BW)

B.3.2.1. IL-1β injections

Strong activation of the HPA axis can be achieved by an intraperitoneal (i.p.) injection of IL-1β (Besedovsky et al., 1986). IL-1β leads to the stimulation of afferent nerves that project to the NTS (nucleus tractus solitarii), which gives input to the PVN (paraventriclar nucleus) (Turnbull and Rivier, 1999). Hence, IL-1β mainly activates the HPA axis by increasing CRH release (Berkenbosch et al., 1987; Sapolsky et al., 1987). The activation of the HPA axis can then easily be measured by determination of plasma ACTH and CORT levels.
Recombinant mouse IL-1β was purchased from R&D Systems. Each mouse received a dose of 100 ng, which is sufficient to achieve a sound HPA axis response. Injections started 2 h after lights on. Decapitation started 2 h after the first mouse received its injection. Order of the mice and time intervals between two mice were the same as for the injections. A decapitation 2 h post injection was chosen, since it has been shown that at this time point plasma CORT levels reach their maximum (Besedovsky et al., 1986).

IL-1β injection:

- Inject mice i.p. either with 200 µl IL-1β stock solution (0.5 ng/µl IL-1β in 0.1% BSA-PBS) (experimental group)
  or with 200 µl 0.1% BSA-PBS (vehicle injected control group) (see I.2.(c))
- Inject alternately one SM-Iβ rescue mouse and one control mouse
- Interval between injections should be 4 min.
- Start decapitation of the first injected mouse 2 h after the injection
- Collect trunk blood in 50 µl 5% EDTA-PBS and tap Eppendorf reaction tube several times to mix well
- Store immediately on ice
- Dissect tissues of interest, snap freeze on dry ice and store in liquid nitrogen

- Centrifuge blood samples at 600 x g at 4 °C for 10 min.
- Transfer 20 µl EDTA-plasma in a new Eppendorf reaction tube for CORT measurements and 100 µl for ACTH measurements
- Store at −80 °C until CORT and ACTH measurements

B.3.2.2. ACTH injections

ACTH stimulation tests are commonly used in the clinics and in basic research to distinguish between primary (decreased responsiveness to ACTH) and secondary (ACTH deficiency) adrenal insufficiency. To examine if the reduced stress-induced CORT levels in SM-Iβ rescue mice are due to an impaired steroidogenesis of the adrenal gland, two ACTH stimulation tests were performed. A low dose (10 µg/kg) and an intermediate dose (100 µg/kg) of $ACTH_{1-24}$ (*Bachem*) were i.p. injected in female 3-7-month-old SM-Iβ rescue mice and litter-matched controls. Two separate experiments were performed for the stimulation with a low and intermediate dose. Injections started 2 h after lights on, and blood collection started 1 h after the first injection. SM-Iβ rescue mice and controls were injected alternately. A control group received an equal volume (0.1 ml/10 g) of vehicle solution (0.1% BSA-PBS).

ACTH injection:

- Inject mice i.p. with 0.1 ml/10 g of a 1:500 dilution (low dose) or 1:50 dilution (intermediate dose) of a ACTH stock solution (experimental group) (see I.2.(c))
- Vehicle injected control group receives 0.1 ml/10 g of 0.1% BSA-PBS
- Inject alternately one SM-Iβ rescue mouse and one control mouse
- Inject in 4 min. intervals
- Decapitation of the first injected mouse should be started 1 h after the injection
- Collect trunk blood in 50 µl 5% EDTA-PBS and mix well
- Store samples on ice
- Centrifuge blood samples at 600 x g at 4 °C for 10 min.
- Transfer 60 µl EDTA-plasma in a new Eppendorf reaction tube for IL-6 measurements and at least 20 µl for CORT measurements
- Store at −80 °C until CORT measurements

B.3.3. Restraint stress

Restraint or immobilisation stress is a well-established method to induce stress in mice. It is considered to be a mixed physical and psychological stressor (Pacak, 2000) that leads to a rapid rise in stress hormone levels (Goldstein and Kopin, 2008). In two different age-groups of female SM-Iβ rescue mice the acute effects of restraint stress were investigated: a young group (3 months old) and an old group (7 months old). Restraint stress experiments were performed in

the morning (2 h after lights on), when endogenous CORT levels are low. Mice were placed in a tube-shaped mouse restrainer (self-made from the staff of the IFIB workshop). This plastic cylinder had an internal diameter of 3 cm and a variable plug, which was adjusted to the animal size. It was ensured that mice could freely breathe but without being able to perform significant movements or turning around. Between two mice the restrainer was properly cleaned with ddH_20 and 70% $EtOH/H_2O$. This should prevent additional uncontrollable stress that can be caused by olfactory traces from the former mouse. After 30 min. of immobilisation, mice were decapitated and trunk blood was collected in 50 µl 5% EDTA-PBS (see also B.3.2.). Blood samples were centrifuged at 600 x g for 10 min. at 4 °C. Plasma was stored until CORT measurement at −80 °C.

For the catecholamine measurements, the immobilisation time was reduced to 10 min. Before and after immobilisation, mice were anaesthetised with Forane® (Isoflurane, *Baxter*) and blood was collected by retro-orbital puncture. Mice were fixed and the tip of a Na-heparin capillary (minicaps®, end-to-end, 44.7 µl, #9000244, *Hirschmann Laborgeräte*) was carefully inserted into the corner of the eye socket. The capillary was moved forward while rotating between the finger tips. As soon as blood appeared in the capillary, it was withdrawn and a few drops of blood (~300 µl) were collected in an Eppendorf reaction tube and immediately placed on ice. Samples were centrifuged at 600 x g for 10 min. at 4 °C. Serum was stored at −80 °C until catecholamine measurements.

B.3.4. Behavioural test: Forced swim test

Depression is one of the diseases that have been associated with a dysfunction in HPA axis regulation (Ising and Holsboer, 2006). Certainly, it is difficult to model complex human psychiatric disorders in animals, but the Porsolt forced swim test (FST) is commonly used as an animal model of depression. It was first published in 1977 as a test to measure antidepressant effects of drugs on the behaviour of mice (Porsolt et al., 1977). The impossibility of mice to escape from the situation and the forced swimming can be considered as a mixture of physical and psychological stress.

In our studies a slightly modified version of the originally published procedure was used (Porsolt et al., 1978; Porsolt et al., 1977). Mice were placed for 6 min. in a plastic beaker (height 18 cm, diameter 14 cm) filled with 23 °C water. The same test was repeated 24 h later. Both, test and re-test were performed in the morning hours when the mice are still active and endogenous CORT levels are low. Between two mice the water was discarded, the beaker cleaned to remove olfactory traces and filled with fresh water. After refilling, the water temperature was controlled with a thermometer. The water level was adjusted at a height, at which the mice had no other option but to swim. This means, they were not able to rest on their tails or to escape from the plastic beaker (see **Figure 6**). Directly after swimming, the mice were dried with towels and placed in front of an infrared lamp (InfraPhil 100 W, HP1511, *Philips*). Behaviour during the FST

was recorded with an USB camera (WebcamPro 9000, *Logitech*), and the videos were analysed by a researcher unaware of the genotype of the mice. The scoring of the behaviour was done with a simple Unix-programme and analysed with an Excel-Macro ("winrat-the improved version"). The software was kindly provided by Dr. Alana Knapman, Max Planck Institute of Psychiatry, Munich. Three different behaviours were scored: swimming, struggling and floating. Struggling was defined as escape behaviour with both front paws above the water surface. Floating was defined as an immobile state, in which the mouse only moves the tail or one limb to keep the head above the water surface. Swimming was defined as calm swimming movements. For all three behaviour types, the time spent within this behaviour and the latency when this behaviour occurred for the first time was calculated.

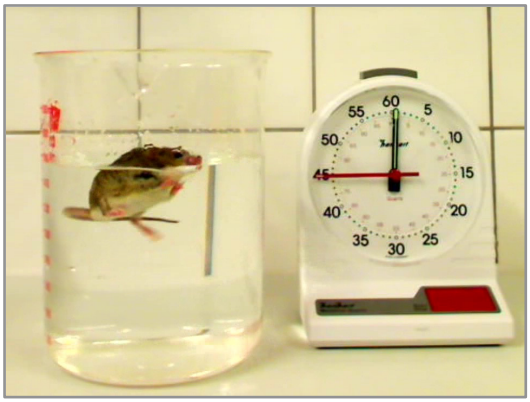

Figure 6: Set-up for the forced swim test (FST). Mice were placed in 23 °C-warm water and the stop watch started. During the test, the researchers stayed in the background to avoid falsifications of the behavior. Behaviour was recorded with an USB camera and scored from a blinded experimenter. The experimental part of the FST was performed by Anneysha Mohanty.

B.3.5. Cold stress

Another stressor effectively activating the HPA axis is cold stress (Djordjević et al., 2003). However, besides the stress effect, acute cold stress is commonly used to reveal deficits in thermoregulation. For this purpose, core body temperature was measured in 2 female SM-Iα and 7 female SM-Iβ rescue mice (3-6 months old) as well as in 10 cGKI brain-KO (6-10 months old) and corresponding controls. Temperature was measured under baseline conditions and at 4 °C. With this experiment, possible changes in thermoregulation and in the tolerance to cold stress should be accessed. All temperature measurements were performed with a radio telemetry system from Data Sciences International (*DSI*). This system consists of an implantable wireless transmitter (PhysioTel® TA-F20) and a receiver (PhysioTel® RPC-1) placed underneath the home cage of the single-caged mice (see **Figure 7**). Temperature and activity data from each animal were collected by the transmitter, and the digitized data were broadcasted as radio frequency signals to the receivers, which converted the data to a form that could be analysed with the DSI Dataquest A.R.T.™ Analysis software. For the transmitter implantations, the mice were

anaesthetised with a mixture of Midazolam, Medetomidin and Fentanyl applied as intraperitoneal injection (i.p.) (see 0). Depth of anaesthesia was controlled with the toe pinch reflex. During the surgery the animals were placed on a heating pad (AccuLux ThermoLux, *Reptilica*) to prevent hypothermia and eyes of the mice were covered with a sterile ophthalmic ointment (Bepanthen®, *Bayer*) to prevent drying out. After disinfection of the surgical area, a 1.5 cm incision was made along the midline with sharp sterile scissors to the abdominal wall. The transmitter was placed loosely without fixation inside the abdomen. The peritoneum was sutured with an absorbable suture (#V391, Ethicon Vicryl, *Johnson&Johnson*) and the abdominal skin with a non-absorbable suture (#EH7823, Ethicon Ethilon®II, *Johnson&Johnson*). Before antagonising the anaesthesia with a mixture of Naloxon, Flumazenil and Atipamezol (subcutaneous s.c. injection) (see I.2.(d)), mice received a s.c. injection of the analgesic Carprofen (Rimadyl®, *Pfizer*). Mice were allowed to recover for at least one week until temperature recordings started. Basal temperature was recorded for one week, in which the mice where left undisturbed without cage changes and any researcher or animal technicians entering the room. For the cold stress experiment, the mice were transferred with the complete set-up into a cold room (4 °C). No food and bedding was provided during the cold stress and the cages were pre-cooled at 4 °C. The mice were subjected to the cold stress for 4-6 h starting ~8 h after lights on (in accordance with pilot experiments performed by Dr. S. Feil). Temperature was controlled regularly and when core body temperature dropped below 20 °C, mice were excluded from the experiment and immediately warmed.

Figure 7: Mouse with an implanted transmitter to measure core body temperature and activity. Eight mice were measured simultaneously with the DSI set-up. Each mouse was single-caged and placed in its home cage upon the encoded receiver. Distance between the cages was 50 cm to all sides and signals were checked for cross-talk and electromagnetic interference of other devices such as computers.

Temperature and activity data were measured and recorded in 2 min. intervals. Subsequently, the telemetry data were further processed with the DSI Dataquest A.R.T.™ Analysis software. For the baseline data, moving averages were calculated as 1 h, 3 h, 6 h and 12 h bins for each day. Then the bins of 5-7 consecutive days were combined as a 24 h baseline. Moving averages and 24 h baseline were first calculated for each mouse before the mean of mutant and control groups

was calculated. Analysis of the cold stress experiment was done in 15 min., 30 min., 1 h and 2 h bins.

B.3.6. Fasting stress

As the stressor types mentioned before, also acute food deprivation leads to an increase in stress hormone levels (Djordjević et al., 2003). Given that mice consume the majority of their daily food at night, an overnight fasting is very effective leading in wild type mice to 2-fold increased plasma CORT levels (Hoekstra et al., 2008). However, besides acting as a mild stressor, overnight fasting can also cause metabolic changes and influences core body temperature (Overton and Williams, 2004). The food deprivation can cause mice to enter torpor, a controlled rapid drop in body temperature and metabolic acitivity (Swoap, 2008). To further investigate thermoregulation in our cGKI-deficient mouse lines, the core body temperature was investigated in 2 female SM-Iα and 7 female SM-Iβ rescue mice (3-6 months old) and 10 female cGKI brain-KO mice (6-10 months old) in response to overnight fasting. The same groups of mice as in the cold stress experiment were used. Mice were given at least one week between cold stress and fasting stress to recover. Fasting started at lights off and lasted between 16-18 h. Mice were placed in new cages with water supplied, but without food and bedding. Weight of the mice was determined before and after the fasting stress. Temperature and activity data were recorded in 2 min. intervals and moving averages were calculated as 15 min., 30 min., 1 h and 2 h bins. Moving averages of each individual animal were calculated before the group means for mutant and control mice were computed.

B.4. Statistical analysis

Data are always represented as group means ± SEM and were analysed with GraphPad Prism® 5.0 (*GraphPad Software, Inc.*). Statistical analyses were performed by an unpaired Student's t-test to compare two groups. For all other statistical analyses (comparing more than two groups, conditions or time-points) a two-way ANOVA followed by Bonferroni's post hoc test or an ANOVA with repeated measures was applied. Significance levels are given as p with $p<0.05$ and $p<0.01$ being statistically significant. Significance levels with $p<0.001$ are considered to be highly significant.

B.5. *Ex vivo* analysis of blood and tissues

B.5.1. Protein analysis

B.5.1.1. Preparation of protein extracts

To compare and analyse the expression levels of different genes in control and mutant mice, protein was extracted from various organs. Isolated organs were snap frozen and either immediately lysed in SDS protein lysis buffer or stored at −80 °C.

Protein extraction:

- Prepare SDS lysis buffer right before usage
- Add appropriate amount of SDS lysis buffer to the frozen tissue (placed in a FastPrep™ lysing matrix tube; for 10 mg tissue ~100 µl lysis buffer)
- Homogenise with the FastPrep®-24 instrument (*MP biomedicals;* 2 x 30 s; 6.5 m/s; pause for 5 min. and place samples on ice between the two homogenisation steps)
- Denature at 95 °C for 10 min.
- Centrifuge at room temperature for 5 min. at 18,000 x g
- Transfer supernatant in a new 1.5 ml Eppendorf reaction tube
- Store at −20 °C until determination of protein concentration

B.5.1.2. Determination of protein concentration

Protein concentration was determined with the Lowry method. This method is especially suitable for low protein concentrations (0.1 - 400 µg/ml). It combines the biuret reaction, in which alkaline copper (II) sulfate forms complexes with peptide bonds, followed by a reduction of Cu^{2+} to Cu^{+}, with the Folin Ciocalteau's phenol reagent which is reduced by the formed Cu^{+}. The resulting blue colour can be photometrically measured at OD_{650}. The unknown protein concentration is determined by comparison with BSA standards. The reaction is sensitive to interference by reducing agents like β-mercaptoethanol. Therefore, protein extraction was performed without β-mercaptoethanol and a small aliquot of the protein lysate was kept for protein determination while the rest was substituted with β-mercaptoethanol. The Lowry assay was performed in duplicates in 96-well plates with the Micro-Lowry-Total-Protein Kit (*Sigma*). Tissue lysates were diluted ~1:5 with SDS lysis buffer depending on the tissue.

Protein determination:

- Add 10 µl cell lysate in a 96-well plate and fill with 90 µl H_20
- Add 100 µl of each BSA standard (12.5, 25, 50, 100, 200 µg/ µl) into the 96-well plate
- Add 100 µl H_20 (blank) and 10 µl lysis buffer filled with 90 µl H_20 (negative control) into the 96-well plate
- Add 100 µl Lowry Reagent Solution to each well
- Shake on the microplate reader and incubate at room temperature in the dark for 20 min.
- Add 50 µl Folin Ciocalteu's Phenol Reagent Working Solution to each well
- Shake on the microplate reader and incubate at room temperature in the dark for 30 min.
- Measure OD_{650} with the microplate reader
- Calculate protein concentrations from the standard curve (plot absorbance values against corresponding BSA concentrations)

B.5.1.3. SDS-PAGE and Western blotting

Proteins can be separated with SDS-PAGE (sodium dodecyl sulfate polyacrylamide gel electrophoresis) according to their molecular weight. SDS, an anionic detergent, denatures proteins and by binding applies a negative charge to them. Since proteins bind SDS at a constant weight ratio (1.4 g SDS / 1 g protein), the negative charge is proportional to the protein mass and this allows a separation by size during electrophoresis. During electrophoresis proteins are compiled in a 4% stacking gel and separated in a 8-12% resolving gel. Whole protein content can be visualised by staining the gel with Coomassie brilliant blue. Or the separated proteins can be blotted onto a PVDF (polyvinylidene difluoride) membrane in a semi-dry blotting chamber. Particular proteins within the multi protein extract can then be detected with specific antibodies (Western blotting).

The Mini-PROTEAN® 3 system (*BioRad*) was used for the preparation of polyacrylamide gels. Gels were prepared with a thickness of 0.75 mm and 10 wells (15 wells) for a maximal loading volume of 18 µl (12 µl). After determination of protein concentration, the concentration was adjusted to 1-2 µg/µl with 5x Lämmli sample buffer. Before protein samples were loaded onto the gel, they were denatured at 95 °C for 5 min. For an efficient detection of the protein of interest, 10-30 µg protein was loaded onto the gel. For solutions and buffers see appendix (I.2.(e)).

SDS-PAGE

- Clean glass plates with 70% ethanol
- Arrange glass plates in the Mini-PROTEAN® 3 system clamps
- Prepare solution for resolving gel (see Table 3) and pour between glass plates until ~1 cm below the rim of the small glass plate
- Cover with isopropanol and allow the gel to polymerise for ~45 min.
- Remove isopropanol and pour stacking gel solution (see **Table 3**) on top of the resolving gel
- Place comb immediately in the gel and allow polymerization for ~45 min.
- Load protein samples and run gels in the electrophoresis chamber at 100 V for ~15 min. until samples reach the resolving gel
- Run the gels at 150 V for ~60-90 min.

Coomassie staining

- Heat gel together with Coomassie stainer in the microwave for 1 min. at 800 W
- Incubate at room temperature for ~30 min. with gentle shaking
- Remove Coomassie stainer and destain with Coomassie destainer for 2-3 h (replace destainer every 30 min.)

Table 3: Composition of Glycin-SDS-PAGEs. The indicated quantities are for 2 gels with 0.75 mm thickness. TEMED and APS should be added last.

reagents	stacking gel	resolving gel	
	4%	**8%**	**12%**
Rotiphorese® Gel 30 (*Roth*) (30% acrylamide/ bisacrylamide, ratio 37.5:1)	0.65 ml	2.7 ml	4 ml
4x TrisCl/SDS, pH 8.8	_	2.5 ml	2.5 ml
4x TrisCl/SDS, pH 6.8	1.25 ml	_	_
ddH_20	3.05 ml	4.7 ml	3.4 ml
tetramethylethylenediamine (TEMED) (stored at 4 °C)	10 µl	10 µl	10 µl
20% ammonium persulfate (APS) (stored at –20 °C)	25 µl	50 µl	50 µl

Western blotting

- Cut 16 Whatman papers (~9 x 8 cm) per blot
- Soak 4 pieces in anode solution I, 4 pieces in anode solution II, and 8 pieces in cathode solution
- Cut PVDF-membrane (Immobilon™-P Transfer Membrane, *Millipore*) to the correct size, activate in methanol and bathe briefly in anode solution II
- Stack the blot in a MAXI-Semi-Dry-Blotter (*Roth*) in the following order:
  - (Cathode/top)
  - 8 Whatman papers soaked in cathode solution
  - Gel
  - PVDF membrane
  - 4 Whatman papers soaked in anode solution I
  - 4 Whatman papers soaked in anode solution II
  - (Anode/bottom)
- Smooth out any air bubbles by gently rolling over the stack with a plastic pipette
- Blot at 50 mA per blot for ~60-70 min.
- Before blocking the membrane, cut membrane to the size of the gel and label the marker bands with a pencil
- Block membrane for 1 h at room temperature (optionally overnight at 4 °C) in 5% milk powder in TBS-T
- Wash 2 x 5 min. in 1% milk powder in TBS-T
- Wash 1 x 5 min. in TBS-T
- Incubate membrane in a 50 ml Falcon with primary antibody dilution (I.4) overnight at 4 °C with constant rotating
- Wash 3 x 5 min. in 1% milk powder in TBS-T
- Incubate with secondary antibody diluted 1:5,000 in 1% milk powder in TBS-T for 1 h at room temperature
- Wash 1 x 5 min. in 1% milk powder in TBS-T
- Wash 2 x 5 min. in TBS-T
- Develop the blot with commercially available ECL reagent (Amersham ECL Western Blotting Detection Reagent, *GE Healthcare*):
  - Mix solution A and B with a ratio of 1:1
  - Dilute with TBS-T 1:10 (up to 1:15, depending on the expected signal strength)
- Place membrane in a small plastic container and cover with diluted ECL reagent (1 ml per membrane)
- Develop the blot with a digital imaging system (FluorChem® FC3, *Biozym Scientific GmbH*)

B.5.2. Histological methods

B.5.2.1. Preparation of paraffin sections and cryosections

Two different methods can be used for tissue sectioning: paraffin embedded sections and cryosections. Compared to cryosections, paraffin sections display a better morphology of the tissue, but require extensive fixation and processing. Cryosections can be more rapidly processed and antigenicity is in general better preserved than in paraffin sections.

Paraffin sectioning

For paraffin embedded sections, mice were euthanised with diethyl ether. Tissues were dissected immediately and immersion-fixed in a sufficient volume of Cell fix (see 0) (~5-10x greater than the tissue volume) for 30-60 min. at room temperature. Fixation time needs to be long enough to ensure immersion of the complete tissue, but short enough to prevent extensive cross-linking of proteins by form- and/or glutaraldehyde.

Preparation of paraffin sections

- Wash fixed tissue 2-3 x in PBS to ensure complete removal of the fixative
- Dehydrate tissue with an increasing alcohol series:
  - 60% EtOH/H_2O for 1 h at RT
  - 70% EtOH/H_2O for 1 h at RT
  - 80% EtOH/H_2O for 1 h at RT
  - 90% EtOH/H_2O for 1 h at RT
  - 2 x 100% EtOH for 20 min. at RT
  - 2 x 100% toluene for 20 min. at RT
- Pass tissue through 3 changes of liquid paraffin (Paraplast®X-TRA, *Roth*) at 57 °C
- Each paraffin step should be at least overnight
- Embed tissue in clean liquid paraffin using an embedding system consisting of a metallic cassette and a plastic mould
- Store paraffin embedded tissue at room temperature until further processing

For histological staining, paraffin embedded tissue was cut in 10 µm sections with a microtome (HM335E, *MicromInternational*). Afterwards paraffin sections were placed in a waterbath (*Medax*) with 40 °C water temperature to flatten. Sections were mounted onto poly-L-lysine coated slides (Polysine™, *Menzel-Gläser*) and allowed to dry first on the rim of the waterbath and afterwards at 37 °C overnight. Sections need to be deparaffinised and rehydrated to enable histological staining.

Rehydration of paraffin sections

- Deparaffinize with toluene:
  - 2x 100% toluene for 10 min. at room temperature
- Rehydrate paraffin sections with a decreasing alcohol series:
  - 2 x 100% EtOH for 5 min. at RT
  - 90% EtOH/H_2O for 2 min. at RT
  - 80% EtOH/H_2O for 2 min. at RT
  - 70% EtOH/H_2O for 2 min. at RT
  - 60% EtOH/H_2O for 2 min. at RT
- Wash slides in PBS (for immunohistological staining) or H_20 (for HE staining) for 5 min. at RT

Cryosectioning

For cryosections, mice were euthanised with diethyl ether and tissue was perfusion-fixed. In order to do this, a 12-gauge needle was inserted in the left ventricle and the right atrium was cut open. Mice were transcardially perfused through this ventricular catheter with ice-cold heparin solution (~5 min.) followed by ice-cold 4% PFA solution (~10 min.) (see also I.2.(f)). Perfusion flow rate was kept at 1 ml/min. Tissues were dissected and post-fixed in 4% PFA overnight. Tissue was washed twice with PBS and placed in 30% sucrose for cryoprotection. After tissue has sunk in sucrose solution, it was placed in moulds filled with Tissue-Tek® O.C.T compound (*Sakura Finetek*). A beaker filled with isopentane (2-methyl-butane) was cooled in liquid nitrogen (−176 °C) until isopentane was close to freezing (opaque bubbles occured). Subsequently, tissue in Tissue-Tek® was frozen in the cooled isopentane and the tissue was stored at −20 °C until sectioning. Later, tissue was cut in 5-10 µm sections at −25 °C using a cryostat (HM525, *MicromInternational*). Sections were immediately mounted on slides (SuperFrostPlus®, *Menzel-Gläser*) via electrostatic charging of the slide surface. Slides were air-dried and subsequently stored at −20 °C until histological staining.

B.5.2.2. Hematoxylin and eosin (HE) staining

For the HE-staining, 10 µm serial paraffin sections were rehydrated as described and washed in ddH_20. This staining method is commonly used to recognise morphological changes and was used in this project to compare the morphology of adrenal glands from SM-Iβ rescue and control mice. Hematoxylin stains nucleic acids which appear in a deep-blue purple colour. Proteins are nonspecifically stained by eosin in pink. Consequently, in HE-staining nuclei appear blue while the cytoplasm and extracellular matrix are stained in pink.

HE- staining

- Incubate slides for 3-5 min. in Mayer's hemalaun solution (#T865.1, *Roth*)
- Wash slides briefly in ddH_20
- Rinse slides with tap water for ~15 min. until staining has the desired blue intensity
- Wash in ddH_20 for 2 min.
- Incubate slides in Eosin G solution (#7089.1, *Roth*) supplemented with a drop of glacial acetic acid (1 drop/100 ml Eosin G solution) for 3 min.
- Rinse slides briefly with tap water
- Dehydrate slides in an increasing alcohol series (80% EtOH/H_20, 90% EtOH/H_20, 2 x 100% EtOH) for 30 s each step
- Incubate for 2 x 2 min. in 100% toluene or xylene
- Mount with DePeX mounting medium (*Serva*)

B.5.2.3. Cresyl violet staining

Cresyl violet staining is commonly used to visualise neuronal cell bodies in the brain. This basic dye binds to the acidic components in the cytoplasm of cells, especially to RNA rich ribosomes. Since neurons possess nissl bodies (rough endoplasmic reticulum), cresyl violet can be used to stain neurons in the brain blue. Cryosections were stained for 2 min. in Cresyl violet staining solution (see I.2.(g)) and washed in ddH_20. After dehydration in an increasing alcohol series and toluene, slides were mounted with DePeX mounting medium.

B.5.2.4. X-gal (5-bromo-4-chloro-3-indolyl-β-D-galactopyranoside) staining

X-gal staining was used to analyse and confirm the recombination pattern of the Nes-Cre transgenic mice. Therefore, the Nes-Cre mouse line was crossed to a Rosa26 Cre reporter mouse strain (R26R) (Soriano, 1999) and the resulting offspring expressed β-galactosidase upon Cre-mediated recombination of a lacZ reporter gene. Recombination events can be visualised by a β-gal activity assay, in which X-gal, a chromogenic substrate of β-galactosidase, is processed by the enzyme resulting in a blue precipitate. For X-gal staining, mice were euthanised with diethyl ether, tissues of interest were rapidly dissected and fixed in Cell fix for 30-60 min. Tissues were incubated in X-gal staining solution (see I.2.(h)) overnight at RT. Subsequently, tissues were washed at least twice for 1 h in PBS before pictures of the whole organs were taken. Afterwards, tissues were further processed for paraffin sectioning as described (see B.5.2.1).

B.5.2.5. Oil Red O staining

Oil Red O, a fat soluble dye, is used to stain neutral triglycerides and lipids on frozen sections. Oil Red O staining can thus reveal differences in the cholesterol storage capacities of adrenal glands. This is a helpful tool in assessing deficits in steroidogenesis since cholesterol esters stored in the cytoplasm of steroidogenic cells serve as the primary source for steroidogenesis (Bisgaier et al., 1985). Cryosections were obtained as described (see B.5.2.1).

Oil Red O staining

- Incubate slides in 100% propylene glycol for 5 min.
- Stain slides in pre-warmed Oil Red O solution (see I.2.(i)) for 10 min. at 57-60 °C
- Differentiate slides in 85% propylene glycol for 5 min.
- Dip slides several times in two changes of ddH_2O
- Counterstain slides with Mayer's hemalaun solution (#T865.1, *Roth*)
- Wash in running tap water for 3-5 min.
- Wash in ddH_2O
- Mount slides with Aquatex® (*Merck*)

B.5.2.6. Immunohistochemistry

To show the expression and localisation of specific proteins in tissue sections, immunohistochemistry and immunofluorescence (see B.5.2.7) were used. For immunohistochemistry, deparaffinised and rehydrated 10 µm sections of tissues were first treated with citrate buffer for antigen retrieval and afterwards incubated with a primary antibody against the protein of interest. An indirect method was used for the visualisation of the antigen-antibody immunoreactivity. The signal of the primary antibody was amplified by using a biotinylated secondary antibody against the host species of the primary antibody and a preformed complex of avidin and a biotinylated enzyme (in this case: horseradish peroxidase, HRP) (VECTASTAIN® Elite ABC Kit, *Vectorlabs*). Visualisation of the signal was achieved by adding 3,3'-diaminobenzidine (DAB), a chromogenic enzyme substrate that is converted by HRP to an insoluble brown dye. Alternatively, in tissues with high endogenous peroxidase activity or for double-stainings, alkaline phosphatase was used for visualisation of the immunoreactive signal (VECTASTAIN® Standard ABC-AP Kit, *Vectorlabs*). In those cases the Vector blue alkaline phosphatase substrate kit (*Vectorlabs*) was used as chromogenic substrate resulting in a blue staining. When a monoclonal mouse antibody was used as primary antibody, unspecific binding sites were blocked with the Vector Mouse on Mouse Kit (M.O.M.™ Kit , *Vectorlabs*) instead of serum in TBS-T.

Immunohistochemical staining (see I.2.(j)):

- Following rehydration, wash slides in PBS for 5 min. at RT
- Incubate slides for 20 min. at RT in peroxidase blocking solution to destroy endogenous peroxidase activity
- Wash slides in PBS for 3 min.
- Antigen retrieval:
  - Incubate slides in citrate buffer for 15 min. at RT
  - Heat in a microwave oven (600 W) until buffer starts boiling
  - Let slides cool down in TBS-T for 10 min.
- Blocking of unspecific binding sites:
  - Block sections with 10% serum in TBS-T for 2 h at RT (source of serum depends on the host species of the secondary antibody; in most cases: normal goat serum)
- Incubate slides with primary antibody dilution in 5% serum-TBS-T overnight at 4 °C (I.4)
- Wash slides in TBS-T for 3 x 10 min.
- Add biotinylated secondary antibody dilution (1:200 in 5% serum-TBS-T) and incubate for 1 h at RT
- Prepare ABC reagent and incubate in the dark for 30 min.
- Wash slides in TBS-T for 3 x 10 min.
- Incubate slides with pre-formed ABC complex for 45 min. in the dark
- Wash slides in TBS-T for 3 x 10 min.
- Incubate slides with DAB staining solution until a brown staining gets visible (check staining under a microscope to avoid too intense background staining)
- Wash slides in PBS
- Counterstain sections with Hoechst 33258 (stock diluted 1:1000 in PBS; *Sigma*) for 15 min. at RT in the dark
- Wash slides in PBS for 5 min.
- Wash slides in ddH_20 for 5 min.
- Mount sections with Aquatex® (*Merck*) or Shandon Immu-Mount (*Thermo Fisher Scientific*)

B.5.2.7. Immunofluorescence

Immunofluorescence uses fluorescent dyes coupled to antibodies (instead of enzymes as in immunohistochemical stainings) to visualise the distribution of an antigen in the cell or tissue. Immunofluorescent staining was used to gain more information about the cell types that expressed cGKI in the tissues of interest. For these co-localisation studies, 10 µm perfusion-fixed cryosections were incubated with primary antibodies. Secondary antibodies labeled with different fluorophores were used to visualise immunoreactivity. In those cases, in which primary and secondary antibodies were derived from different host species and no cross reaction was expected, co-localisation staining was performed in parallel. In the other cases, serial stainings

were performed with particular attention on the order of staining to avoid cross reactions between e.g. the second and the first secondary antibody. In the rare cases, in which both primary antibodies were derived in rabbit, additional blocking steps between first and second staining were performed with normal rabbit serum (5% in PBS) and Fab fragments.

Immunofluorescence staining (see I.2.(k)):

- Incubate slides in PBS for 5-10 min.
- Permeabilize sections by incubation with 0.5% Triton-X-100 (in PBS) for 10 min. at RT
- Wash slides in PBS for 5 min. at RT
- Blocking of unspecific binding sites:
  - Incubate in 4% serum-PBS (serum from the host species of the secondary antibody) for 30 min. or longer at RT
- Incubate sections with primary antibody dilution in reaction buffer (I.4) overnight at 4 °C
- Wash slides 3 x 15 min. in PBS
- Incubate sections with secondary antibody dilution in reaction buffer (1:500) and Hoechst 33258 at the same time (Hoechst stock solution diluted 1:1000 in the secondary antibody dilution) for 1 h at RT
- Wash slides 3 x 30 min. in PBS
- Mount sections with Shandon Immu-Mount (*Thermo Fisher Scientific*)

B.5.2.8. Morphometric analysis

To reveal morphological differences of the adrenal glands that could contribute to the phenotype of SM-Iβ rescues in steroidogenesis, 10 µm-thick HE-stained sections (B.5.2.2) of adrenal glands from female SM-Iβ rescue mice and gender- and litter-matched controls were analysed. For each animal, between 5-8 consecutive sections from the middle part of the left and right adrenal gland were photographed under a microscope (Axioskop 20, *Zeiss*) with a colour CCD progressive scan camera (Marlin F-046C, *Allied Vision Technologies GmbH*). Digital images were evaluated with the free software Image J. For each section, the area of the whole adrenal gland and the area of the medulla were measured by tracing the surrounding borders and calculating the corresponding areas with Image J in mm^2. The area of the cortex was then calculated by subtracting medullary area from adrenal gland area. For each individual animal, the mean over the consecutive sections was calculated, before the mean for SM-Iβ rescues and controls was calculated. The evaluation procedure was done blind, without knowledge of the genotype of the mice.

B.5.3. RIA, ELISA and HPLC

RIA (radioimmunoassay) and ELISA (enzyme-linked immunosorbent assay) are antibody-based detection assays, which were used in this project to quantify hormone (CORT) and cytokine (IL-6) levels in plasma and cell culture supernatants.

B.5.3.1. RIA

The commercially available ImmuChem™ double antibody corticosterone RIA (*MP Biomedicals)* was used to determine CORT concentrations in cell culture supernatants and in plasma samples of SM-Iβ rescue and cGKI brain-KO and corresponding controls. The test is based on the competition between the CORT in the sample and radioactively (iodine-125) labelled CORT for the limited binding sites of a specific antibody. After incubation with the competitive ^{125}-I CORT and a specific rabbit anti-CORT antibody for 2 h, the amount of ^{125}-I CORT was inversely proportional to the CORT that shall be quantified. The formed antigen-antibody complex is precipitated with a mixture of PEG (polyethylene glycol) and an excess of goat anti-rabbit IgGs. After a centrifugation step, the supernatant containing unbound antigen was aspirated, radioactivity in the precipitate was measured in a γ-counter (*Berthold Technologies*) and CORT concentrations in the sample were calculated by comparison with defined standards. The RIA was performed according to the manufacturers' instructions at the isotope lab of the University of Tuebingen. Plasma samples and cell culture supernatants were diluted 1:50 and 1:25 in steroid diluent. According to the manufacturer, the detection limit was at 7.7 ng/ml and the intra- and interassay coefficient of variation was 4.4% and 6.5%, respectively.
ACTH concentrations were determined in unextracted plasma samples with a commercially available immunoradiometric assay (IRMA) (*IDS Ltd, Boldon,Tyne and Wear, UK*). IRMA is a special type of RIA, in which the first antibody is brought onto a solid phase, e.g. coated on tubes or beads, and the secondary antibody is radioactively labelled. Sensitivity of the assay was at 5 pg/ml and intraassay variation <7%. All ACTH measurements were kindly conducted by our collaborator Prof. Michael J. Shipston (Centre for Integrative Physiology, University of Edinburgh, Edinburgh EH8 9 XD, Scotland, UK).

B.5.3.2. ELISA

For the determination of IL-6 in plasma and cell culture supernatants the commercially available Quantikine® mouse IL-6 immunoassay (*R&D Systems*) was used. In this sandwich ELISA a specific monoclonal anti-IL-6 antibody has been pre-coated onto a 96-well plate. IL-6 present in the samples was captured by the immobilized antibody, and a second polyclonal IL-6 antibody conjugated to HRP was added to the antigen-antibody complex. Washing steps removed any unbound HRP-coupled antibodies before a chromogen (3,3',5,5'-tetramethylbenzidine) was

added together with hydrogen peroxide. This chromogen was converted by HRP to a blue product, and the reaction was stopped by adding hydrochloric acid solution turning the product yellow. The intensity of the colour is proportional to the amount of IL-6 in the sample and was measured with the Multiskan EX Microplate Photometer (*Thermo Fisher Scientific*) at a wavelength of 450 nm (the correction wavelength was set at 550 nm). Concentration of IL-6 was calculated by comparison with a standard curve. The ELISA was performed according to the manufacturers' instructions. Plasma samples as well as cell culture supernatants were measured undiluted. Detection limit was at 7.8 pg/ml and the intra- and interassay coefficient of variation was 4% and 7.5%, respectively.

B.5.3.3. HPLC

High-performance liquid chromatography (HPLC) was used to determine catecholamine concentrations in plasma samples of cGKI-deficient mouse lines and corresponding controls. HPLC is a liquid chromatographic method that can be used to separate, identify and quantify substances (analytes) in a mixture of compounds. A stationary phase (in this case: a reversed-phase C18 column, nonpolar) is combined with a mobile phase that is moved through the column with the help of a pump (flow rate 0.8 ml/min). Depending on the strength of the interaction with the column, analytes have varying characteristic retention times. Analytes were quantified with an L 3500 eletrochemical detector (*Recipe*; potential of +500 mV). As internal standard DHBA (3,4-Dihydroxybenzylamine) was used. All HPLC measurements were kindly performed by S. Hasanovic from the Central Laboratory (Department of Internal Medicine IV, Clinical Chemistry, Tuebingen). A commercially available set-up was used (Chromsystems).

B.5.4. Semi-quantitative RT-PCR

A variant of the PCR (B.2.2) is the RT-PCR (reverse transcription polymerase chain reaction), that is used to reverse transcribe mRNA into cDNA using RNA-dependent DNA polymerases (reverse transcriptases). Following the transcription step, the cDNA is then amplified using PCR and can be analysed after separation in 1-2% agarose gels providing good information on mRNA expression levels. For a semi-quantitative analysis of mRNA levels, a "housekeeping" gene (a gene expressed in all cells at relatively constant levels) was co-amplified in the same reaction as the gene to be analysed. HPRT (hypoxanthine-guanine-phosphoribosyl-transferase) or GAPDH (glyceraldehyde 3-phosphate dehydrogenase) were used as internal standards depending on the amplicon size and primer annealing temperature of the gene of interest.
For RNA isolation, three 4-months-old SM-Iβ rescue mice (two females, one male) and three litter-matched controls (two females, one male) were deeply anaesthetised with Forane® (Isoflurane, *Baxter*), and the tissues of interest were rapidly excised. Liver lobes were weighed and directly snap frozen in liquid nitrogen, while adrenal glands were first freed of surrounding fat

under a binocular. This step was performed as fast as possible in PBS on ice. Afterwards adrenal glands were also weighed and snap frozen in liquid nitrogen. Since RNA is extremely sensitive to degradation by RNAses, all steps for RNA isolation were performed rapidly under a cleaned hood and if possible on ice. Filtered pipette tips, RNAse-free H_2O (DEPC-treated H_2O) and either sterile, RNAse-free plasticware or glassware (baked for 4 h at 300 °C) were used. Total RNA from adrenal glands was isolated using the NucleoSpin® RNA XS Kit (*Macherey-Nagel*) following the manufacturers' instructions. Homogenisation was performed with the FastPrep®-24 instrument (*MP biomedicals).* RNA from liver lobes was isolated with peqGOLD RNAPure™ (containing a mixture of phenol and guanidine isothiocyanate for cell lysis and inhibition of RNAses, *Peqlab*) according to the following protocol.

RNA isolation (from liver) (see I.2.(I)):

- Add 2 ml peqGOLD RNAPure™ (*Peqlab*) to 100 mg tissue
- Homogenise in a FastPrep™ Lysing Matrix tube with the FastPrep®-24 instrument (*MP biomedicals*) (60 s; 6.5 m/s)
- Incubate 5 min. at RT
- Transfer lysate into a new 1.5 ml Eppendorf reaction tube
- Add 0.2 ml chloroform (per 1 ml RNAPure isolation reagent)
- Vortex for 15 s
- Incubate for 5 min. at 4 °C (on ice)
- Centrifuge at 12,000 x g for 15 min. at 4 °C
- Transfer the upper aqueous phase (containing the RNA) to a new 1.5 ml Eppendorf reaction tube. (Avoid transfer of traces of the lower organic phase and interphase containing proteins and DNA.)
- Add an equal volume of isopropanol to the transferred aqueous phase (~50% of initial volume)
- Mix well and allow to precipitate overnight at 4 °C
- Centrifuge at 12,000 x g for 15 min. at 4 °C (RNA precipitate should be visible as white-yellowish pellet at the bottom of the tube)
- Discard supernatant and wash pellet twice with 75% EtOH/H_20 by vortexing and subsequent centrifugation at 12,000 x g for 10 min at 4 °C
- Discard supernatant and let pellet air-dry for ~10 min.
- Solve pellet in RNAse free H_2O (60 µl for RNA from livers)

To remove DNA contaminations, samples are subsequently submitted to DNAse digestion. For the adrenal gland samples, the DNAse digestion was already performed on column at the end of the isolation procedure.

DNAse digestion (for liver samples):

- Mix 100 µl reaction buffer for rDNAse with 10 µl rDNAse (part of the NucleoSpin® RNA XS Kit, *Macherey-Nagel*)
- Add 1/10 volume to the eluted RNA (for liver: 6 µl)
- Incubate for 10 min. at 37 °C
- Add 0.1 volume of 3 M sodium acetate (pH 5.2) and 2.5 volumes of 100% EtOH to one volume of sample (for liver: 6.6 µl sodium acetate, 165 µl EtOH)
- Mix thoroughly and allow to precipitate overnight at −20 °C
- Centrifuge at 18,000 x g for 10 min. at 4 °C
- Discard supernatant
- Wash pellet twice in 75% EtOH/H_2O
- Air-dry for 10 min. at RT
- Resolve RNA-pellet in RNAse free H_2O (50 µl for RNA from livers)
- Measure RNA concentration with a Nanodrop® ND-1000 Spectrophotometer (*NanoDrop Technologies*) at a wavelength of 260 nm

The absorption maximum of nucleic acids is at OD_{260} and an OD_{260} = 1 corresponds to 40 µg/ml RNA. Therefore RNA concentration can be calculated by the following formula:

Concentration [µg/ml] = OD_{260} x 40 µg/ml x dilution factor

OD_{280} (the absorption maximum of proteins) and OD_{230} were also measured to assess the purity of the extracted RNA. Pure RNA has a 260/280 ratio of ~2. If the ratio is lower than ~1.8, the sample is probably contaminated with proteins. The 260/230 ratio should be around ~1.8 or higher. A lower ratio indicates contaminations with organic solvents.
The yield for two adrenal glands (one animal) was between 0.75-3 µg RNA, for liver the yield was around 2 µg RNA per 1 mg tissue. RNA concentration for livers was adjusted to 1 µg/µl with RNAse free H_2O and stored at −80 °C. Since the yield for adrenal glands was very low, only 150 ng to 500 ng RNA were reverse transcribed.

Mix for RT (cDNA synthesis):

RNA (0.5-1 µg/µl for liver)		1 µl
Random primer mix (60 µM, *NEB*)	6 µM	2 µl
10x PCR buffer		2 µl
ddH_2O		14 µl
M-MuLV reverse transcriptase (10,000 U, *NEB*)	500 U	1 µl

RT:

- Incubate at 75 °C for 5 min. to denature RNA
- Incubate at 75 °C (−0.5 °C/s) until 8 °C are reached (this allows primer annealing)
- Add 1 µl of M-MuLV reverse transcriptase
- Incubate at 25 °C for 5 min.
- Incubate at 42 °C for 60 min.
- Incubate at 80 °C for 5 min. to inactivate M-MuLV reverse transcriptase
- Fill volume to 50 µl with ddH_2O and store at −20 °C

To examine the gene expression levels of genes involved in steroidogenesis, published primers were used whenever possible. A list of the primer pairs and PCR conditions is attached in I.3.2. Published primers and newly designed primers had to fulfill certain criteria. To ensure that amplification is from the cDNA template and not from remaining contaminations of genomic DNA, primers were checked, if they were either intron flanking or bridging exon-exon junctions. It was also checked that both primer pairs had similar melting points and that they did not bind to many other sites in the mouse genome. Vector NTI® software (*LifeTechnologies*) was used for alignment and analysis of primers. All primers were ordered at MWG biotech and dissolved in ddH_20 to a stock concentration of 100 µM. A touchdown PCR protocol was used to reduce nonspecific background.

Standard RT-PCR protocol:

Initial denaturation	94 °C	3 min.	
Denaturation	94 °C	20s	10 x
Annealing (Touchdown)	66-59 °C (−0.5°C/cycle)	30 s	
Elongation	72 °C	1 min.	
Denaturation	94 °C	20s	31 x
Annealing	53-60 °C	30 s	
Elongation	72 °C	1 min.	
Final elongation	72 °C	5 min.	

Standard RT-PCR Mix:

cDNA	(~7.5-10 ng RNA)	1 µl
10x PCR buffer		2 µl
Primer A+ B (25 µM)	0.08-0.25 µM	0.2-0.6 µl
GAPDH or HPRT-Primer (25 µM)	0.08-0.25 µM	0.2-0.6 µl
ddH_2O		ad 60 µl

The PCR protocol was programmed to pause after certain cycles (26-41) in 3 cycle steps to allow taking an aliquot of 10 µl. With a starting volume of 60 µl it was possible to take 5 samples that were mixed immediately with 2 µl 6x DNA loading dye. Amplicons were separated with electrophoresis using 1-2% agarose gels (containing 300 ng/ml ethidium bromide) depending on the amplicon size. Photographs of the gels were taken under UV-light, saved digitally and analysed with the software ImageJ. Pixel intensity was measured for each band by framing it with a box and using the measurement option of the software. Background intensity was determined in an equally sized box and subtracted from the band intensity. Each band was normalized to the corresponding band of the housekeeping gene at the same cycle. Bands that were too weak or vague were not included in the analyses. Only bands in the linear range of amplification were analysed, and therefore bands of high cycles were excluded when saturation was obviously reached.

C Results

C.1. cGKI expression

Before investigating a potential role of cGKI in the stress response, expression patterns in tissues involved in HPA axis regulation were examined. Additionally, the expression pattern of cGKI in brown adipose tissue was analysed since this organ is involved in the thermoregulatory aspects of the cold stress response. Western blotting was used to detect general cGKI expression in tissue extracts of hypothalamus, pituitary gland and adrenal gland. Also brown and white adipose tissue was analysed with Western blotting. The general expression was confirmed and localised on the cellular level with immunohistochemistry. For both methods (Western blotting and immunohistochemistry) the cGKI common (DH) antibody (abbreviated as cGKIc) was used (Valtcheva et al., 2009). This polyclonal antiserum from rabbit was raised against the bovine cGKIα and affinity-purified using cGKIα coupled to BrCN-Sepharose. Both isoforms of cGKI, cGKIα and cGKIβ, are recognised by this antibody.

C.1.1. cGKI expression in tissues of the HPA axis

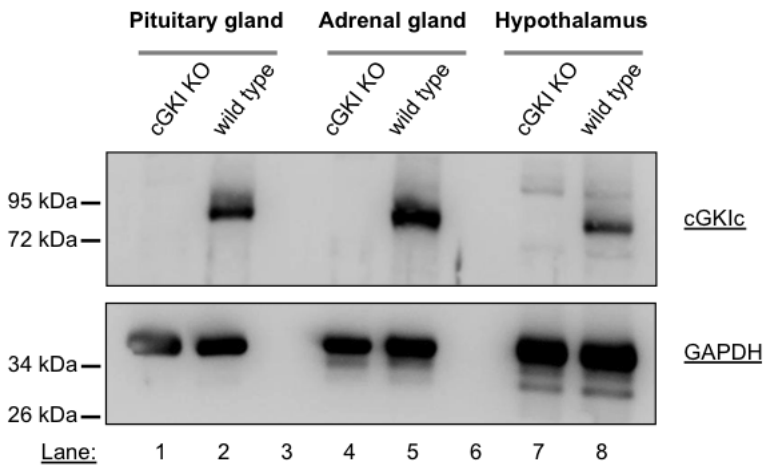

Figure 8: Western blot analysis of tissue extracts from cGKI KO and wild type mice. Tissues from three mice were pooled for pituitary and adrenal gland lysates. Using SDS-PAGE, 10 µg of protein was separated and blotted onto a PVDF membrane. cGKI (~78 kDa) and GAPDH (as loading control, ~37 kDa) were detected by overnight incubation at 4 °C with the corresponding antibodies. Immunoreactive signals were visualised with secondary antibodies coupled to horseradish peroxidase and subsequent enhanced chemiluminescence.

A signal at ~78 kDa was detected by Western blotting with the cGKIc antibody in tissue extracts of hypothalamus, pituitary and adrenal gland from wild type mice (**Figure 8**). This band size

corresponds to the molecular weight of cGKI, and the specificity of the signal was confirmed by its absence in tissue lysates of cGKI KO mice. Assuming GAPDH as a housekeeping gene and thus being expressed at constant levels in all tissues, the expression level of cGKI in the hypothalamic region seems to be lower as the expression levels in the pituitary and adrenal gland. Both pituitary and adrenal gland show almost equal expression levels of cGKI in the Western blot.

To gain further insight into the localisation of cGKI expression in the tissues of the HPA axis, immunohistochemical stainings were performed. In the hypothalamus, cGKI was detected in the paraventricular nucleus among other brain nuclei (**Figure 9**). In line with the relatively weak Western blot signal (**Figure 8**), cGKI expression in the PVN was restricted to a few neurons.

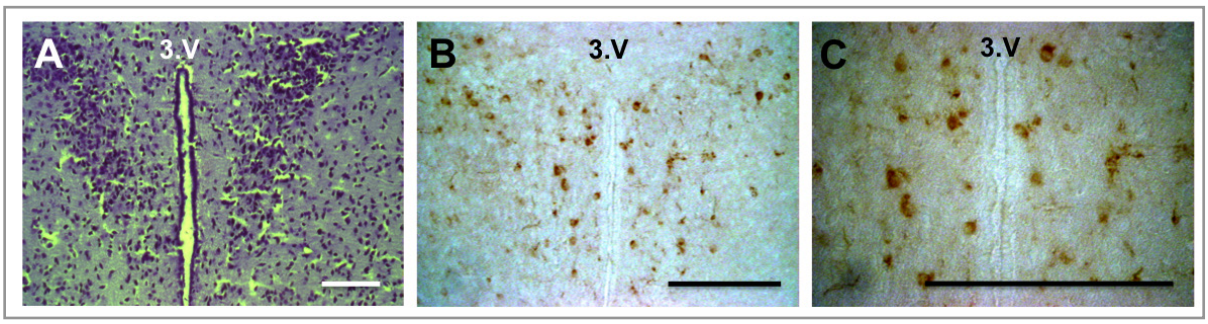

Figure 9: Representative sections of a Nissl staining (A) and an immunohistochemical staining for cGKI in the PVN of a 1-year-old wild type mouse (B,C). (A) Nissl staining identifies the two clusters of neurons of the PVN on both sides of the 3rd ventricle. (B) The diaminobenzidine method was used to visualise cGKI immunoreactive cells. Only few cells in the PVN are strongly cGKI-positive. (C) A higher magnification of (B) shows the morphology of cGKI-positive cells, which resemble magnocellular neurons. PVN, paraventricular nucleus; 3.V=3rd ventricle; scale bar=100 µm. (These stainings were kindly prepared and provided by Hui Wang.)

In the pituitary gland, immunohistochemical staining revealed abundant cGKI expression in the pars intermedia and in fewer scattered cells of the pars distalis (**Figure 10**). No cGKI-expressing cells were detected in the pars nervosa.

cGKI expression in the adrenal gland was mainly localised to the fibrous capsule surrounding the gland and to the vasculature. Especially large arteries underneath the capsule showed strong cGKI expression. Additionally, some cGKI-positive cells were scattered in the adrenal cortex between the CORT-producing cells of the zona fasciculata. At the transition from the cortical area to the medullary area of the gland also some cGKI-positive cells were observed as well as in the medulla, between the chromaffin cells, which were themselves cGKI-negative (**Figure 11**).

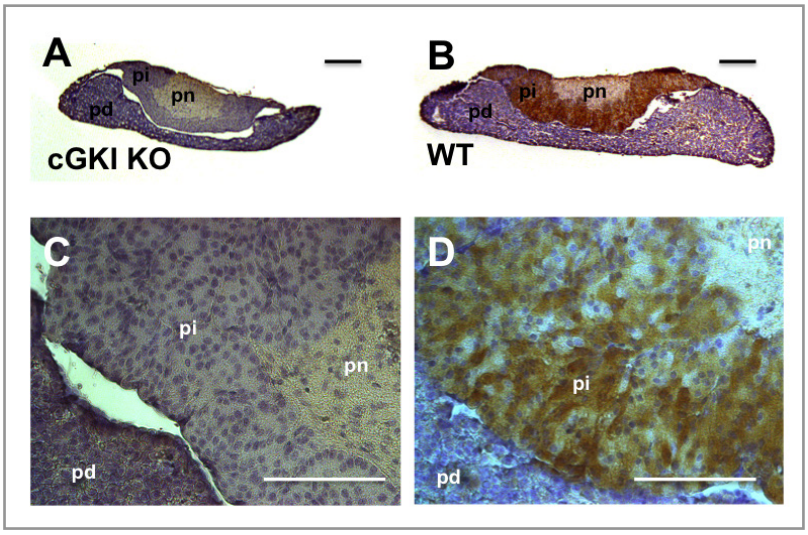

Figure 10: Hematoxylin staining (to visualise nuclei) combined with an immunostaining for cGKI (brown staining) in representative sections of pituitary glands from a 5-week-old cGKI KO mouse (A,C) and a wild type mouse at the same age (B,D). pn, pars nervosa; pi, pars intermedia; pd, pars distalis; WT, wild type; (A,B) scale bar=200 µm, (C,D) scale bar =100 µm.

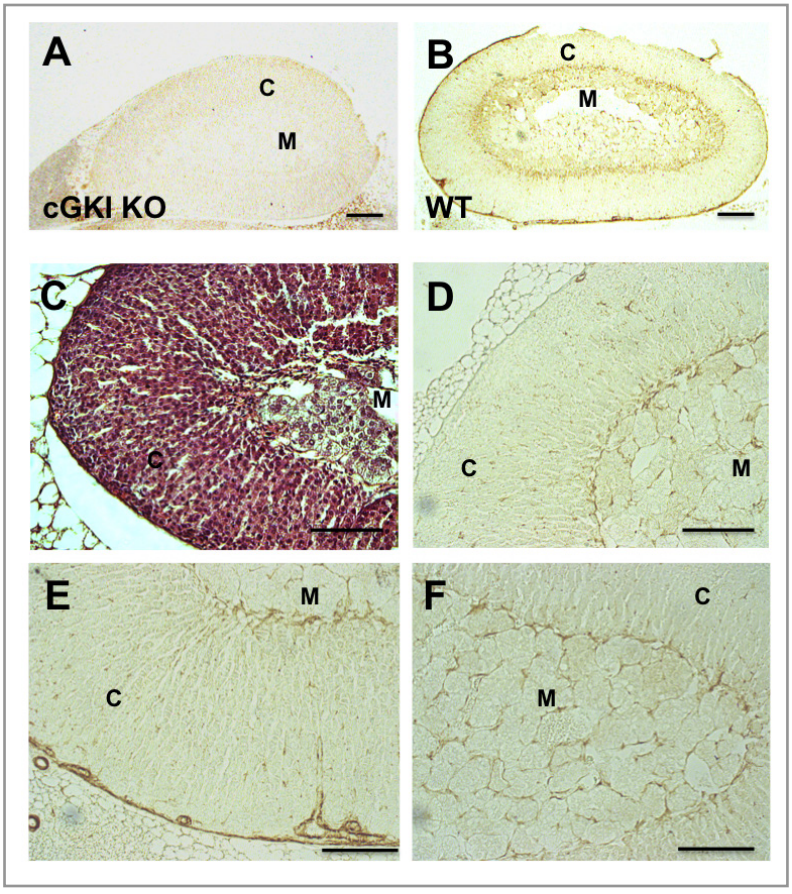

Figure 11: Immunostaining for cGKI in representative sections of 6-week-old GKI KO (A) and wild type (B,D,E,F) adrenal glands. (C) Higher magnification of an HE-staining of a wild type adrenal gland. M, medulla; (A,B) scale bar=200 µm.; (C-F) scale bar=100 µm.

C.1.2. cGKI expression in brown adipose tissue (BAT)

A signal at the height of the molecular weight of cGKI (~78 kDa) was detected by Western blotting with the cGKIc antibody in white and brown adipose tissue extracts from wild type mice (**Figure 12**). cGKI is thus expressed in both tissues, and the absence of the signal in tissue extracts of cGKI KO mice confirmed the specificity of the signal. To estimate the expression level of cGKI in these tissues, they were compared to tissue extracts of cerebelli from wild type and cGKI KO mice. In cerebellar Purkinje cells, cGKI is expressed at high levels and hence they provide a good possibility to assess the expression level of cGKI in other tissues (Lohmann et al., 1981). Despite the unequal amount of protein loaded (20 µg protein for the cerebellum, 8 µg protein for adipose tissues), cGKI seems to be strongly expressed in both types of adipose tissue; even stronger in brown adipose tissue since the signal strength of the cGKIc band in wild type WAT and BAT is comparable while less protein was loaded. In this Western blotting, β-actin was used as a control to recognise differences in protein loading.

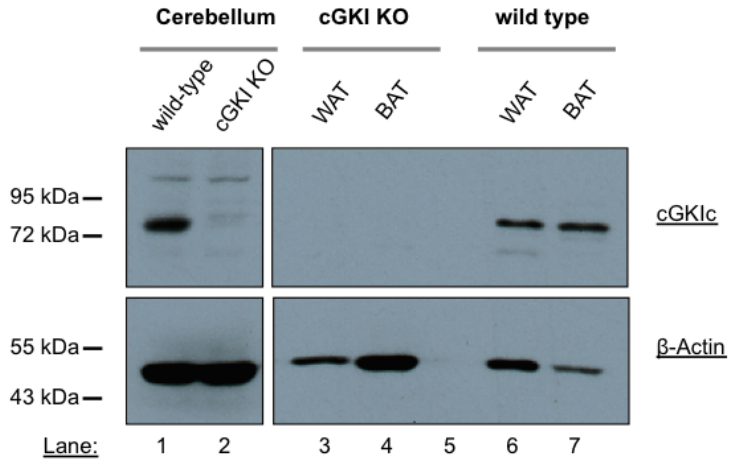

Figure 12: Western blot analysis of white and brown adipose tissue extracts from cGKI KO and wild type mice. Cerebellum tissue extract (20 µg protein loaded) was used for comparison of expression levels. cGKI is expressed in white and brown adipose tissue (8 µg protein loaded). The absence of an immunoreactive signal in cGKI KO tissue confirms the specificity of the signal. β-actin (~45 kDa) was used as a loading control. WAT, white adipose tissue; BAT, brown adipose tissue.

Immunohistochemistry was used to gain further insight into the localisation of cGKI in brown adipose tissue. BAT is well vascularised and therefore the strong expression level of cGKI could be due to cGKI expression in arteries and vessels. Indeed, expression in the vasculature was confirmed by immunohistological staining (**Figure 13**). But additional cGKI expression was observed in cells with a characteristic morphology. These cGKI-positive cells in BAT had round shaped cell bodies and long extensions spreading from the cell bodies.

Immunohistochemical staining of cGKI in WAT was inconsistent and due to a high background staining, it remained unclear whether cGKI expression in WAT is restricted to the vasculature or whether additional cell types in WAT express cGKI.

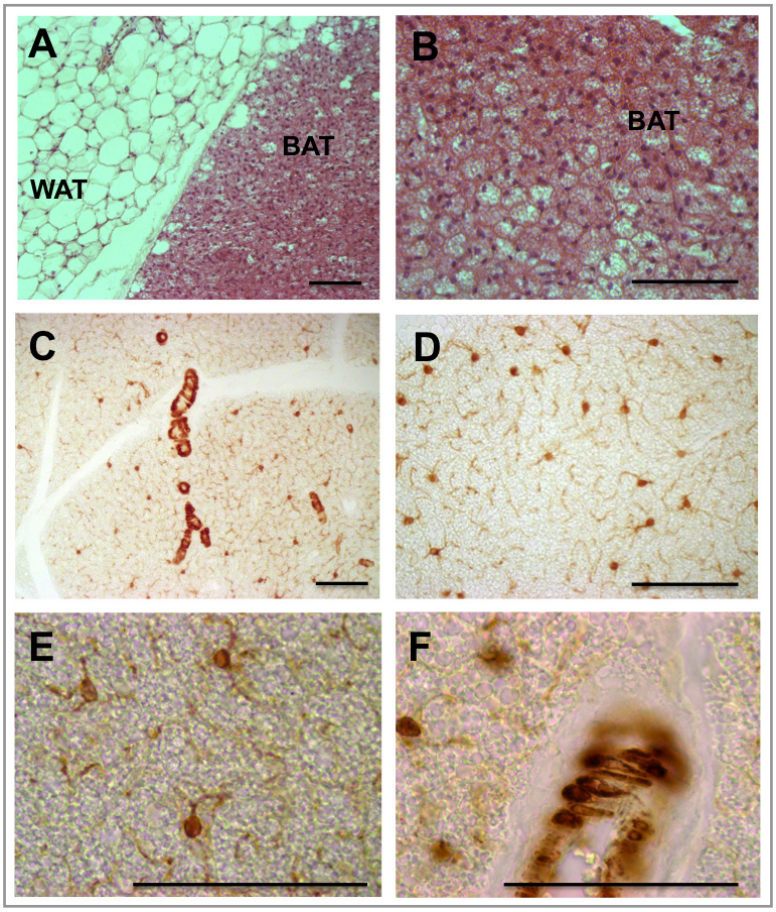

Figure 13: HE-stainings (A,B) and immunohistochemical stainings with an cGKIc antibody (C,D,E,F) in interscapular brown adipose tissue of a 6-month-old wild type mouse. (A) White fat is in close contact with brown fat in the interscapular region. A clear difference between the unilocular white adipocytes containing single lipid droplets and the multilocular brown adipocytes can be seen. (B) Higher magnification of interscapular brown adipose tissue. Each fat cell contains numerous lipid droplets. (C) cGKI immunoreactivity is localised in the vasculature and in characteristically shaped round-bodied cells with long branches. (D,E,F) In the higher magnifications the morphology of the cGKI-positive cells can be clearly seen. WAT, white adipose tissue; BAT, brown adipose tissue; scale bar=100 µm.

C.2. In vivo analysis in cGKI-deficient mouse lines

C.2.1. HPA axis

In order to determine the physiological significance of the abundant cGKI expression in tissues of the HPA axis, basal and stimulated plasma stress hormone levels were measured in different cGKI-deficient mouse lines.

C.2.1.1. Stress hormone and IL-6 levels

Basal plasma CORT and ACTH levels

Basal plasma CORT levels were determined in total cGKI KO and SM-Iβ rescue mice. Trunk blood was collected in the morning hours, when CORT levels are at a minimum. No difference between the plasma CORT levels in cGKI KO mice (214.03 ± 25.34 ng/ml) and wild type controls (229.99 ± 22.34 ng/ml) was observed (**Figure 14 A**). Also CORT levels in SM-Iβ rescue mice (118.12 ± 27.69 ng/ml) were indistinguishable from controls (136.73 ± 21.94 ng/ml) (**Figure 14 B**). In the plasma samples of SM-Iβ rescues, ACTH was additionally measured. Again, plasma ACTH concentrations in SM-Iβ rescues (430.14 ± 57.23 pg/ml) were similar to concentrations measured in the control group (405.04 ± 53.55 pg/ml) (**Figure 14 B**). Although basal CORT levels were almost equal between cGKI-deficient mouse mutants and corresponding controls, the levels between the cGKI-deficient mouse lines (cGKI KO mice vs. SM-Iβ rescues, **Figure 14 A** vs. **Figure 14 B**) were considerably different.

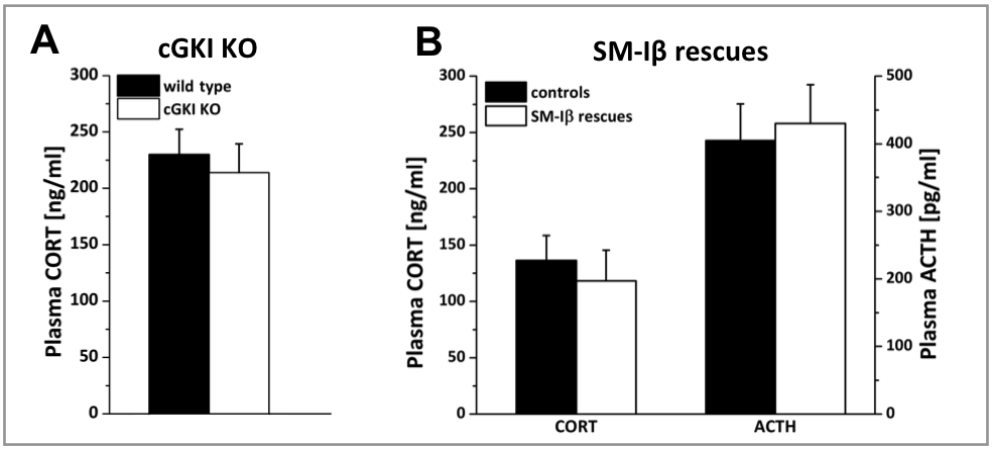

Figure 14: Basal CORT levels in cGKI-deficient mouse lines (open bars) compared to controls (black bars). Trunk blood was taken in the morning, and CORT levels were measured with a commercially available RIA. (A) Plasma CORT levels in cGKI KO mice (n=10; 4♂, 6♀) and litter-matched wild type controls (n=10; 5♂, 5♀). Mice were sacrificed at an age of 6-8 weeks. (B) Basal plasma CORT and ACTH levels in SM-Iβ rescues (n=7♀) compared to controls (n=9♀). Mice were decapitated at an age of 7-12 months.

Another group of SM-Iβ rescue mice (5-7 months old) was used to investigate CORT levels in the evening, when plasma CORT levels reach their maximum due to their circadian secretion pattern (**Figure 15 A**). Basal CORT levels in SM-Iβ rescues and litter-matched controls were again measured in the morning (2 h after lights on) and this time also in the evening (1 h before lights off). In this experiment, blood was taken via tail nick to make repetitive blood sampling in the same mouse possible. Again, morning levels did not differ between the genotypes (63.23 ± 10.18 ng/ml in SM-Iβ rescues vs. 63.74 ± 11.64 ng/ml in controls). However, plasma CORT levels taken in the evening were significantly lower (p=0.033) in SM-Iβ rescues (148.02 ± 17.02 ng/ml) compared to controls (217.88 ± 24.31 ng/ml) (**Figure 15 B**).

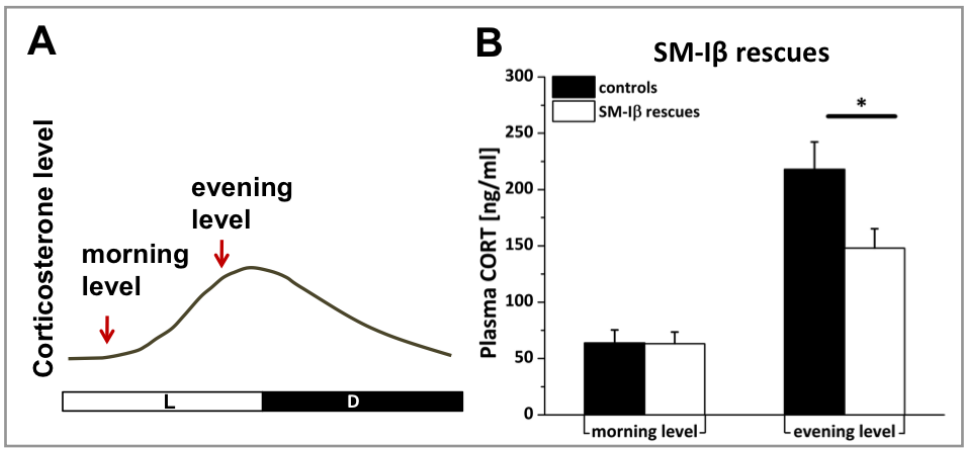

Figure 15: Basal plasma CORT levels in 5-7-month-old SM-Iβ rescue mice and litter-matched controls.
(A) Ultradian variation in CORT levels in nocturnal rodents. In the early morning hours plasma CORT concentrations are at their nadir and peak in the late afternoon shortly before the onset of the activity phase in mice. Red arrows mark the time of blood sampling by tail nick. (B) Unstimulated plasma CORT levels in the morning (2 h after lights on) and evening (1 h before lights off) in SM-Iβ rescues (open bars; n=11♀) compared to litter-matched controls (black bars; n=13♀). *, p<0.05.

Basal and stimulated plasma catecholamine levels

Not only CORT, but also catecholamines are released from the adrenal gland into the blood circulation in response to stress. It was long believed that the cortex of the adrenal gland (where CORT is produced) and the medulla (where catecholamines are produced) act completely independent of each other, but numerous studies have shown that there is a close bidirectional relationship between the two of them (Ehrhart-Bornstein et al., 1998). Therefore, catecholamine levels in cGKI-deficient mouse lines before and after exposure to restraint stress (10 min.) were measured (**Figure 16, Table 4**). Blood was collected via retro-orbital puncture in the morning. In total cGKI KO mice, adrenaline and noradrenaline levels were elevated in the basal and in the stimulated state (restraint) compared to wild type controls. For noradrenaline this difference reached significance in both states (**Figure 16 A**).
In cGKI brain-KO mice, the adrenaline values are difficult to interpret since only in a few mice adrenaline concentration were above the detection limit. Noradrenaline levels in cGKI brain KO

are extremely low when compared to the other cGKI-deficient mouse lines. Therefore, it is doubtful whether the restraint stress was successful and effectively stimulated the SNS. Nevertheless, cGKI brain-KO mice have higher noradrenaline levels compared to controls, but this difference was not statistically significant, probably due to the low animal number (**Figure 16 B**).

Adrenaline levels in SM-Iβ rescue mice were higher in both states, basal and after restraint. However, noradrenaline levels were lower in the basal state in SM-Iβ rescues than in controls. After stimulation, noradrenaline levels in the SM-Iβ rescue mice were higher than in controls. Again this difference did not reach significance, probably due to low animal numbers (**Figure 16 C**). Values for each group are listed in **Table 4**.

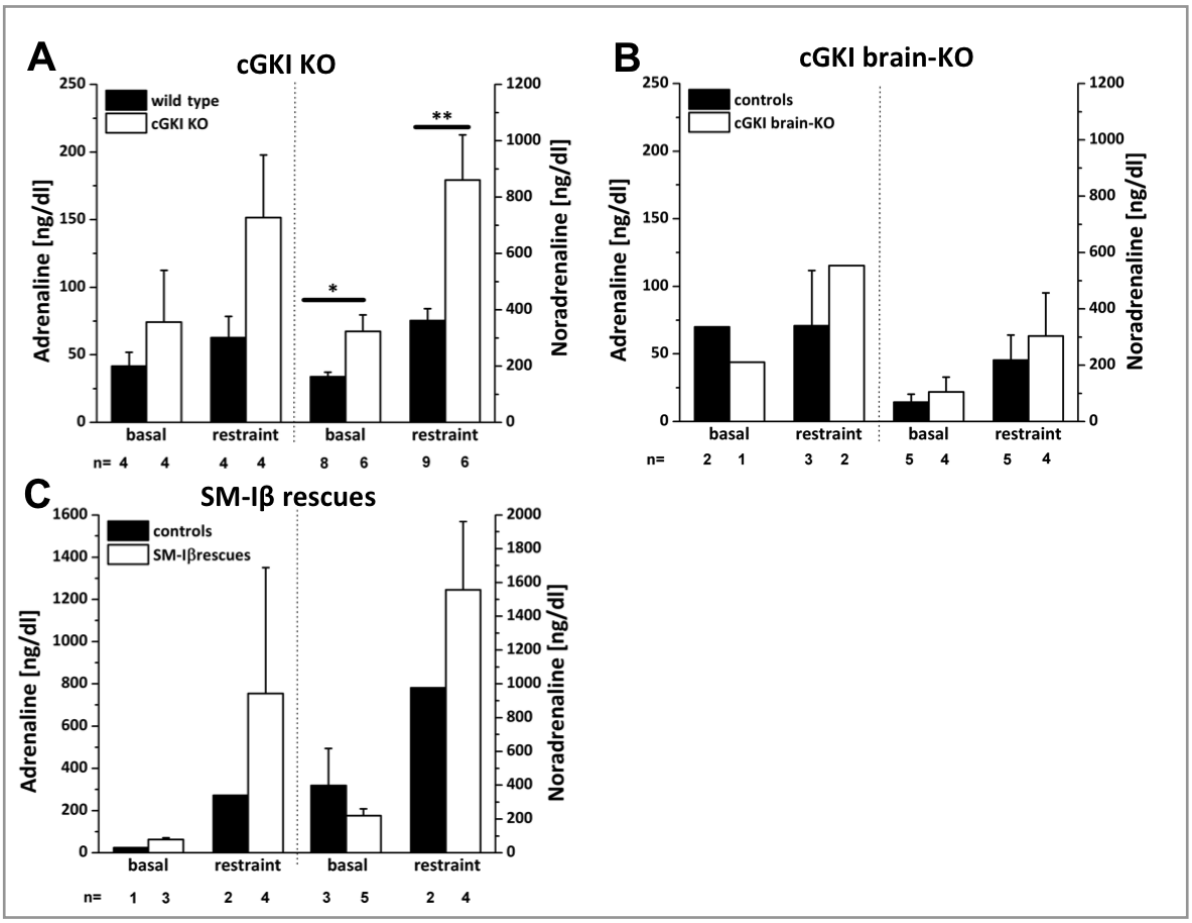

Figure 16: Catecholamine measurements in cGKI-deficient mouse lines before (basal) and after 10 min. restraint stress. Blood was collected in the morning via retro-orbital puncture. (A) cGKI KO mice (5-8 weeks old; open bars) compared to wild type controls (black bars). (B) Catecholamine levels in 8-12-month-old female brain-KO mice (open bars) compared to controls (black bars). (C) Adrenaline and noradrenaline levels have been determined in 2-3-month-old female SM-Iβ rescue mice. HPLC measurements were kindly performed by S. Hasanovic, Central laboratory, Tuebingen. *, p<0.05; **p<0.01.

Table 4: Catecholamine levels in cGKI-deficient mouse lines before and after 10 min. restraint. Significant differences are indicated by asterisks. *, p<0.05; **, p<0.01.

Mouse line	Adrenaline [ng/dl]		Noradrenaline [ng/dl]	
	basal	restraint	basal	restraint
cGKI KO	74.33 ± 38.34	151.43 ± 46.83	323.67 ± 58.36*	860.33 ± 160.96**
wild-type controls	41.58 ± 10.38	62.65 ± 15.8	163.09 ± 15.22	361.88 ± 41.71
cGKI brain-KO	44.0	115.25	104.75 ± 52.38	304.20 ± 152.10
controls	77.85	70.83 ± 40.90	69.00 ± 28.7	218.15 ± 89.06
SM-Iβ rescues	63.67 ± 7.84	754.00 ± 596.82	220.20 ± 40.22	1557.25 ± 404.50
controls	24.00	272.50	399.67 ± 217.80	978.50

Bassal plasma IL-6 levels

HPA axis activation can be influenced by cytokines and most of them have a stimulatory effect on the stress response system (Dunn, 2000). It was recently observed that SM-Iβ rescue mice have elevated plasma IL-6 levels with increasing age (Lutz et al., 2011). Therefore, IL-6 plasma levels were determined in an unstimulated group of SM-Iβ rescue mice having the same age (5-7 months) as the mice used in the *in vivo* HPA axis stimulation experiments. As expected, at this age SM-Iβ rescues had significantly elevated IL-6 levels (11.45 ± 1.58 pg/ml) compared to controls (1.68 ± 0.36 pg/ml) (**Figure 17**). Only 3 out of 15 SM-Iβ rescue females had low IL-6 levels at this age. The remaining 12 animals displayed moderately elevated IL-6 levels (ranging from 9.12 to 26.94 pg/ml).

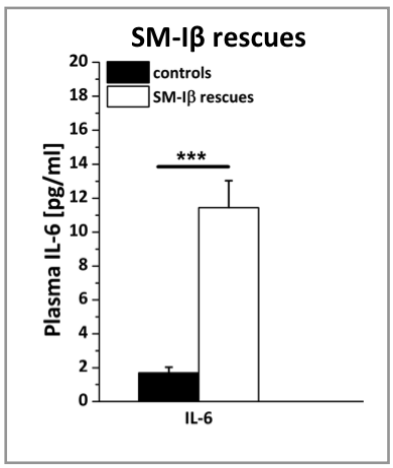

Figure 17: IL-6 levels in plasma samples of unstimulated SM-Iβ rescue mice. Blood was collected via decapitation in the morning. SM-Iβ rescues (n=15♀; 5-7 months old) had significantly higher basal IL-6 levels (open bar) than litter-matched controls (black bar; n=15♀; 5-7 months old). ***, p<0.001.

C.2.1.2. IL-1β stimulated CORT and ACTH levels

Interleukin-1β, a cytokine effectively stimulating the HPA axis (Besedovsky et al., 1986), was injected in two cGKI-deficient mouse lines to investigate the potential role of cGKI in the stress response. IL-1β injections in control and cGKI brain-KO mice (2-6 months old), which lack cGKI in the central and peripheral nervous system, resulted in the expected elevations in plasma ACTH (**Figure 18 A**) and plasma CORT concentrations (**Figure 18 B**) compared to vehicle-injected control groups. However, no significant difference between cGKI brain-KO and control mice was observed (see also **Table 5**).

Control and SM-Iβ rescue mice (4-6 months old), which lack cGKI in all tissues of the HPA axis except in smooth muscle cells, showed also the expected elevations in plasma ACTH levels after injection of IL-1β (**Figure 18 C**). However, SM-Iβ rescue mice had significantly higher ACTH levels than controls, whereas after vehicle injection no difference in plasma ACTH levels was observed between the genotypes. Based on the higher stress-induced ACTH levels in SM-Iβ rescue mice, one would expect higher CORT levels as well. Interestingly, the contrary was observed. IL-1β-injected SM-Iβ rescue mice had significantly lower plasma CORT concentrations than control mice after vehicle and IL-1β injection (**Figure 18 D**, see also **Table 5**). Hence, already the vehicle injection seemed to cause a slight activation of the HPA axis, which becomes obvious when the levels are compared to the basal CORT levels in SM-Iβ rescue mice (**see also Figure 15 B**).

Table 5: Plasma ACTH and CORT concentrations after vehicle and IL-1β stimulation. For statistical analysis a two-way ANOVA was performed. *, p<0.05; **, p<0.01; ***, p<0.001.

Mouse line	ACTH [pg/ml]		CORT [ng/ml]	
	vehicle-injected	IL-1β injected	vehicle-injected	IL-1β injected
cGKI brain-KO	121.93 ± 34.43	404.96 ± 52.99	80.47 ± 30.33	454.43 ± 18.24
controls	80.05 ± 15.80	332.14 ± 28.66	101.61 ± 12.91	441.94 ± 33.25
SM-Iβ rescues	189.56 ± 32.88	481.38 ± 29.74**	120.10 ± 13.42*	480.62 ± 27.87***
controls	227.98 ± 31.30	340.99 ± 30.12	189.96 ± 11.48	615.21 ± 20.46

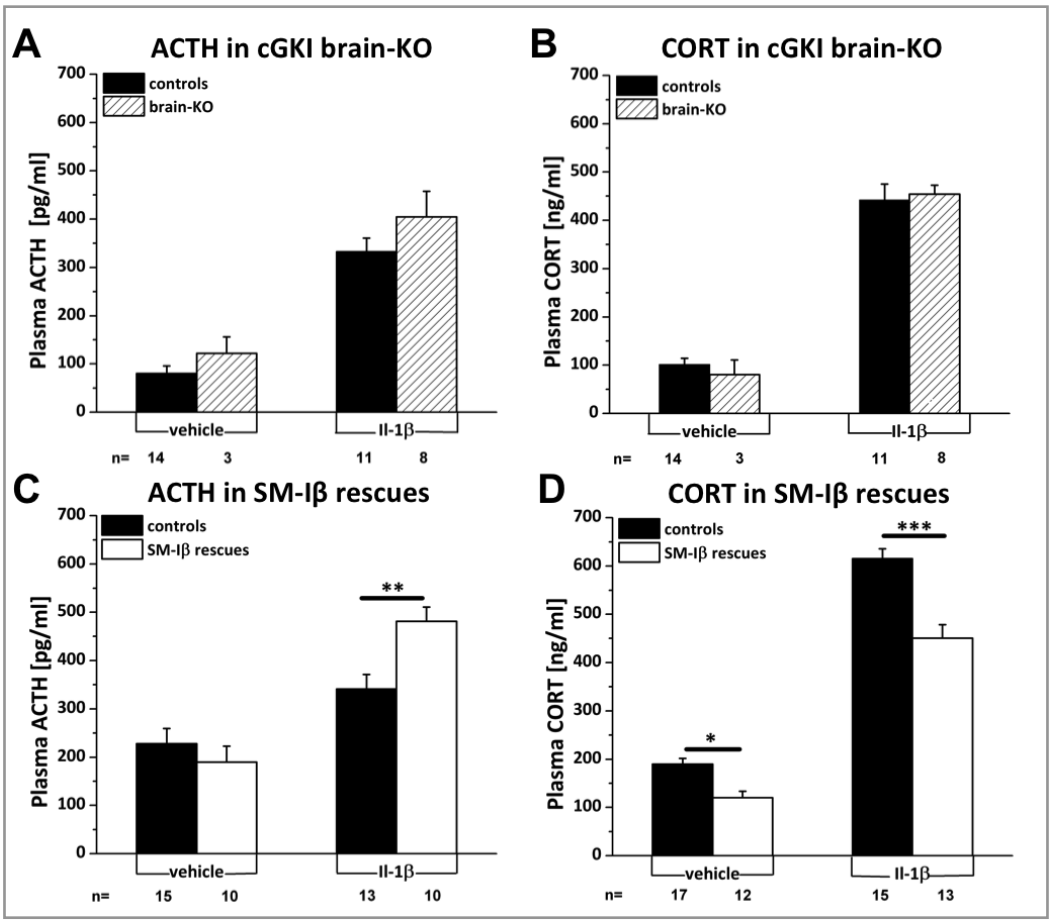

Figure 18: Effect of i.p. injections of 100 ng IL-1β on stress hormone levels in female cGKI brain-KO (A,B) and SM-Iβ rescue mice (C,D). Trunk blood was collected 2 h after injection. IL-1β stimulated ACTH (A) and CORT (B) levels in cGKI brain-KO mice (2-6 months old; striped bars) and litter-matched controls (black bars), compared to a vehicle-injected control group. (C) ACTH levels in unstimulated (vehicle) and stimulated (IL-1β) SM-Iβ rescues (4-6 months old; open bars) compared to litter-matched controls (black bars). (D) CORT levels in SM-Iβ rescues compared to controls. For statistical analysis a two-way ANOVA followed by Bonferroni's multiple comparison was performed. *, p<0.05; **,p<0.01;, p<0.001.***

C.2.1.3. Restraint stress stimulated ACTH, CORT and IL-6 levels

Restraint stress was applied as another stressor type. The aim of the experiment was to figure out whether the observed phenotype of attenuated CORT secretion in response to an immunological stressor in SM-Iβ rescues holds also true for another stressor type. A 30 min. restraint stress led to the expected elevated plasma CORT levels in 7-month-old control and SM-Iβ rescue mice, but CORT levels were significantly lower in the SM-Iβ rescue mice (**Figure 19 A**). High plasma IL-6 levels were expected in SM-Iβ rescue mice at this age as it has been shown in a previous study (Lutz et al., 2011). And indeed, plasma IL-6 levels were elevated in this group of mice compared to controls (**Figure 19 A**). To exclude the possibility that the higher plasma IL-6 levels contributed or even caused the altered stress response in SM-Iβ rescue mice,

a younger group of mice (3 months old) selected for normal plasma IL-6 levels was also tested in the restraint stress paradigm. Again CORT levels after 30 min. restraint stress were attenuated in the SM-Iβ rescues compared to controls (**Figure 19 C**). These results indicate that the observed phenotype in SM-Iβ rescues is independent of the type of stressor and independent of the elevated plasma IL-6 levels in older mice. Additionally, plasma ACTH levels were determined in both age-groups (**Figure 19 B, D**). Mice of the 7-months-old group had a tendency to higher plasma ACTH levels compared to controls (p=0.056) (**Figure 19 B**). Values of the restraint stress experiment are given in **Table 6**.

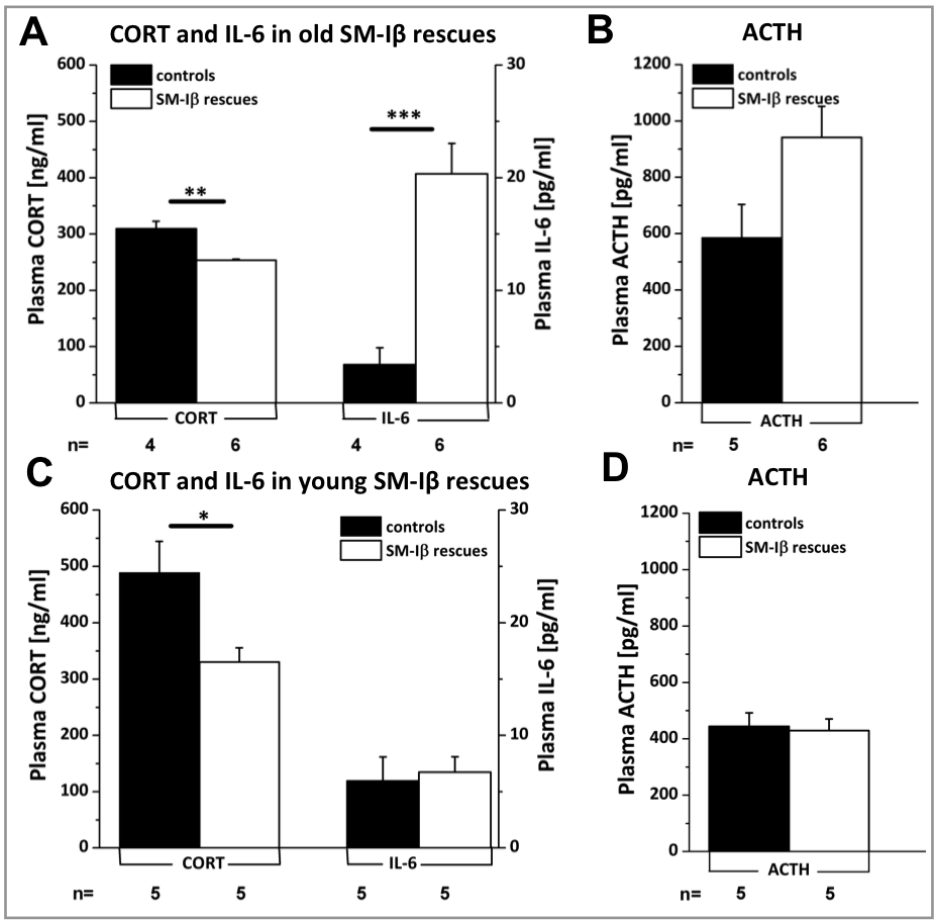

Figure 19: Effect of 30 min. restraint stress on plasma ACTH (B,D), CORT and IL-6 levels (A,C). Plasma of SM-Iβ rescue mice (open bars) and controls (black bars) was assayed for CORT and IL-6. Mice were grouped according to their age and plasma IL-6 levels. (A) "old mice" (7 months old) with high (>15 pg/ml) IL-6 levels and (C) "young mice" (3 months old) with low (<15 pg/ml) IL-6 levels. For statistical analysis a student's t-test was performed. *, p<0.05; **, p<0.01; ***, p<0.001.

Table 6: ACTH, CORT and IL-6 levels after 30 min. restraint stress. A student's t-test was performed for statistical analysis and significant differences are indicated by asterisks. *, p<0.05; **, p<0.01; ***,p<0.001.

Mouse line	age	ACTH [pg/ml]	CORT [ng/ml]	IL-6 [pg/ml]
SM-Iβ rescues	young	429.54 ± 40.72	330.4 ± 24.96*	6.73 ±1.38
controls	young	444.28 ± 47.75	489.0 ± 55.24	5.97 ± 2.1
SM-Iβ rescues	old	941.58 ± 111.08	253.29 ± 2.17**	20.36 ± 2.69***
controls	old	585.78 ± 118.08	309.42 ± 13.41	3.42 ± 1.49

C.2.1.4. ACTH-induced CORT levels

An *in vivo* ACTH stimulation test was performed to investigate, if the observed phenotype in SM-Iβ rescue mice is due to an impaired responsiveness of the adrenal glands to ACTH. Two different doses of $ACTH_{1-24}$ were i.p. injected in SM-Iβ rescue mice and litter-matched controls. The first group (7-month-old females) received a low dose (10 µg/kg) of $ACTH_{1-24}$, the second group (3-month-old females) received an intermediate dose (100 µg/kg) of $ACTH_{1-24}$. Plasma CORT levels were determined in trunk blood collected 1 h after injection.

SM-Iβ rescue mice injected with the low dose of ACTH displayed significantly lower levels of plasma CORT (**Figure 20 A**) compared to controls. However, CORT levels in the vehicle injected mutant mice were even higher than in the ACTH injected group suggesting that the low dose of ACTH is not sufficient to induce a robust CORT increase. In line with this, CORT levels in control mice were also not elevated in the ACTH-injected group compared to the vehicle-injected control mice (**Figure 20 A**).

When the intermediate dose of $ACTH_{1-24}$ (100 µg/kg) was used, CORT levels were significantly increased in ACTH-injected SM-Iβ rescue mice compared to vehicle-injected SM-Iβ rescue mice (**Figure 20 B**). CORT levels in ACTH-injected controls were also elevated compared to vehicle-injected control mice, but the difference was not statistically significant (p=0.08) (**Figure 20 B**). This is probably due to the low number of vehicle-injected mice (n=2 controls). However, no difference was observed between the genotypes.

Since CORT levels were already quite elevated after the vehicle-injection compared to basal CORT levels (compare **Figure 20** to **Figure 14 B**) and stimulation with the intermediate dose of $ACTH_{1-24}$ (100 µg/kg) in younger animals (3 months old) resulted in only slightly elevated CORT levels, experimental problems can not be excluded. Therefore, it might be worth repeating the experiment with a higher dose of $ACTH_{1-24}$ in older (~6 months old) mice.

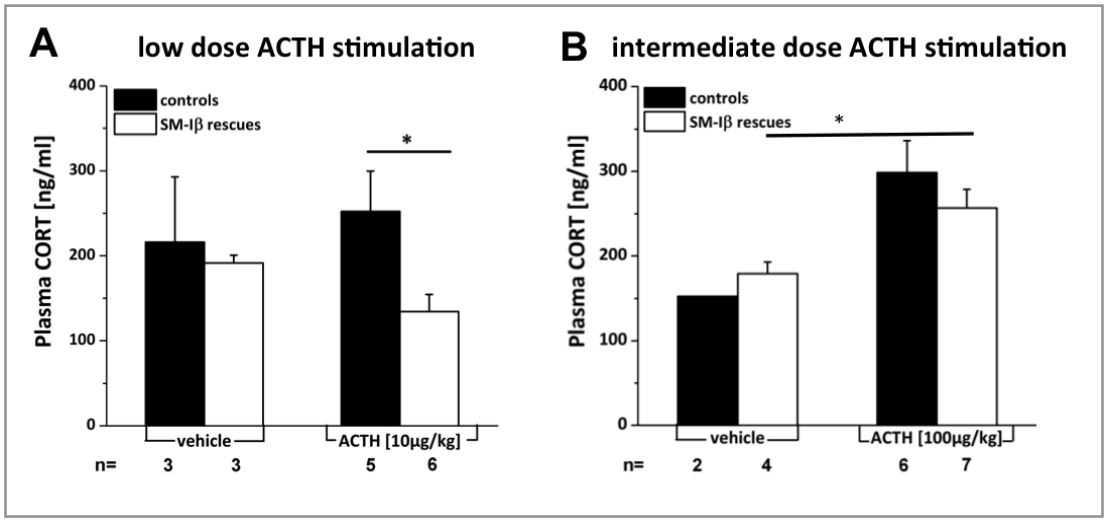

Figure 20: ACTH stimulation test for adrenal insufficiency in SM-Iβ rescue mice (open bars) and litter-matched controls (black bars). (A) A low dose of $ACTH_{1-24}$ (10 µg/kg) was injected i.p. in 7-month-old mice, and trunk blood was collected 1 h after injection. A vehicle injected group served as control. CORT levels were determined in the plasma. (B) Another group of SM-Iβ rescue mice (3 months old) was injected with an intermediate dose of $ACTH_{1-24}$ (100 µg/kg). Student's t-test was performed for statistical analysis. *, p<0.05.

C.2.1.5. Behaviour in the forced swim test (FST)

Behaviour in the forced swim test was analysed in SM-Iβ rescue mice to investigate if the reduced CORT levels in this mouse mutant had an influence on immobility behavior in the test. Behavioural immobility in this test seems to be associated with the absence or presence of CORT. It was shown that adrenalectomy (Jefferys et al., 1983), inhibition of CORT synthesis (Baez and Volosin, 1994) and antisense treatment of glucocorticoid receptors (GR) (Korte et al., 1996) lead to a decrease of the time spent in an immobile or floating posture.

Consistent with lower stress-induced CORT levels, SM-Iβ rescue mice showed a tendency (p=0.096) towards decreased immobility time (floating behavior) in the FST during the test (**Figure 21 A**, see also **Table 7**). Also in the re-test, 24 h later (**Figure 21 B**), floating behaviour was reduced compared to controls (p=0.063), while struggling behaviour was significantly increased. In accordance with the reduced floating times, the floating latency was also significantly increased during the test in SM-Iβ rescue mice (**Figure 21 C**). The reduced immobility time in SM-Iβ rescue mice suggests a rather "depression-resistant" behaviour, which is in line with their reduced CORT levels.

Table 7: Time spent in the different behavioural states during test and re-test (24 h later) of the FST. Student's t-test was used for statistical analysis. *, p<0.05.

Mouse line	test/re-test	Struggling [s]	Swimming [s]	Floating [s]	Latency [s]
SM-Iβ rescues	test	54.13 ± 7.39	230.3 ± 21.07	75.58 ±19.39	121.76 ±13.85*
controls	test	60.5 ± 10.71	176.27 ± 16.27	122.22 ± 17.63	75.95 ± 13.59
SM-Iβ rescues	re-test	73.38 ± 11.02	143.23 ± 19.43	143.39 ± 27.25	14.26 ± 2.74
controls	re-test	36.07 ± 10.75	120.35 ± 17.38	203.32 ± 16.51	9.39 ± 1.99

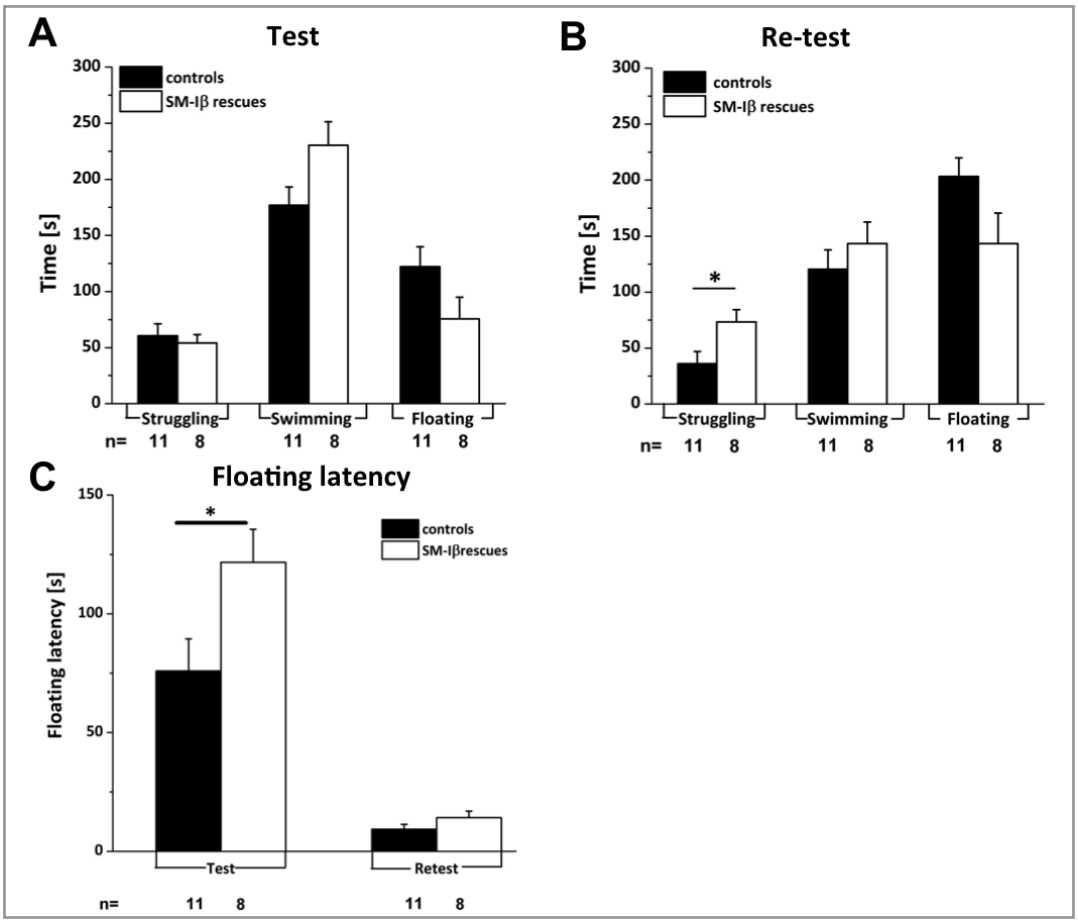

Figure 21: Stress coping behaviour of 3-4-month-old female SM-Iβ rescue mice (open bars) was assessed in the forced swim test (FST) and compared to litter-matched controls (black bars). Mice were placed in a cylinder filled with 23 °C-warm water for 6 min. and behaviour was evaluated. Three different behaviours were distinguished: struggling, swimming and floating. (A) Behaviour during the test, which was performed in the early morning hours. (B) Behaviour in the re-test, performed 24 h later. (C) Floating latency was defined as the time until the onset of the first characteristic immobile posture (floating). Statistical analysis was performed with Student's t-test. *, p<0.05.

C.2.2. BAT

The abundant expression of cGKI in brown adipose tissue (C.1.2) suggests a function for cGKI in thermoregulation. Therefore, core body temperature was measured under normal conditions and during cold- and fasting stress. All temperature measurements were performed with the DSI telemetry system (B.3.5).

C.2.2.1. Core body temperature under normal conditions

Core body temperature and activity in female SM-Iα (n=2) and SM-Iβ rescue mice (n=7) (3-6 months old) and female cGKI brain-KO mice (6-10 month old) were measured for 7 days under constant conditions (LD 12:12; lights on at 0500 h; 21°C) and averaged as a 24 h baseline with 3 h bins (**Figure 22** and **Figure 23**, see also I.5.1.1).
Locomotor activity followed a circadian rhythm in rescue mice and controls with increased activity during the dark phase. No differences in activity were observed between the genotypes. Body temperature in rescue mice and controls also followed a circadian rhythm with an increase during the activity phase at night. But core body temperature in rescue mice was about 0.5 °C below the temperature of controls. During the light phase, which corresponds to the resting phase in mice, the temperature difference reached statistical significance (**Figure 22**).
The circadian rhythm of locomotor activity recorded in cGKI brain-KO mice and controls was even more pronounced than in the SM-Iβ rescue mice, probably due to the different genetic background (C57BL/6 vs. 129/Sv). cGKI brain-KO mice had significantly higher activity levels than controls in the dark phase, which corresponds to the active phase in mice. In contrast, no differences were observed in the core body temperature between the genotypes (**Figure 23**).

C.2.2.2.Core body temperature under cold stress

The same groups of mice were exposed to 4 °C for 4-6 h, and changes in temperature and activity were analysed. In SM-Iα and SM-Iβ rescue mice and controls core body temperature decreased slightly after starting the cold challenge. Locomotor activity peaked twice, at the beginning of the cold stress and at the beginning of the subjective night. No differences between the genotypes were found in core body temperature and activity (**Figure 24**, see also I.5.1.2). In cGKI brain-KO mice core body temperature decreased more rapidly during cold exposure than in controls, being significantly lower after 4 h of cold stress. Activity was similar in both genotypes during the cold exposure (**Figure 25**, see also I.5.1.2).

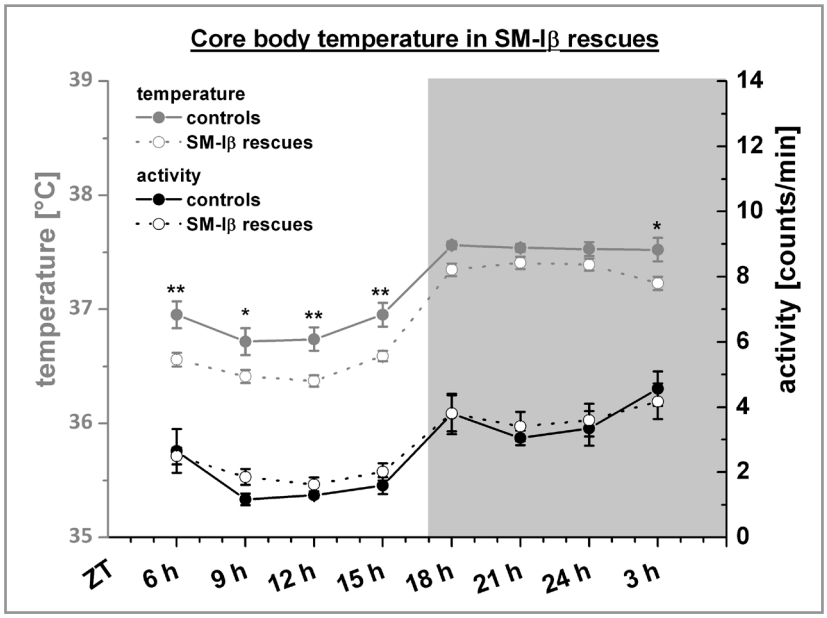

Figure 22: Baseline of core body temperature (dark grey lines) and locomotor activity (black lines) over 24 h in freely moving 3-6-month-old female SM-Iα (n=2♀) and SM-Iβ rescue (n=7♀, ; dashed line, open circles) and control mice (n=7♀; solid line, filled circles). A moving average with 3 h bins of a continuous 7 day recording is shown. Data from two independent experiments are summarised in this graph. A two-way ANOVA with repeated measures was performed for statistical analysis followed by a Bonferroni post-hoc test. *, p<0.05; **, p<0.01.

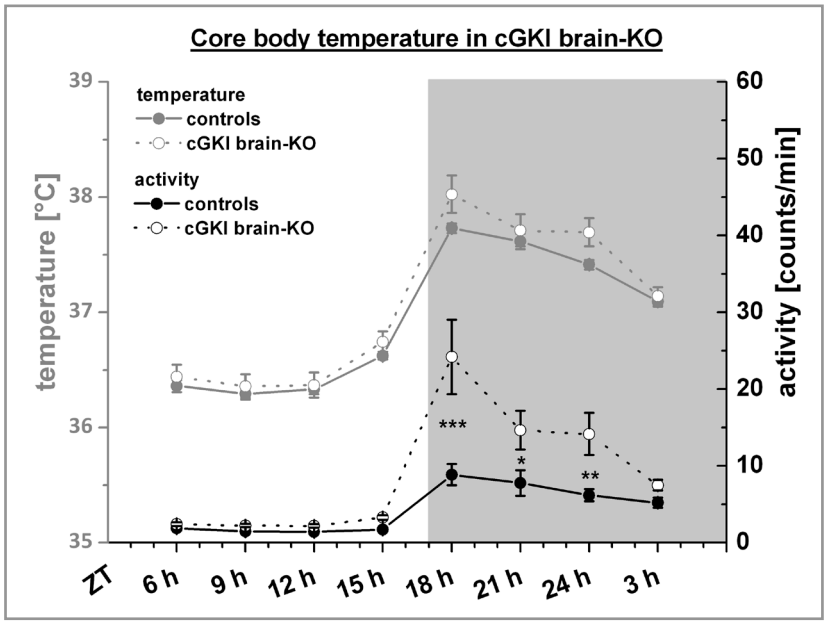

Figure 23: Core body temperature (dark grey lines) and locomotor activity (black lines) in cGKI brain-KO mice (n=10♀, dashed line, open circles) and controls (n=11♀, solid line, filled circles). Parameters were recorded in 2 min. intervals over 5-7 consecutive days and summarised as 3 h moving averages over 24 h. Recorded mice were 6-10 months old. Data from three independent experiments with similar results were summarised and statistically analysed with a two-way ANOVA with repeated measures. *, p<0.05; **, p<0.01; ***, p<0.001.

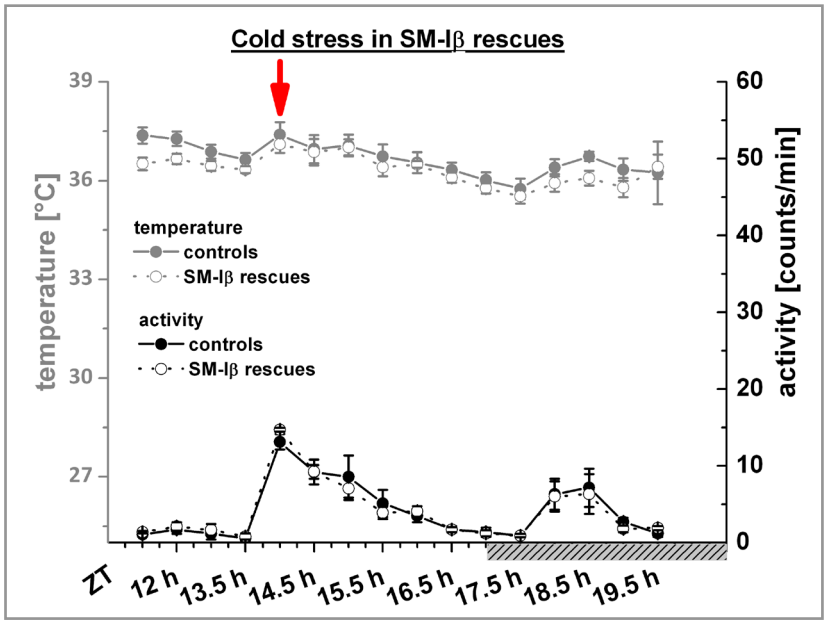

Figure 24: Core body temperature (dark grey lines) and locomotor activity (black lines) in SM-Iα and SM-Iβ rescue (n=9♀, dashed line, open circles) and control mice (n=7♀, solid line, filled circles) exposed to 4 °C for 6 h. The red arrow marks the start of the cold stress. Lights were not turned off in the evening, but the time point (ZT 17 h), when lights normally went off is marked on the time line with stripes. Data from two independent experiments in 3-6-month-old mice are summarised in this graph. A two-way ANOVA with repeated measures was performed for statistical analysis.

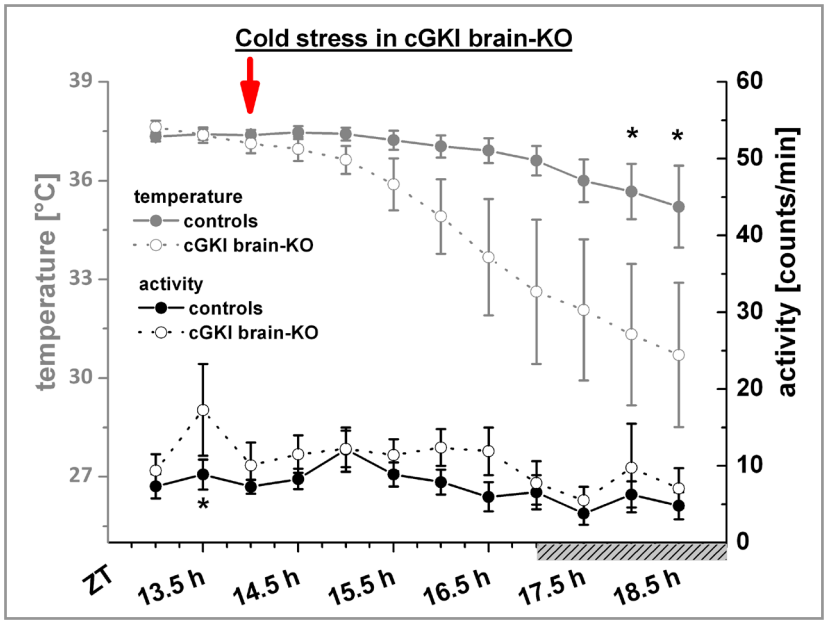

Figure 25: Cold stress in 6-10-month-old cGKI brain-KO mice (n=10 ♀, dashed line, open circles) and controls (n=11, solid line, filled circles). Core body temperature (dark grey lines) and activity (black lines) were measured in freely moving animals with implanted transmitters. Cold exposure started at ZT 14 h (marked with a red arrow) and ended at ZT 19 h. Lights were turned on during the whole experiments, but the time point when lights normally went off is marked at the time line with stripes. Data from three independent experiments with similar results were summarised and statistically analysed with a two-way ANOVA with repeated measures. *, p<0.05.

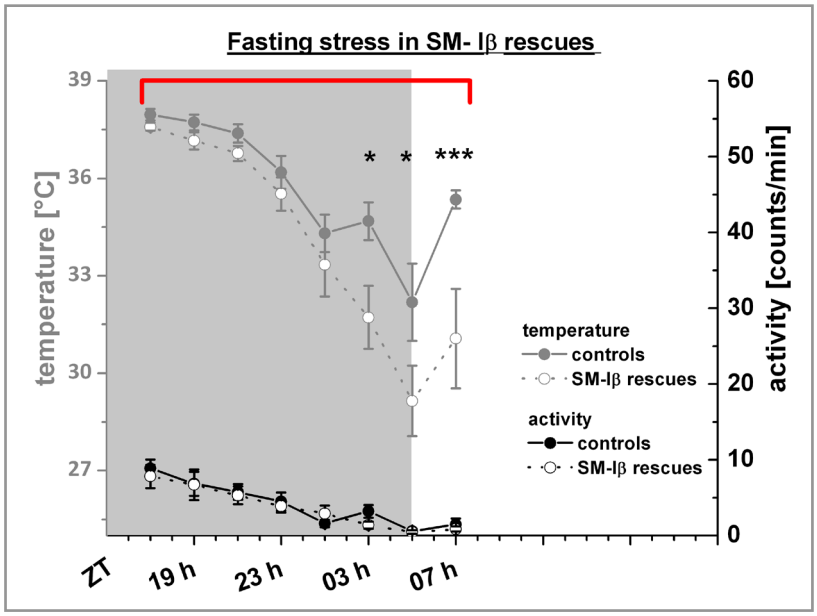

Figure 26: SM-Iα and SM-Iβ rescue mice (n=9♀, dashed line, open circles) and controls (n=7, solid line, filled circles) were fasted overnight (red bracket indicates the time free of food). Locomotor activity (lower black lines) as well as core body temperature (upper dark grey lines) was measured with telemetry. Data from two independent experiments in 3-6-month-old mice are summarised in this graph. A two-way ANOVA with repeated measures was performed for statistical analysis. *, p<0.05; ***, p<0.001.

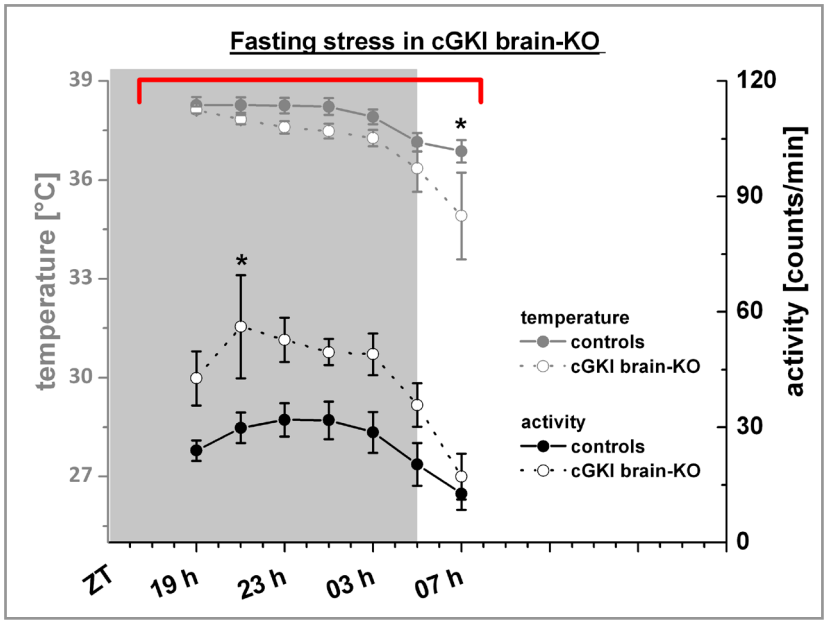

Figure 27: cGKI brain-KO mice (6-10 months old, n=10 ♀, dashed line, open circles) and controls (n=11, solid line, filled circles) were fasted overnight (red bracket indicates the time without food). Core body temperature (dark grey lines) and activity (black lines) were measured and data from three independent experiments with similar results were summarised. Data were statistically analysed with a two-way ANOVA with repeated measures. *, p<0.05.

C.2.2.3. Core body temperature under fasting stress

After exposure to the cold challenge, mice were allowed to recover for at least one week before they were food-deprived overnight. In SM-Iα and SM-Iβ rescue mice and controls core body temperature decreased during fasting (**Figure 26**, see also I.5.1.3). Core body temperature was significantly lower in SM-Iα and SM-Iβ rescue mice than in controls after 10 h free of food. Locomotor activity was indistinguishable between mutant mice and controls.
Also in cGKI brain-KO mice and controls core body temperature decreased during the food deprivation, but the decrease was not as pronounced as in rescue mice and controls (**Figure 27**, see also I.5.1.3). This might be due to the different genetic background or age. However, after 14 h of fasting core body temperature in cGKI brain-KO was significantly lower than in controls, whereas locomotor activity, which was higher in the mutant mice during the dark phase, was indistinguishable between cGKI brain-KO mice and controls.

C.3. *Ex vivo* analysis of cGKI-deficient mouse lines

C.3.1. HPA axis: analysis of adrenal glands in SM-Iβ rescue mice

The observed *in vivo* phenotype with increased ACTH and decreased CORT levels in stressed SM-Iβ rescue mice suggested an involvement of cGKI in the regulation of CORT release from the adrenal cortex. Therefore, adrenal glands of SM-Iβ rescue mice and controls were analysed in more detail.

C.3.1.1. Weight of adrenal glands

The reduced CORT level after stress may result from a reduced size of adrenal glands in SM-Iβ rescue mice. Hence, adrenal glands of naive 7-9-month-old female SM-Iβ rescue and control mice were weighed. The weight was normalised to the body weight of the mice since SM-Iβ rescue mice are in general slightly smaller than control mice (Weber et al., 2007). The macroscopic appearance of adrenal glands of SM-Iβ rescue mice and controls was indistinguishable (**Figure 28 A**). Colour, shape and size were also similar. Additionally, the weight of both adrenal glands normalised to the body weight of the animal was almost equal in controls (240.07 ± 17.37 µg adrenal gland/g BW) and SM-Iβ rescue mice (213.43 ± 16.81 µg adrenal gland/g BW) (**Figure 28 B**).

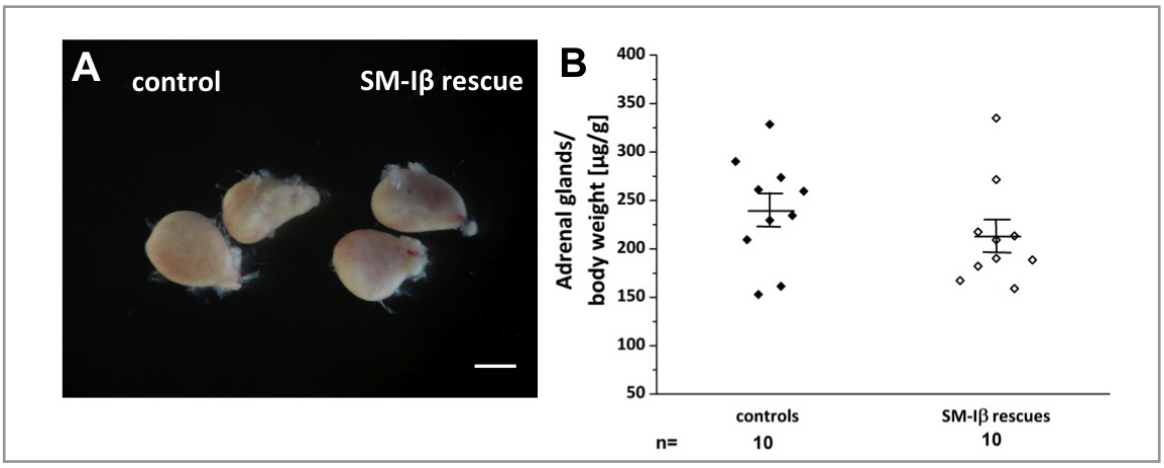

Figure 28: (A) Representative image of right and left adrenal gland of a 6-month-old control and SM-Iβ rescue mouse. Scale bar = 0.1 cm. (B) Distribution of adrenal gland weight normalised to the body weight of the mouse in 7-9-month-old controls (n=10♀; closed symbol) and SM-Iβ rescue mice (n=10♀; open symbol). Statistical analysis of the data was performed with a Student's t-test.

C.3.1.2. Morphological analysis of adrenal glands

Adrenal glands of SM-Iβ rescue mice were morphologically analysed to investigate, if the reduced CORT release in these mutants was associated with morphological differences such as hypo- or hyperplasia of the adrenal cortex. Thus, analysis of HE-stainings of consecutive sections from the middle part of adrenal glands of SM-Iβ rescue mice and controls was performed by measuring the area of the whole adrenal gland and the area of the medulla. The cortical area was calculated by subtracting the medullary area from the adrenal gland area.

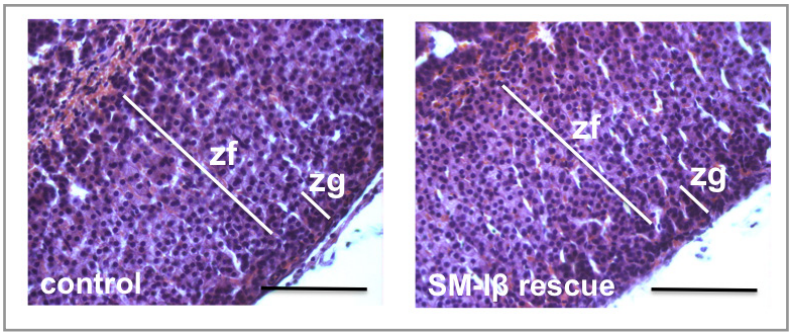

Figure 29: Representative micrographs of HE-stained 10 µm-sections from the middle part of the adrenal gland of a 6-month-old female control (left picture) and litter-matched SM-Iβ rescue mouse (right picture). Zf, zona fasciculata; zg, zona glomerulosa; scale bar = 100 µm.

No obvious morphological differences between HE-stained sections of control and SM-Iβ rescue mice were observed by visual inspection (**Figure 29**). Measurements of the sections revealed a significantly reduced adrenal gland, medullary and cortical area in SM-Iβ rescue mice compared

to controls. However, the ratio of cortical to whole adrenal gland or medullary area was similar in both genotypes (**Table 8**).

Table 8: Morphometric analysis of adrenal glands from SM-Iβ rescue mice and controls. Statistical analysis was performed using a Student's t-test. *, p<0.05; **, p<0.01.

Measured area	SM-Iβ rescue mice (n=5♀)	Control mice (n=9♀)
Adrenal gland area [mm^2]	1.15 ± 0.05*	1.63 ± 0.09
Medullary area [mm^2]	0.42 ± 0.02*	0.64 ± 0.05
Cortical area [mm^2]	0.73 ± 0.03**	0.99 ± 0.05
Cortical/adrenal gland area [mm^2]	0.63 ± 0.01	0.62 ± 0.02
Cortical/medullary area [mm^2]	1.73 ± 0.06	1.62 ± 0.13

C.3.1.3. Neutral lipid content

Cholesteryl esters stored in the steroidogenic cells of the zona fasciculata of the adrenal gland serve as primary source for CORT synthesis. To exclude the possibility that the deficits in CORT release in SM-Iβ rescues are caused by a problem in the cholesterol storage capacity of the adrenal glands, frozen sections of SM-Iβ rescue mice and controls were stained with Oil Red O, a fat-soluble dye. Red staining was observed mainly in the zona fasciculata and surrounding white and brown adipose tissue in both genotypes (**Figure 30**). Sections from three control and three SM-Iβ rescue mice were examined, but no difference between the genotypes was observed.

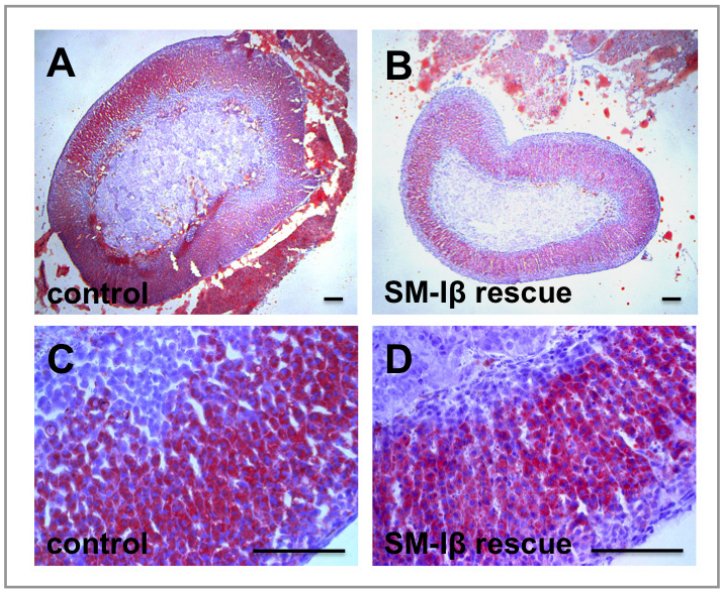

Figure 30: Representative staining of neutral lipids with Oil Red O in 10 µm sections of adrenal glands from a 6-month-old female control (A,C) and litter-matched SM-Iβ rescue mouse (B,D). Scale bar = 100 µm.

C.3.1.4. Protein expression in adrenal glands

Western blot analysis of cGKI expression in individual adrenal glands of control and SM-Iβ rescue mice revealed a clear reduction in cGKI expression levels in mutant mice (**Figure 31**). In the same mice, proteins of the IL-6 signalling pathway and Mac2, a macrophage marker, were examined, because it has been shown that SM-Iβ rescue mice have increased plasma IL-6 levels at higher ages with markedly increased IL-6 mRNA expression in the liver and upregulated IL-6 regulated genes. Additionally, SM-Iβ rescue mice show an increased infiltration of Mac2-positive macrophages in the liver (Lutz et al., 2011). Neither the important IL-6 effector SOCS3 (suppressor of cytokine signaling) nor Phospho-Akt (Ser^{473}), which is part of the IL-6 activated phosphoinositide-3-kinase (PI3K) pathway, were expressed to a different extent in SM-Iβ rescue mice. Likewise, Mac2 expression in SM-Iβ rescue mice did not differ between mutant mice and controls.

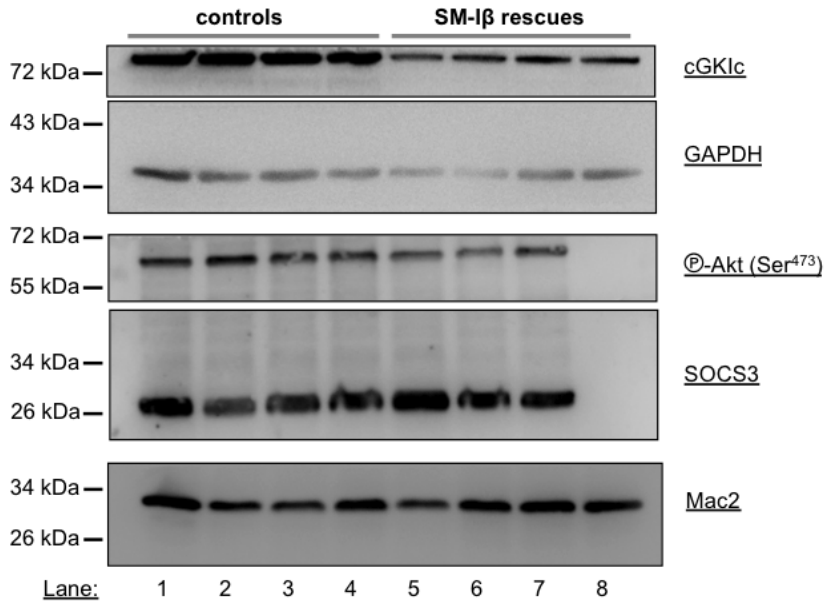

Figure 31: Western blot analysis of proteins expressed in adrenal glands of individual 6-month-old control (n=4) and SM-Iβ rescue mice (n=3-4). Protein lysates (40 µg protein) were separated with SDS-PAGE and blotted onto PDVF membranes. Specific primary antibodies were used for the detection of cGKI, Phospho-Akt (Ser^{473}) and SOCS3 (components of the IL-6 pathway), Mac2 (a macrophage marker) and GAPDH, which served as loading control.

To analyse which cGKI isoform is mainly expressed in wild type adrenal glands, a Western blot with the common cGKI antibody and antibodies specific for the cGKIα and cGKIβ isoform was performed (**Figure 32**). Both cGKI isoform-specific antibodies recognised their respective purified protein (cGKIα and cGKIβ) that was loaded as a positive control, but the cGKIα isoform-specific antibody caused high background staining and multiple bands were detected in the adrenal gland

lysates of cGKI KO, wild type, SM-Iα rescue and SM-Iβ rescue mice. The low signal-to-noise ratio made it impossible to define a specific signal for cGKIα in adrenal gland lysates, and thus no conclusion could be drawn from the Western Blot about the expression of the cGKIα isoform in adrenal glands (data not shown). However, the cGKIβ isoform-specific antibody gave a positive signal in adrenal gland lysates of wild type and SM-Iβ rescue mice (**Figure 32**). Hence, cGKIβ is expressed in wild type adrenal glands.

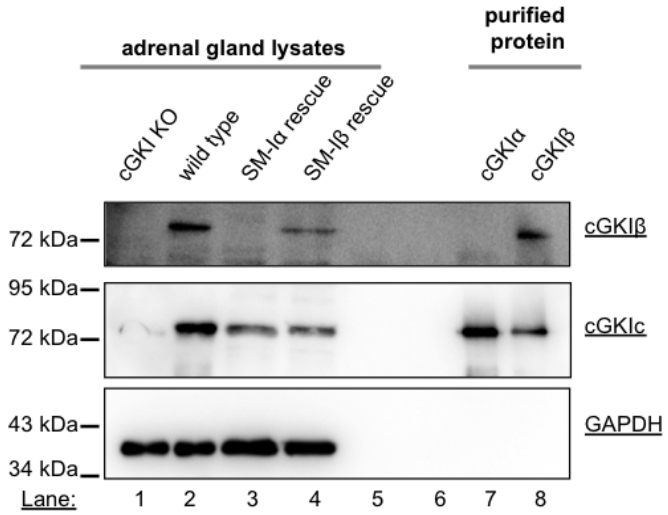

Figure 32: Western blot analysis of adrenal gland tissue lysates of cGKI KO, wild-type, SM-Iα and SM-Iβ rescue mice to determine, which cGKI isoform is expressed in the adrenal gland. Tissue lysates (10 µg protein) and purified cGKIα and cGKIβ (4 ng protein) were separated with SDS-PAGE, blotted onto PDVF membranes and expression levels were detected with specific antibodies. GAPDH was used as a loading control.

C.3.1.5. Characterisation of cGKI-positive cells in the adrenal gland

The stress-induced phenotype of reduced CORT levels in SM-Iβ rescue mice implies a problem at the level of the adrenal gland as the site of CORT production and secretion. Thus, cGKI expression in the adrenal gland of wild type mice was further analysed with immunofluorescence stainings to localise the site of cGKI expression in detail. cGKI expression was mainly detected in the capsule of the adrenal gland, in the vasculature and in characteristically shaped cells in the cortex (**Figure 33**). CORT-producing cells, which are arranged in columns in the zona fasciculata did not show any immuno-positive signals. cGKI-positive cells in the cortex displayed a characteristic shape with meager cytoplasm around the nucleus and elongations traversing from the cell body through the cortex (**Figure 33 D**). Similar staining patterns were observed with immunohistochemical staining methods (data not shown). The number of cGKI-positive cells in

the cortex varied strongly and was most abundant in young (4-10-week-old) mice. In older mice (>3 months) the number of cGKI-positive cells in the cortex was markedly reduced.

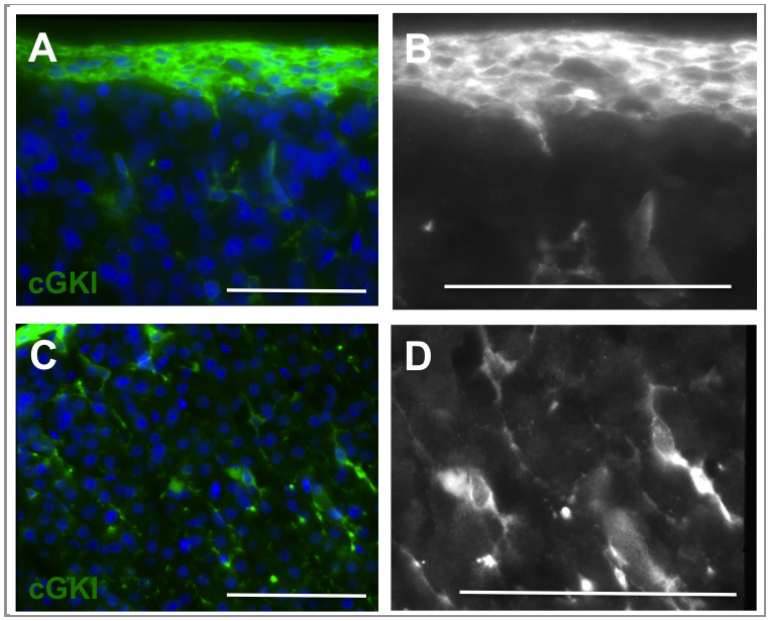

Figure 33: Immunofluorescence staining of 8-week-old wild type adrenal glands with an antibody against cGKI (detected with a secondary antibody labelled with AlexaFluor488). (A) A strong immunoreactive signal can be seen in the fibrous capsule of the gland. (B) Higher magnification shows several cell layers that stain positive for cGKI. (C) In the cortex single scattered cells can be detected. (D) These cells show a characteristic shape with large nuclei and elongations branching from the cell body. Scale bar= 100 µm.

Comparison of cGKI expression in adrenal glands from SM-Iβ rescue and control mice revealed similar staining patterns in the capsule and in large arteries underneath the capsule. The capsule was sometimes less intensely stained in SM-Iβ rescue mice and expression seemed to be restricted to only one layer of the capsule, whereas in wild type and control mice several layers of the capsule stained positive for cGKI. Most interestingly, in SM-Iβ rescue mice almost no cGKI-positive cells were detected in the cortex (**Figure 35**). To characterise the cGKI-positive cells, co-localisation studies with markers for different cell types were performed. Positive signals for CD31 (an endothelial marker) and βIII-tubulin (a neuronal marker) were detected in the endothelial layer of large vessels (CD31) and in fibers traversing the cortex and medulla (βIII-tubulin), but no overlap with cGKI-positive signals was observed (**Figure 36 A, B**). The macrophage marker, Mac2, stained a high number of cells in the cortex with a similar morphology than cGKI-positive cells, but again no overlap in the immunoreactive signals was detectable (**Figure 36 C**). Immunoreaction with antibodies against VaChT (vesicular acetylcholine transporter), FSP1 (fibroblast specific protein 1), Thy1.2 (CD90.2) and GFAP (glial fibrillary acid protein) was also observed in the adrenal gland, but was again not localised to the same cells as cGKI (data not shown).

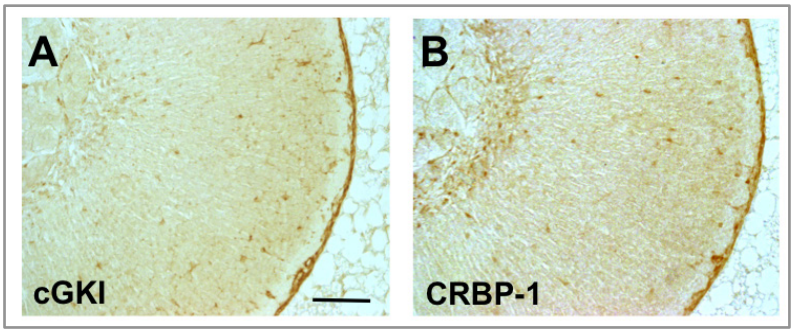

Figure 34: Immunohistochemical staining for cGKI (A) and CRBP-1 (B) in the adrenal gland of a 6-month-old control mouse. Parallel sections (10 µm) are shown. Scale bar = 100 µm.

CRBP-1 (cellular retinol binding protein 1) has been suggested as a fibroblast marker for the stellate cells of the liver (Van Rossen et al., 2009), in which cGKI was also detectable (Lutz et al., 2011). Therefore, the cGKI-positive cells in the adrenal gland cortex might also express CRBP-1. Immunohistochemical staining with a rabbit antibody against CRBP-1 revealed a similar staining pattern as the cGKI staining, mainly the capsule showed strong immunoreactions for both antibodies (**Figure 34**). However, the CRBP antibody emerged as not suitable for immunofluorescent staining, thus co-localisation studies were not possible.

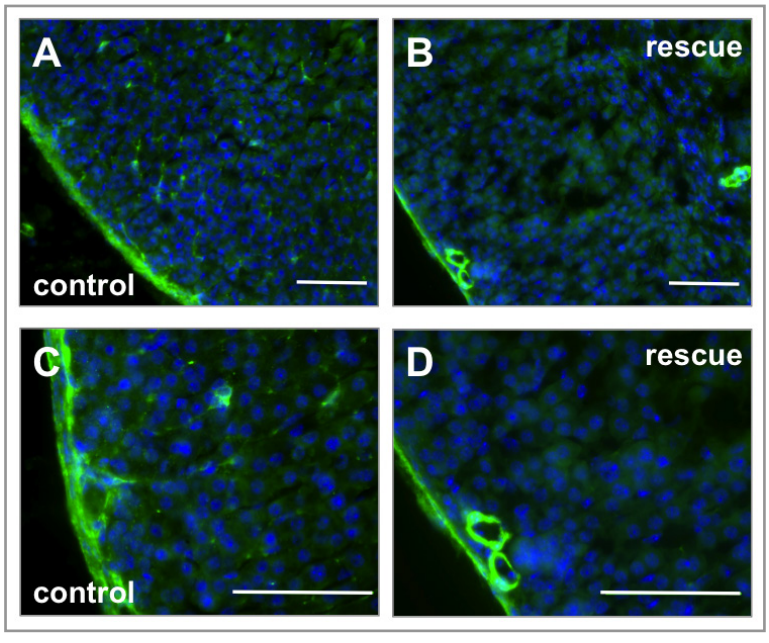

Figure 35: Immunofluorescence staining for cGKI of the adrenal gland of a 3-month-old control (A,C) and a litter-matched SM-Iβ rescue mouse (B,D). Immunoreaction was detected with an anti-rabbit AlexaFluor488-labelled secondary antibody. Scale bar = 100 µm.

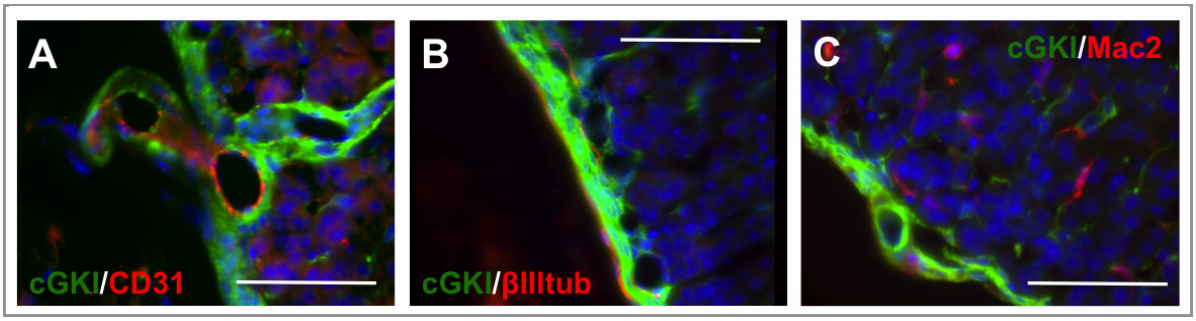

Figure 36: Double staining of wild type adrenal gland sections with an antibody for cGKI (shown in green; secondary antibody labelled with AlexaFluor488) and different cellular markers. An endothelial marker (CD31), a neuronal marker (βIII-tubulin) and a macrophage marker (Mac2) are shown in red (secondary antibody labelled with AlexaFluor555 or 594). Scale bar = 100 µm.

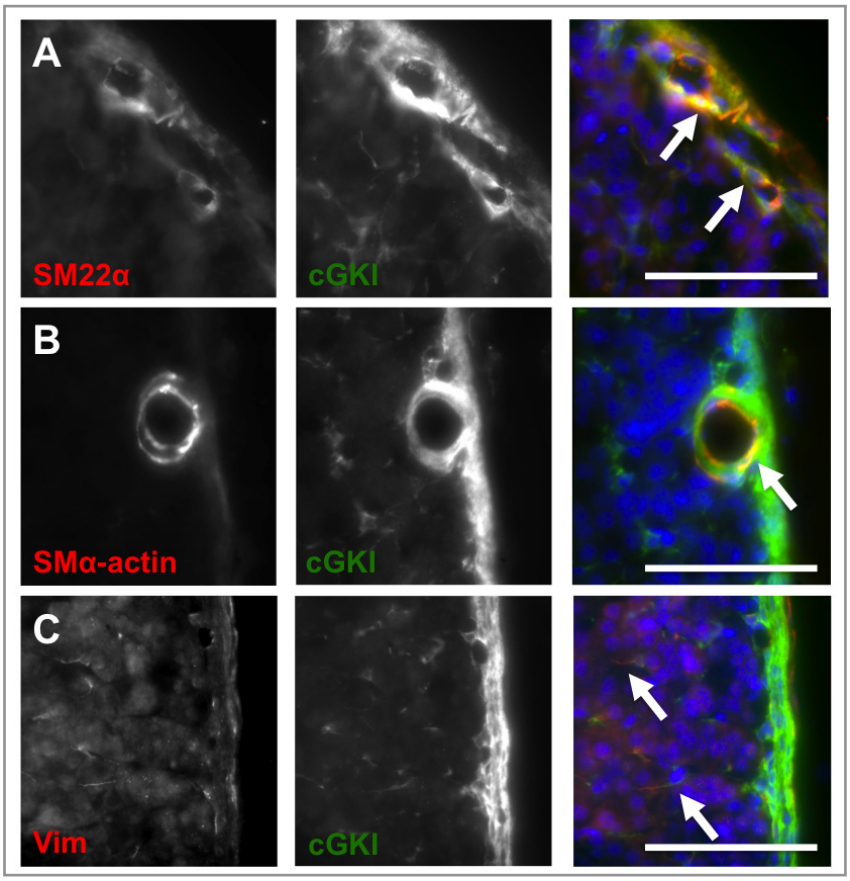

Figure 37: Double staining of wild type adrenal gland sections with antibodies for cGKI (shown in green; secondary antibody labelled with AlexaFluor488) and smooth muscle and fibroblast markers (shown in red; secondary antibody labelled with AlexaFluor555 or 594) reveals partial overlap in the positive signals. Vim, Vimentin. Scale bar = 100 µm.

At least partial co-localisation was found between the smooth muscle markers SM22α and SMα-actin and cGKI (**Figure 37 A, B**). Both smooth muscle markers were expressed in large vessels underneath the capsule. SM22α was more abundantly expressed than SMα-actin.

Immunoreactive signals for SM22α were additionally detected in the vessels of the medulla and in parts of the capsule. Neither SMα-actin nor SM22α was detectable in the cGKI-positive cells scattered in the cortex. Vimentin, which has been used as a myofibroblast marker in some studies (Gabbiani, 1981, 1996), gave an immunoreactive signal in small fibers in the cortex, which were often part of branches from cGKI-positive cells (**Figure 37 C**). Positively stained fine cellular structures were hardly distinguishable from the high background staining, thus detection of double-positive cells was extremely difficult. Additionally, only few cells stained positive for vimentin, whereas cGKI immunoreactivity was more abundant.

C.3.1.6. Gene expression in adrenal gland and liver

Using semi-quantitative RT-PCR, mRNA levels of the cGKI isoforms in wild type adrenal glands were investigated. Both isoforms were present in the adrenal gland (**Figure 38**).

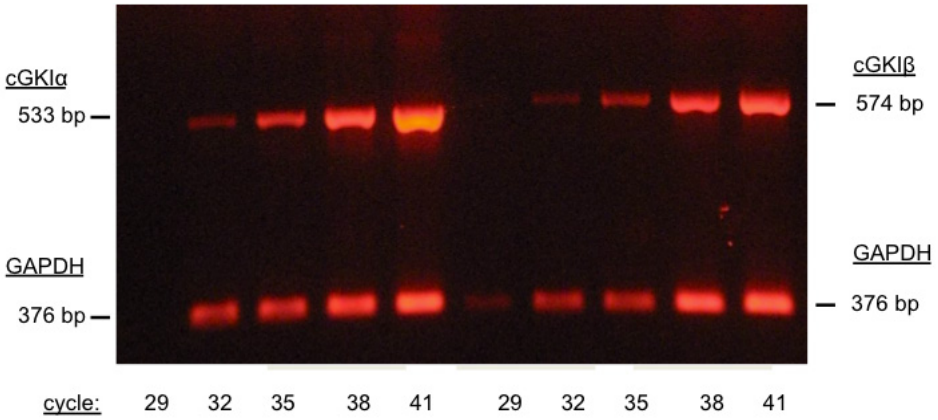

Figure 38: Semi-quantitative RT-PCR for cGKIα and cGKIβ mRNA expression levels in the adrenal gland of a 7-week-old wild type mouse. Samples were taken at the indicated cycles.

In order to reveal potential deficits in CORT synthesis in SM-Iβ rescue mice, RT-PCRs for genes involved in steroidogenesis were performed (**Figure 39**). Neither mRNA expression levels of enzymes involved in CORT synthesis (MC2R, the ACTH receptor; StaR, which is the rate limiting enzyme in this process; Cyp11A1 and Cyp11B1) nor of those involved in CORT transport in the blood (corticosterone binding globulin=CBG) were significantly different between SM-Iβ rescue and control mice. Also mRNA levels of the lipoprotein receptors LDLR (low density lipoprotein receptor) and SR-BI (scavenger receptor BI for high density lipoproteins), which regulate the substrate availability for CORT synthesis by modulating cholesterol influx in adrenal cells, were similar in mutant and control mice. Another enzyme that is critically involved in active CORT production is the 11β-hydroxysteroid dehydrogenase (11β-HSD1), which converts the inactive dehydrocortisone and cortisone into active glucocorticoids. Again, mRNA levels reflecting its gene expression were similar between mutant and control mice. Some of the enzymes are expressed

at higher levels in the liver, and therefore mRNA levels for 11β-HSD1, CBG, LDLR and SR-BI were also determined in livers of SM-Iβ rescue mice and controls. As in the adrenal glands, no differences between mutant and control mice were detected.

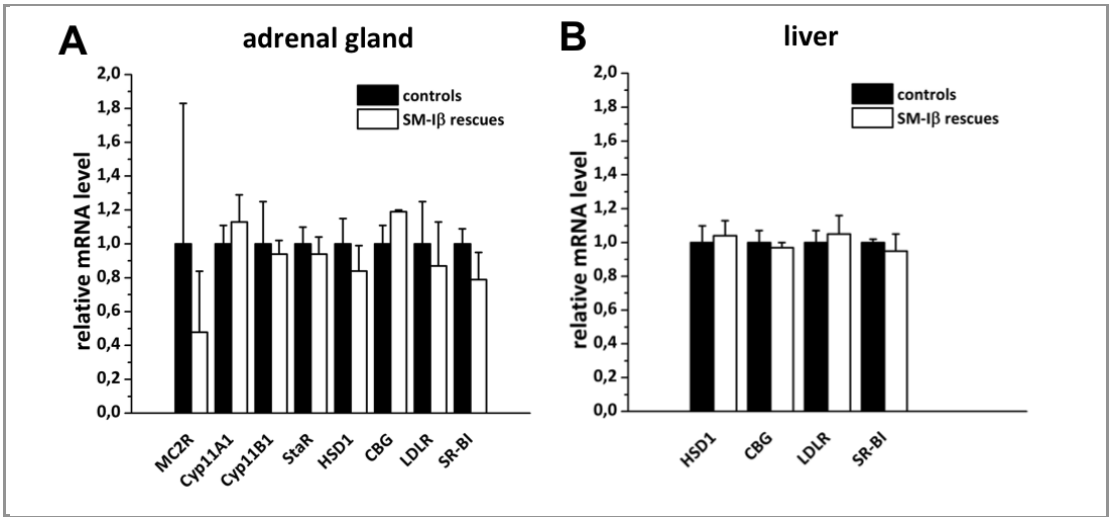

Figure 39: Relative mRNA levels for genes involved in CORT synthesis and CORT availability in adrenal gland (A) and liver (B). RNA was isolated from 4-month-old SM-Iβ rescue mice (n=1♂, 2♀) and controls (n=1♂, 2♀). Semi-quantitative RT-PCRs were performed as described in (B.5.4) and expression was normalised to GAPDH or HPRT expression. Control mRNA levels were set as 1 for each gene. No statistical differences were detected between the genotypes applying Student's t-test.

C.3.1.7. ACTH sensitivity in acute primary adrenal cells

To test, if the sensitivity for ACTH in CORT producing cells is *per se* reduced in SM-Iβ rescue mice, a cell culture approach was used. Dispersed cells were acutely isolated from 5-9-month-old female SM-Iβ rescue and control mice. After a regeneration period of 1 h, cells were stimulated with increasing concentrations of $ACTH_{1-24}$ for another hour before CORT levels in the supernatant were measured using RIA. A dose-dependent release of CORT was observed in cell preparations of both genotypes. With the highest ACTH concentration (10 nM), absolute CORT values reached a maximum ranging from 20 to 60 ng/ml CORT depending on the cell culture preparation. However, in 2 out of 3 experiments no differences in the absolute CORT values were observed between the genotypes. In the 3 independent experiments, normalised values gave similar dose-dependent CORT release curves for SM-Iβ rescues and controls with an $EC_{50} \approx 0.2$ nM (**Figure 40**).

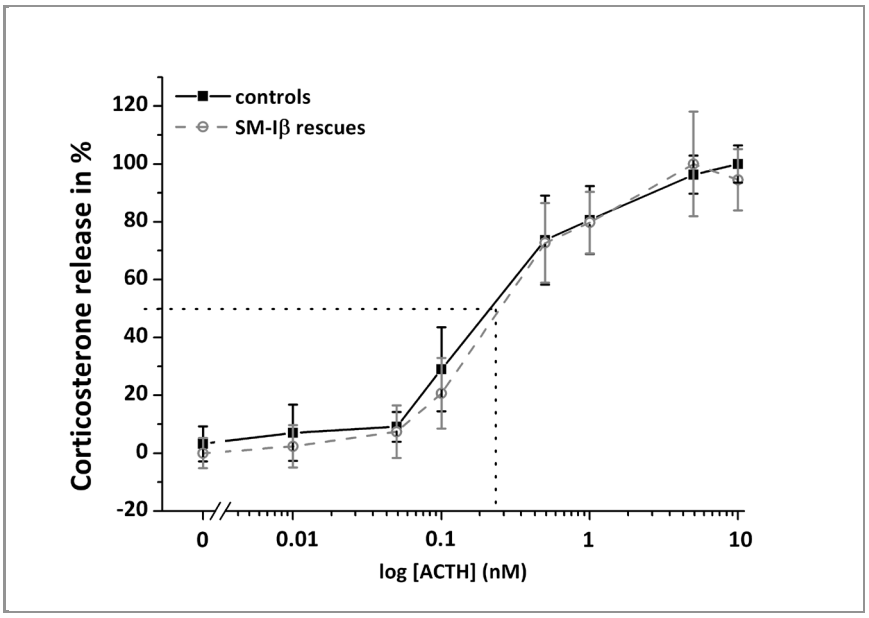

Figure 40: ACTH sensitivity in dispersed adrenal gland cells derived from 7-month-old female SM-Iβ rescue (n=6) and control mice (n=6). Results of CORT measurements in the supernatant were normalised to the protein content of single cell suspensions of SM-Iβ rescue and control mice. An aliquot was kept for this purpose before seeding of the cells. Statistical analysis was performed with two-way ANOVA for repeated measures. One out of three experiments with similar results is shown. Each data point represents n=3 wells. Data were normalised taking the highest mean value as 100%. EC_{50} was between 0.2-0.3 nM and is indicated by the dotted line.

C.3.1.8. ACTH sensitivity in adrenal slice cultures

The sensitivity of steroidogenic cells to ACTH might not necessarily be a deficit of the cells themselves, but could be influenced by surrounding cells via paracrine factors. Therefore, ACTH stimulation was performed in adrenal gland slices of a SM-Iβ rescue and a control mouse. In organotypic slice cultures, intact cell-cell contacts are preserved and a better reflection of the *in vivo* situation is given in this way. Adrenal gland slices were stimulated with ACTH in the presence or absence of 8-Br-cGMP for up to 19 h, and CORT release into the medium was measured (**Figure 41**). In adrenal slices from a mutant and a control mouse, the synthesis rate of CORT production increased rapidly after starting the stimulation with ACTH and reached the maximal rate between 15 to 30 min. Afterwards synthesis rate decreased slowly and returned almost to baseline. When stimulated with ACTH alone, the peak of the synthesis rate was even slightly higher in the SM-Iβ rescue mouse. In the additional presence of the cGMP analogon 8-Br-cGMP, this difference disappeared. Without any stimulating substance in the medium, the CORT synthesis was low in both genotypes showing also a small increase after medium change.

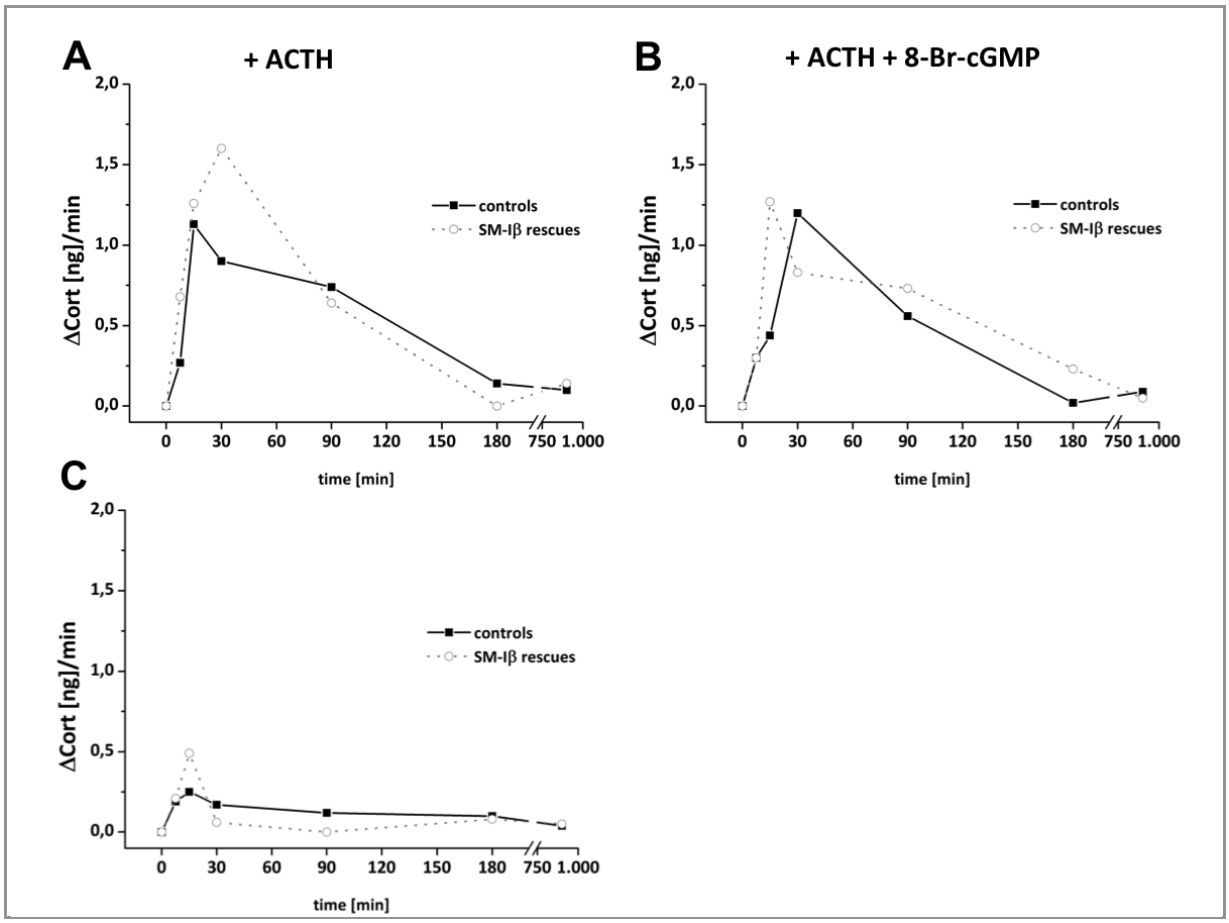

Figure 41: Incubation of adrenal slices from a 4-month-old SM-Iβ rescue (dashed line, open symbols) and control mouse (solid line and symbols) with 20 nM ACTH (A,B) and 100 µM 8-Br-cGMP (B). The supernatant from untreated slices was measured as a control to estimate the level of CORT leakage from the slices. For each condition aliquots from 3 wells were taken at several time points (0, 15, 30, 60, 120, 240, 1800 min) and pooled for measurements. Synthesis rate was calculated by determining the mass in the remaining volume (corrected for the taken aliquots) and calculating the mass increase per minute. For each time period the synthesis rate is displayed between the two time points of taking aliquots. Statistical analysis was not performed because pooled values were measured. Preparation of adrenal slices was performed at the Institute of Physiology II with the kind permission of Prof. Olga Garaschuk.

C.3.2. Thermoregulation: analysis of brown adipose tissue (BAT)

In our *in vivo* studies, SM-Iβ rescue mice as well as cGKI brain-KO mice displayed deficits in thermoregulation. Therefore, brown adipose tissue, as the main site of non-shivering thermogenesis, in which heat is produced during cold stress, was investigated in more detail in these mouse mutants.

C.3.2.1. Protein expression in BAT

Western blot analysis in brown adipose tissue revealed a clear reduction of cGKI protein expression in cGKI brain-KO and SM-Iβ rescue mice when compared to the corresponding controls (**Figure 42**).

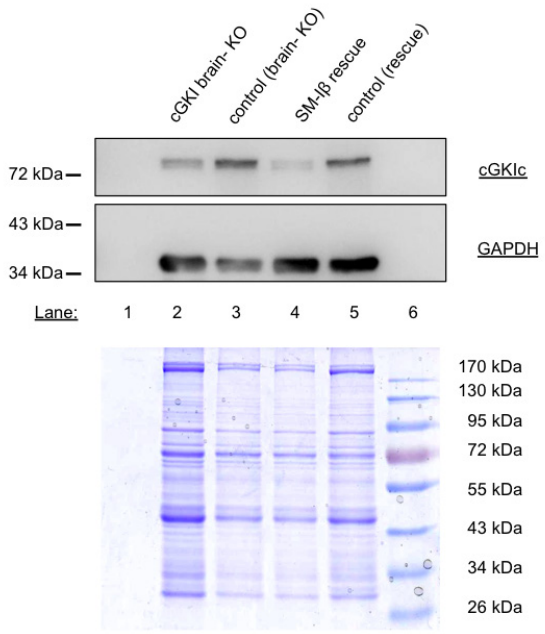

Figure 42: Western blot analysis of cGKI protein expression in brown adipose tissue lysates (~20 µg protein loaded) of cGKI brain-KO, SM-Iβ rescues and corresponding controls. GAPDH was used as a loading control. Loading amounts can also be estimated from the Coomassie staining in the lower half of the figure.

C.3.2.2. Characterisation of cGKI-positive cells in BAT

As mentioned above (C.1.2), analysis of the localisation of cGKI expression in brown adipose tissue revealed expression in the vasculature and in small cells with thin processes. In both cGKI mutants (cGKI brain-KOs and SM-Iβ rescues) cGKI expression in the vasculature was detectable, but expression in the small cells was completely missing in the SM-Iβ rescue mice and reduced to a few cells in the GKI brain-KO mice (**Figure 43**).

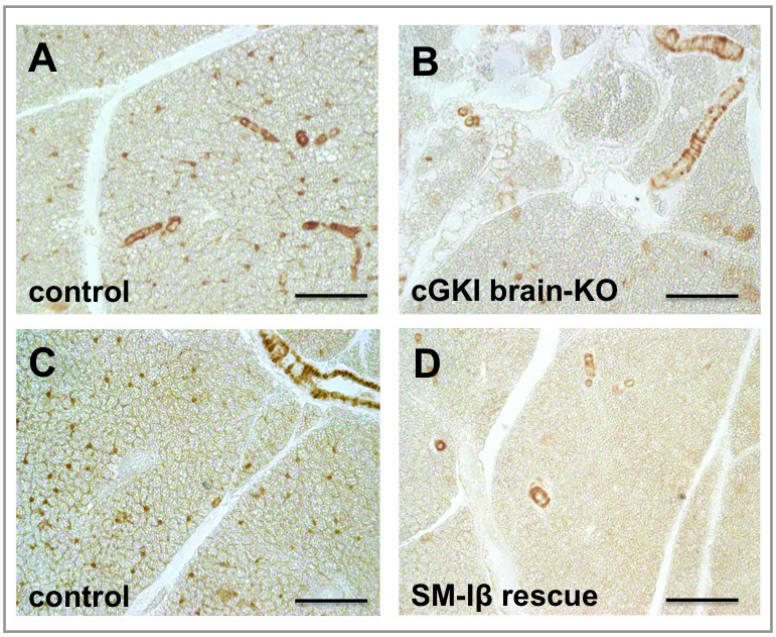

Figure 43: Immunohistochemical staining for cGKI in sections of interscapular brown adipose tissue of cGKI mutant mice. Scale bar = 100 µm.

Additionally, cGKI expression was found in structures that morphologically resembled peripheral nerve bundles. In SM-Iβ rescue mice (**Figure 44**) and in cGKI brain-KO mice (data not shown), cGKI expression in these structures was missing. Immunohistochemical double-stainings with antibodies detecting cGKI and βIII-tubulin confirmed the nervous origin of these cGKI-positive tissue structures. Whether cGKI and βIII-tubulin co-localise in the same cells in the peripheral nerve bundles was impossible to judge by immunohistochemical staining (**Figure 44**). Double staining using immunofluorescence will be needed to further clarify this.

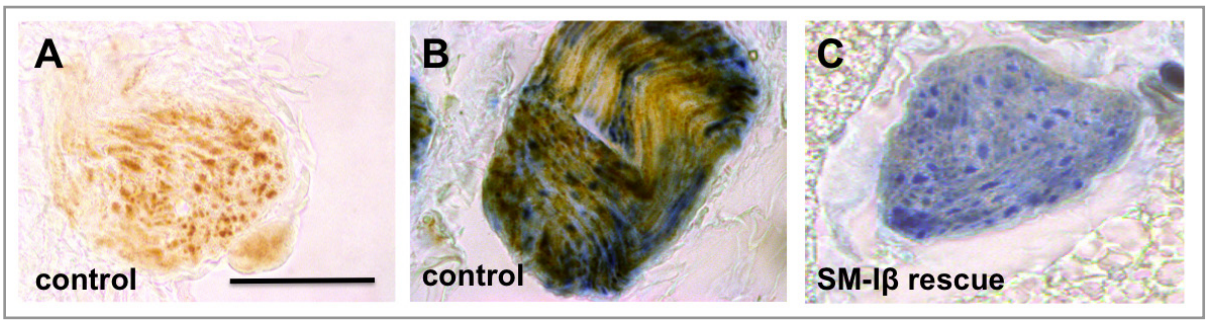

Figure 44: Immunohistochemical staining of peripheral nerve bundles in BAT of a control (A,B) and a SM-Iβ rescue mouse (C). cGKI-positive staining was visualised with a HRP-coupled secondary antibody (DAB, brown colour), and βIII-tubulin-positive staining with an AP-coupled secondary antibody (blue colour), respectively. Scale bar= 50 µm.

To detect the recombination pattern of the Nes-Cre mouse line in BAT, X-gal staining in brown adipose tissue of a reporter mouse (R26R/Nes-Cre mouse) was performed. Peripheral nerve bundles (**Figure 45 A**) and the characteristically shaped cGKI-positive cells in BAT displayed positive blue X-gal staining in addition to their cGKI expression (**Figure 45 B, C**).

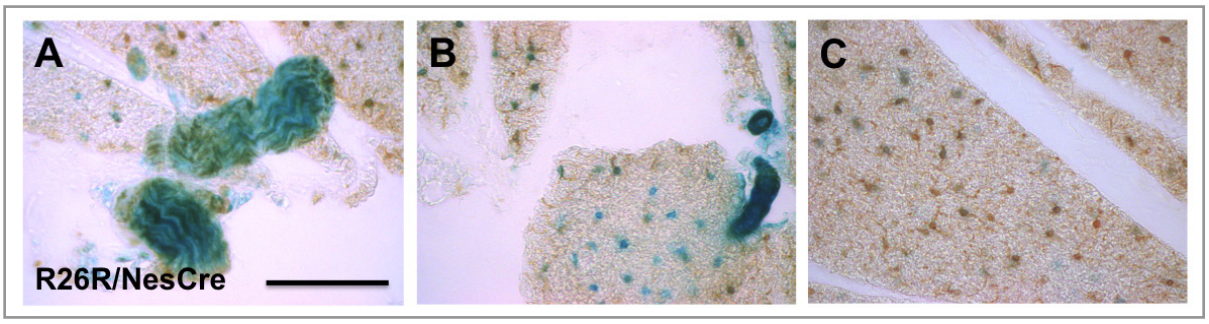

Figure 45: X-gal staining in a R26R/Nes-Cre mouse. To detect the recombination pattern in the Nes-Cre mouse line, the line was crossed to a Rosa26-Cre reporter (R26R) mouse, which expresses β-galactosidase following Cre-mediated recombination of a lacZ reporter gene. X-gal staining (blue) was combined with immunohistochemical staining for cGKI (brown). (A) Peripheral nerve bundles show an intense blue staining (X-gal staining). (B, C) Some of the characteristically shaped cGKI-positive cells in BAT are additionally X-gal stained. Scale bar= 100 µm.

D Discussion

D.1. cGKI modulates HPA axis activation

An organisms' ability to properly respond to stress is fundamental for its survival, and the HPA axis is a key mediator of this stress response (Jessop, 1999). Disturbances in HPA axis regulation result in a variety of diseases (Chrousos, 2009). Thus, profound knowledge of factors involved in its regulation provides the potential to develop treatment strategies.

Studies of NO/cGMP signalling and NP/cGMP signalling in HPA axis modulation are quite controversial and so far the role of cGKI has not been investigated. Hence, in this study the question was addressed, whether cGKI is involved in the regulation of HPA axis responsiveness *in vivo*.

The expression of cGKI in the relevant tissues is the first requirement for a functional role in HPA axis regulation. It has already been shown in previous studies that cGKI is expressed in brain areas relevant for HPA axis regulation such as hippocampus and hypothalamus as well as in the pituitary and adrenal gland (Feil et al., 2005b; Gambaryan et al., 2003; Kleppisch et al., 1999). Expression of cGKI in the hypothalamic PVN, pars intermedia and pars distalis of the pituitary gland and in the adrenal gland of wild type mice was confirmed by Western blot analysis (**Figure 8**) and immunohistochemistry (**Figure 9**, **Figure 10**, **Figure 11**). The adrenal gland expresses considerable levels of cGKI when compared to cGKI protein expression levels in the cerebellum (data not shown), which is known to contain high amounts of cGKI protein (Lohmann et al., 1981). Consequently, the abundant cGKI expression in tissues of the HPA axis suggests a possible role in its regulation.

Thus, the role of cGKI in the stress response *in vivo* was studied by measuring plasma stress hormone levels under basal and stimulated conditions in different cGKI-deficient mouse models (**Table 1**). Lack of cGKI does not influence basal CORT levels in the morning, when CORT levels are at their nadir. This was concluded from the comparison of CORT levels in controls with total cGKI KO mice and SM-Iβ rescue mice, which lack cGKI in all tissues except smooth muscle cells (**Figure 14**). Basal CORT levels were similar between cGKI-deficient mice and corresponding controls, but the levels between cGKI KO mice and SM-Iβ rescue mice were considerably different. Also the corresponding controls differed from each other. The expected basal CORT levels in the morning in mice are ~50 ng/ml depending on the age and gender of the mice as well as the blood sampling technique (Balcombe et al., 2004; Madetoja and Madetoja, 2009; Schmidt et al., 2003; Yoshimura et al., 2003). cGKI KO mice and controls were only 6-8 weeks old and thus much younger than the SM-Iβ rescue mice (7-12 months old) . A later decapitation of cGKI KO mice was not possible, because most of these mice die at an age of 6-8 weeks after developing a severe gastrointestinal phenotype (Pfeifer et al., 1998; Wegener et al., 2002). Additionally, cGKI KO mice were housed in groups > 4 mice and transferred to the room just a few days before blood collection. Adaptation to a new room needs more than 4 days and also

group hierarchical fights between males lead to elevated CORT levels (Tuli et al., 1995; Van Loo et al., 2003). This, together with the younger age, might have contributed to the high basal CORT levels in cGKI KO mice and controls.

In contrast to the similar basal CORT levels in SM-Iβ rescue mice and controls in the morning, CORT levels in the evening were significantly lower in SM-Iβ rescue mice than in controls (**Figure 15 B**). This could either be due to a dampened course in the circadian rhythm of CORT secretion, to a reduced sensitivity of steroidogenic cells to ACTH, or to lower plasma ACTH levels in the circulation. To elucidate, if the circadian rhythm in CORT levels is indeed dampened, one would need to take serial blood samples, which requires the implantation of catheters and consequently an immense experimental effort and thus this was not analysed. It is known that the sensitivity of adrenal glands to ACTH changes during the day and is higher in the evening (Dallman et al., 1978). This circadian change in sensitivity is regulated via splanchnic nerve innervation of the adrenal gland (Dijkstra et al., 1996; Ulrich-Lai et al., 2006a). However, to test the hypothesis of a changed ACTH-sensitivity in SM-Iβ rescue mice *in vivo*, one would need to block endogenous ACTH via dexamethasone injection prior to ACTH application in the morning and in comparison in the evening. This was not tested yet, since the results from other experiments rather suggested an unchanged sensitivity. Also, whether the lower CORT levels are just due to lower plasma ACTH levels could not be tested in these plasma samples, because for the morning/evening measurements a blood sampling method (tail nick) was used, that gives only low amounts of plasma, but instead allows repetitive blood sampling in the same mouse. However, when blood was taken via decapitation in the morning, ACTH levels were similar between SM-Iβ rescue mice and controls (**Figure 14 B**), but so were CORT levels. Consequently, ACTH measurements in evening plasma samples would be of great interest. However, ACTH levels after stress exposure are similar or even higher than in controls (**Figure 18 A, C** and **Figure 19 B, D**), and thus decreased ACTH levels in the basal state are also unlikely.

The stimulation of the HPA axis via IL-1β injection, which is known as a strong activator of the HPA axis (Besedovsky et al., 1986), resulted in a diminished rise in plasma CORT levels in SM-Iβ rescues (**Figure 18 D**). As mentioned above, the lower CORT levels were not a consequence of reduced ACTH secretion, because ACTH levels in SM-Iβ rescues were even higher than in controls following IL-1β injection (**Figure 18 C**). Lower CORT levels with concurrent equal or higher ACTH levels suggest a diminished sensitivity to ACTH in SM-Iβ rescue mice. Already under control conditions (vehicle injection) CORT levels were slightly increased compared to basal CORT levels in both control and SM-Iβ rescue mice (see **Figure 14 B**). But again, CORT levels in SM-Iβ rescue mice did not increase to the same extent as in controls. In contrast to the elevated ACTH levels in IL-1β injected SM-Iβ rescue mice, ACTH levels in vehicle-injected mice were similar in controls and SM-Iβ rescue mice. With the applied experimental procedure, it is difficult to decipher, whether the higher ACTH levels in SM-Iβ rescue mice after IL-1β injection are an effect of the IL-1β injection *per se* or due to the dimished negative feedback inhibiton of the lower CORT levels circulating in the plasma (Dallman, 2005; Hinz and Hirschelmann, 2000;

Shipston, 1995), the latter being more likely. Even though, a direct effect of IL-1β on pituitary corticotrophs has been discussed; the main route of IL-1β action on HPA axis activation is believed to be via afferent nerves projecting to the NTS, which in turn projects to the PVN (Turnbull and Rivier, 1999). Therefore, the main effect of i.p. IL-β injection is at the level of the brain by increasing CRH release (Berkenbosch et al., 1987; Sapolsky et al., 1987). Furthermore, NO has been shown to interfere with this process by inhibiting the IL-1β induced CRH and AVP release in hypothalamic explants (Costa et al., 1993; Yasin et al., 1993). Consequently, to test if the lack of cGKI in the central and peripheral nervous system is the reason for the observed phenotype, cGKI brain-KO mice were also injected with IL-1β. Neither CORT nor ACTH levels were different between mutant and control mice (**Figure 18 A, B**). Thus, we concluded that cGKI expression in the central and peripheral nervous system does not contribute to the modulation of the HPA axis response after IL-1β injection. Yet, when interpreting *in vivo* data from tissue-specific KO mice generated with the Cre/*loxP*-technology, one needs to be cautious due to the limitations of this method (see A.1.1.2). Incomplete recombination and thus a few cells still expressing the protein could mask an existing phenotype. The rat Nestin promoter and enhancer, which was used for the generation of the Nes-Cre mouse line (Tronche et al., 1999), is much less active in the PNS than in the CNS (Zimmerman et al., 1994). Therefore, possible cGKI expression in the PNS, contributing to the innervation of the adrenal gland, might not be completely eliminated. Nevertheless, regarding cGKI expression in the brain, analysis of brains from cGKI brain-KO mice revealed the complete loss of cGKI expression in the PVN and other nuclei of the hypothalamus (Dr. Susanne Feil, personal communication). Hence, cGKI expression in the PVN seems not to contribute to the observed phenotype in SM-Iβ rescue mice after IL-1β injection.

In addition to the common stress response activated by all types of stressors, there are also differences in the neuroendocrine circuits activated by diverse stressor types (see A.2.4). To test whether the role of cGKI in HPA axis modulation is restricted to IL-1β injection, an immunological challenge and thus a physical stressor type, another stressor was applied. Restraint stress can be seen as a mixed physical and psychological stressor (Pacak and Palkovits, 2001). In 7-month-old as well as in 3-month-old SM-Iβ rescue mice the rise in CORT levels following restraint stress was diminished compared to controls (**Figure 19**). These results suggest that the observed phenotype is independent of the applied stressor. Thus, the role of cGKI in the modulation of HPA axis response is conserved across diverse stressor types. The reason for the use of two groups of mice (old and young) in the restraint stress paradigm was that elevated plasma IL-6 levels had been observed in older SM-Iβ rescue mice (Lutz et al., 2011). The constant presence of the cytokine circulating in the plasma could influence HPA axis activation, since a close bidirectional relationship between cytokines and HPA axis is well established (Gaillard, 2001). But, as IL-1β, IL-6 rather stimulates the HPA axis and increases CORT secretion (Mastorakos and Ilias, 2006; Perlstein et al., 1991). This is in contrast to the observed phenotype of lower CORT levels in SM-Iβ rescue mice. On the other hand, during long-term stress such as sepsis, IL-6 is able to

regulate steroidogenesis independently of the CRH-ACTH pathway (Bethin et al., 2000; Venihaki et al., 2001; Willenberg et al., 2002), and the elevated plasma IL-6 levels in SM-Iβ rescue mice could be a compensatory mechanism for the deficit in CORT secretion. This seems not to be the case, because also young (3-month-old) SM-Iβ rescue mice, which were selected for low plasma IL-6 levels (<15 pg/ml), displayed a deficit in CORT production after restraint stress (**Figure 19**). Consequently, the reduced adrenocortical output of SM-Iβ rescues after stimulation is most likely independent of the stressor-type and the chronically elevated plasma IL-6 levels in older SM-Iβ rescue mice. Some research groups have suggested an increase in plasma IL-6 levels induced by restraint stress (Kitamura et al., 1997; Nukina et al., 2001; Zhou et al., 1993). But neither control mice in the old nor in the young group showed an elevation of IL-6 after restraint stress. The discrepancy can be explained by the different time points of measurements. In this study, IL-6 was measured after 30 min. of restraint stress, while Nukina et al. showed an elevation of IL-6 protein in the plasma 1 h after starting the immobilisation. In contrast to the IL-1β injection, ACTH levels in the 3-month-old SM-Iβ rescue mice were comparable to controls after the restraint stress (**Figure 19 D**). This supports the hypothesis that primarily CORT production or secretion is affected in SM-Iβ rescue mice. On the other hand, ACTH levels in the 7-month-old SM-Iβ rescue mice were increased compared to controls (**Figure 19 B**). This might be a consequence of the potential hyposensitivity to ACTH in the adrenal glands of SM-Iβ rescue mice, and old mice could compensate for it with an up-regulation of ACTH levels. The increased ACTH levels might also be linked to the elevated IL-6 levels. For instance, in CRH KO mice it was shown that IL-6 increases ACTH levels (Bethin et al., 2000). Also in male rats high circulating levels of IL-6 have been capable of releasing ACTH in a CRH-independent mechanism (Rivier, 2001).

Taken together, the deficit in adrenocortical output in SM-Iβ rescue mice seems to be independent of stressor type and plasma IL-6 levels, whereas ACTH levels are more diverse and probably not independent of the chronically elevated plasma IL-6 levels. The *in vivo* data obtained from the two investigated mouse models imply that cGKI absence in non-neuronal cells changes steroidogenic output of the adrenal gland.

Hence, it was tested, if the sensitivity to ACTH *in vivo* is changed in SM-Iβ rescue mice and if the reduced plasma CORT levels after stimulation can be attributed to a problem at the level of the adrenal glands. Injection of a low dose of ACTH (10 µg/kg) was not sufficient to increase CORT levels significantly when compared to vehicle injection. However, SM-Iβ rescue mice had significantly lower CORT levels after ACTH injection (**Figure 20 A**). Whereas the intermediate dose of ACTH (100 µg/kg) was able to efficiently increase CORT levels, but without any differences between the genotypes (**Figure 20 B**). The difference seen with the lower dose might thus rather be an unspecific effect of the handling and injection than a specific effect of ACTH. This is in line with the effect of the vehicle injection in the IL-1β experiment. However, in the ACTH injection experiment the effect of vehicle-injection is absent (**Figure 20 A**). The low number of animals (n=3) might partially explain this phenomenon. When the ACTH dose is

increased, the specific effect of ACTH seems to overlay the unspecific effect and both, SM-Iβ rescue mice and controls can be equally stimulated. Overall, the results from the ACTH stimulation tests suggest that the sensitivity to ACTH *in vivo* is not disturbed in SM-Iβ rescue mice, at least when higher doses of ACTH are applied.

Nevertheless, HPA axis responsiveness after stimulation with different stressors is clearly changed in SM-Iβ rescue mice and this could have some impact on their behaviour. For instance, depression is one of the diseases associated with a disturbed HPA axis regulation (Swaab et al., 2005). Indeed, in the FST, a test commonly used to address depressive behaviour in rodents (Porsolt et al., 1977), SM-Iβ rescue mice showed a tendency to reduced floating times during the test (**Figure 21 A**). In accordance with the reduced floating time, also the onset of floating was significantly later in SM-Iβ rescue mice (**Figure 21 C**). Increased floating or immobility time can be interpreted as behavioural despair (Porsolt et al., 1977) and thus SM-Iβ rescue mice show a reduced depressive-like behaviour than controls in the FST. Still, the interpretation of the behaviour observed in the FST is a topic of ongoing discussions. Originally, the test was designed to screen antidepressant drugs, because most of the commonly used antidepressant drugs caused a reduction in the immobility time in this test (Petit-Demouliere et al., 2005). Later, immobility time was also interpreted as an energy conserving behaviour (Holmes, 2003) and as a successful coping strategy in an inescapable situation (West, 1990). Independent of the interpretation, a lack of cGKI is associated with a reduced floating behaviour. Taking the interpretation as reduced depression-like behaviour as basis, it is thus tempting to suggest cGKI inhibitors as potential antidepressant drugs. Further upstream of the NO/cGMP signaling pathway, NOS inhibitors have also been shown to have antidepressant-like effects in the FST, meaning reduced immobility time, without affecting locomotor activity (Harkin et al., 1999). Also sGC inhibitors had the same effect and the NO/sGC/cGMP-pathway was thus suggested to play an important role in the mediation of immobility behaviour in the FST (Heiberg et al., 2002). On the other hand, more recent studies have suggested an antidepressant-like activity of sildenafil. The effect was not seen at clinically used doses (10 mg/kg), but at rather high doses or in combination with muscarinic receptor blockade and was suggested to act via oxytocin signalling (Brink et al., 2008; Liebenberg et al., 2011; Matsushita et al., 2012). The reduced depressive-like behaviour observed in the SM-Iβ rescue mice might be completely independent of the pathway suggested for sildenafil and can rather be attributed to the reduced CORT levels, which is the prominent phenotype in SM-Iβ rescue mice after stress exposure. It has been shown in experiments with adrenalectomized mice (Veldhuis et al., 1985) and by inhibition of CORT synthesis (Baez and Volosin, 1994) that CORT levels influence the time spent in the immobile posture in the FST. Both treatments decreased immobility time in the FST. In this study, CORT levels were not directly measured after the FST to prevent behavioural changes due to the interference. However, considering that CORT levels in SM-Iβ rescue mice were lower compared to controls after two different stressor types, and that the uncontrollable stress during the FST causes an increase in CORT levels (Baez and Volosin, 1994), one can assume that CORT levels

are also lower in SM-Iβ rescues in the FST and this could be the reason for the decreased immobility time. The rise in CORT levels during the test was also suggested to facilitate the switch in the animals' behaviour from an active stress-coping (struggling) to a more passive coping behaviour (immobility) (Baez and Volosin, 1994). Our results from the re-test, performed 24 h later, are in line with this hypothesis. SM-Iβ rescues showed a significantly increased struggling time compared to controls indicating a deficit in the adaptation to the inescapable situation (**Figure 21 B**).

The reduced adrenocortical output following stress exposure in SM-Iβ rescue mice suggests a deficit in steroid production or secretion from adrenal glands. However, comparison of adrenal glands from SM-Iβ rescue mice and controls revealed no obvious differences. Adrenal glands of SM-Iβ rescue mice were slightly lighter, but since SM-Iβ rescue mice are also smaller in size, the weight of adrenal glands was indistinguishable from controls when normalised to the body weight of the mice (**Figure 28 B**). The histology of the adrenal glands of SM-Iβ rescue mice and controls was also similar. Medullary and cortical area of SM-Iβ rescue mice were significantly smaller compared to controls, but again, when normalised to the total area of adrenal glands, no difference was observed (**Figure 29 B**). Hence, morphological differences were probably not the reason for the reduced adrenocortical output in SM-Iβ rescue mice. The results of the morphological analysis additionally support the finding that ACTH levels in the basal state in SM-Iβ rescue mice are similar to controls (**Figure 14 B**), because chronically elevated plasma ACTH levels would lead to an enlargement of the adrenal gland cortex (Lehoux et al., 1998; Ulrich-Lai et al., 2006b).

Further investigation of the steroidogenic function of adrenal glands in SM-Iβ rescue mice revealed no differences between the genotypes. Steroidogenic function was assessed by measuring CORT secretion after ACTH stimulation in dispersed cell cultures (**Figure 40**). Thus, sensitivity to ACTH in steroidogenic cells themselves seems not to be diminished in SM-Iβ rescue mice. In line with this finding, cGKI expression was undetectable in the steroidogenic cells of the zona fasciculata (**Figure 11**, **Figure 33**). Additionally, neither the expression level of enzymes involved in CORT synthesis such as StAR, Cyp11A1 and Cyp11B1 nor of the receptor for ACTH, MC2R, was up- or down-regulated confirming an intact CORT synthesis pathway in SM-Iβ rescue mice (**Figure 39**). Another factor causing the reduced CORT levels in SM-Iβ rescue mice *in vivo* might be limited substrate availability. This would not necessarily change CORT levels in the *in vitro* cell culture experiment, since ACTH stimulation was only performed for an hour and adrenal cholesterol stores are probably sufficient for this short stimulation period. Even though, the adrenal gland is able to synthesise cholesterol *de novo* from acetyl-CoA, the major source of cholesterol for steroidogenesis in mice are lipoproteins. Especially circulating HDL cholesteryl ester that is taken up via the scavenger receptor BI (SR-BI) receptor is necessary for steroidogenesis (Connelly, 2009; Kraemer, 2007; Temel et al., 1997). Interestingly, SM-Iβ rescue mice have slightly decreased plasma HDL levels (Dr. Stefan Z. Lutz, personal communication), but no obvious changes in the expression of SR-BI in adrenal glands was seen

in semi-quantitative RT-PCR experiments (**Figure 39**). Also the expression levels of SR-BI as well as LDLR in liver and adrenal gland were similar to controls making a general problem in lipoprotein metabolism rather unlikely. Additionally, Oil Red O staining of neutral lipids in adrenal glands from SM-Iβ rescue mice was indistinguishable from controls (**Figure 30**) suggesting intact cholesterol storage capacities.

Thus, neither a deficit in steroidogenesis nor a lack of substrate availability seems to cause the observed phenotype in SM-Iβ rescue mice. The difficulty in the interpretation of CORT levels, which are commonly used as a read-out of HPA axis activation, is the fact that changes in plasma CORT levels can have many reasons and might not always be located at the level of the adrenal gland. For example, enhanced degradation of CORT would lead to reduced CORT levels despite intact CORT production and secretion. The metabolic clearance rate of CORT is greatly influenced by the binding of plasma CORT to CBG. The amount of bound protein negatively correlates with the metabolic clearance rate and IL-6 has been shown to decrease CBG synthesis in human hepatocytes (Breuner and Orchinik, 2002; Emptoz-Bonneton et al., 1997; Siiteri et al., 1982). Therefore, CBG levels were investigated in SM-Iβ rescue mice. However, neither mRNA expression levels of CBG in adrenal gland and liver (**Figure 39**), nor protein expression levels in the blood (data not shown) were changed in SM-Iβ rescue mice.

Therefore, the reason for reduced CORT levels in SM-Iβ rescues is most likely located at the adrenal gland itself rather than in processes following CORT secretion. Supporting this, the comparison of cGKI expression in adrenal glands in control and SM-Iβ rescue mice revealed a clear reduction of cGKI protein in SM-Iβ rescue mice (**Figure 31**). Immunohistochemical and immunofluorescent analysis showed that cGKI expression in the capsule and in large arteries underneath the capsule is “rescued” in SM-Iβ rescue mice (**Figure 35**). But the single cGKI-positive cells interjacently located between the steroidogenic cells of the zona glomerulosa and fasciculata that could be detected in wild type and control mice were mostly not cGKI-positive in SM-Iβ rescue mice (**Figure 33**, **Figure 35**). Thus, those cells might modulate CORT secretion, and the lack of cGKI in these cells could contribute to the observed phenotype of reduced plasma CORT levels in SM-Iβ rescue mice. Further attempts to identify the characteristically shaped cGKI-positive cells in the cortex were consequently of great interest. Most of the applied markers for specific cell types (e.g. Mac2, a macrophage marker; FSP-1, a fibroblast marker; βIII-tubulin, a neuronal marker; CD31, an endothelial marker) did not co-localise with cGKI in the cortical cells (**Figure 36**). Even though, no co-localisation of CD31 and cGKI was observed, the results are not perfectly clear yet. CD31 was only found in large arteries and vessels, but stainings from other groups using different endothelial markers or a different antibody against CD31 found a more abundant CD31 expression and intense staining of the dense capillary plexus in the cortex (Berthon et al., 2010; Mallet et al., 2003). Also the cGKI-positive cells are always in close proximity to the vascular lumen, and thus it might be worth, testing another antibody against CD31 or another endothelial marker. On the other hand, cGKI expression in endothelial cells is quite controversial (Draijer et al., 1995; Joyce et al., 1986; Smolenski et al., 2000). Capsule and

vasculature showed partial co-localisation of smooth muscle markers (SMα-actin and SM22α) with cGKI (**Figure 37**). But those cells were also “rescued”, i.e. cGKI positive, in SM-Iβ rescue mice. The only marker showing partial co-localisation with cGKI in the branches of the cortical cells was vimentin (**Figure 37**). However, not all of the cortical cells stained positive for vimentin and thus the exact identity of the cGKI positive cells in the adrenal cortex still needs to be determined. CRBP-1 represents a promising candidate, since recently cGKI-positive cells in the liver have been shown to express CRBP-1 (Lutz et al., 2011), and the staining pattern in immunohistochemical stainings of parallel sections of adrenal glands was very similar to cGKI, especially in the capsule (**Figure 34**). Unfortunately, due to technical reasons a double-staining with immunofluorescence was not possible. In the liver, CRBP stains hepatic stellate (Ito) cells (Van Rossen et al., 2009), which are counted among pericytes, a type of myofibroblasts (Powell et al., 1999). Therefore, it was standing to reason that cGKI-positive cells in the adrenal gland could also represent some type of myofibroblast or fibroblast. Identification of fibroblasts and a clear distinction between smooth muscle cells, myofibroblasts and fibroblasts is difficult, since fibroblasts can transdifferentiate into myofibroblasts and also smooth muscle cells exhibit phenotypic diversity (Powell et al., 1999; Rensen et al., 2007; Serini and Gabbiani, 1999; Sorrell and Caplan, 2009). Fibroblasts are a very heterogeneous cell population and depending on the tissue can express quite different markers (Sorrell and Caplan, 2009). However, none of the fibroblast markers applied (FSP-1, Thy1.2) co-localised with cGKI (data not shown). Additionally, SM22α is also expressed in some types of fibroblasts, and thus cGKI is probably rescued in this type of fibroblasts (Assinder et al., 2009; Lawson et al., 1997). SMα-actin and vimentin could be detected in some of the cortical cells and co-localised with cGKI suggesting a myofibroblastic nature for the cells, but the staining pattern was very inconsistent. The cells of the adrenal gland capsule, for example, have already been suggested to be myofibroblasts rather than fibroblasts (Bressler, 1973). Clearly, the cGKI-positive cells in the adrenal cortex need to be further characterised to help deciphering their potential influence on CORT levels.

Assuming that the cGKI-positive cells in the adrenal cortex represent a myofibroblast- or fibroblast-like cell type, several scenarios are imaginable, in which way they could influence the adrenocortical output. As fibroblast-like cells they could secrete paracrine factors inhibiting or enhancing steroidogenesis. A large variety of paracrine factors influencing steroidogenesis have been identified such as adrenomedullary catecholamines, substance P, neuropeptide Y, PACAP (pituitary adenylate cyclase activating peptide), VIP (vasoactive intestinal polypeptide), adrenomedullin, and cytokines (Ehrhart-Bornstein et al., 1998; Nussdorfer et al., 1999). Furthermore, fibroblasts secrete a variety of cytokines (Sorrell and Caplan, 2009). But despite fibroblasts and adrenocortical cells, immune cells that extensively infiltrate the adrenal gland can also be a source for cytokine production (Bornstein et al., 2004; Chrousos, 1995). Based on the increased infiltration of macrophages into the liver of SM-Iβ rescue mice (Lutz et al., 2011), Mac2 expression was examined in adrenal glands of SM-Iβ rescue mice and controls. Neither Western blot analysis revealed an increase in Mac2 expression (**Figure 31**) nor was an enhanced

infiltration of Mac2-positive cells observed in immunofluorescent staining of SM-Iβ rescue mice (data not shown). Additionally, an activation of the IL-6 pathway, as it has been shown in the liver (Lutz et al., 2011), was not detectable by Western blot analysis of downstream molecules of the IL-6 pathway (SOCS-3, Phoshpo-Akt) (**Figure 31**). Hence, immune cells infiltrating the adrenal gland can rather be excluded as origin of the changed steroidogenic properties of SM-Iβ rescue mice.

To further proof the hypothesis of paracrine effects decreasing CORT output in adrenal glands of SM-Iβ rescue mice, adrenal slices, which possess intact cell-cell contacts in contrast to dispersed cell cultures, were stimulated with 20 nM ACTH. No differences were observed between the genotypes (**Figure 41**). There are several possible explanations for this finding. The dose of ACTH that was used (20 nM ACTH) stimulates a maximal steroidogenic response and therefore possible paracrine effects decreasing steroidogenesis might be masked. Intercellular communication might become more important when submaximal doses of ACTH are used as it has been shown for intercellular communication via gap-junctions, for example (Thomson, 1998). Hence, it should be tested, if lower ACTH concentrations cause differential results. On the other hand, the diminished CORT levels in SM-Iβ rescue mice *in vivo* could also be independent of ACTH. The results of the ACTH stimulation in dispersed adrenal cell cultures (**Figure 40**) and of the *in vivo* ACTH stimulation experiments (**Figure 20**) support this hypothesis. However, finding the ACTH-independent signal resembles the search for a needle in a haystack since a vast number of extra- and intra-adrenal factors have been shown to influence steroidogenesis independently of HPA axis activation (Ehrhart-Bornstein et al., 1998). If the cGKI-positive cells are myofibroblast-like cells, a local regulation of the blood flow is also conceivable. Besides their contractile properties, myofibroblasts secrete a variety of cytokines and are able to locally regulate blood flow. This has been shown for hepatic stellate cells (Kaneda et al., 1998; Powell et al., 1999). Increases in blood flow alone can already stimulate steroid hormone release (Hinson et al., 1986). The ACTH-independent signal leading to the potential release of a paracrine factor from cGKI-positive cells could also be of neuronal nature. Changes in the adrenal glands' sensitivity to ACTH in the course of the diurnal rhythm are regulated by splanchnic nerve innervation, for example (Dickmeis, 2009; Ulrich-Lai et al., 2006a).

In summary, the data demonstrate a role for the cGMP/cGKI signalling pathway in the modulation of HPA axis responsiveness *in vivo*. The deficit in CORT secretion seems to be independent of the stressor type and elevated plasma IL-6 levels and is probably located at the level of the adrenal gland. Possible explanations are a paracrine effect of cGKI-expressing cells in the adrenal gland reducing the sensitivity of steroidogenic cells to ACTH or a reduction in the local blood flow leading to delayed or reduced secretion of CORT. More studies are clearly necessary to decipher the underlying mechanism of the changed HPA axis responsiveness in cGKI-deficient mice.

D.2. cGKI is involved in thermogenesis

Recent studies have evoked new interest in BAT-dependent thermogenesis, since functional BAT, which so far was believed to exist only in hibernators and newborns in relevant amounts, was demonstrated in human adults (Ravussin and Galgani, 2011). NO/cGMP signalling has for a considerable time been implicated in mitochondrial biogenesis in brown adipocytes (Nisoli et al., 2003), but recently also cGKI has been implicated to be involved in mitochondrial biogenesis and was suggested to be essential for BAT differentiation (Haas et al., 2009).

Therefore, one part of the project was focussed on cGKI expression in brown adipose tissue and a potential function of cGKI in thermogenesis. cGKI expression in brown adipose tissue was confirmed by Western blot analysis and immunohistochemistry (**Figure 12** and **Figure 13**). In cGKI KO mice the immunostain signal was completely absent, confirming its specificity (**Figure 12**). The immunohistochemistry revealed strong cGKI expression in the vasculature, in characteristically shaped cells with long branches, and in peripheral nerve bundles (**Figure 13**). The latter were identified by staining with βIII-tubulin (**Figure 44**). Since an immunohistochemical double staining technique was used, it was difficult to judge whether the cGKI-positive cells are concurrently βIII-tubulin-positive or represent one of the other cell-types present in peripheral nerves such as fibroblasts or pericytes (Joseph et al., 2004). In SM-Iβ rescue mice as well as in cGKI brain-KO mice the cGKI-positive cells in the nerve bundles can not be detected suggesting a nervous origin (**Figure 44 C**), but further studies using immunofluorescence double staining are necessary to clarify this. The identity of the characteristically shaped cGKI-positive cells distributed in BAT is also not clear yet. cGKI expression is not detectable in these cells in both SM-Iβ rescue and cGKI brain-KO mice. Again this suggests a cell type of nervous origin. And indeed X-Gal staining of R26R/Nes-Cre reporter mice revealed a blue staining pattern in those cells indicating Cre recombinase expression and thus confirming the absence of cGKI expression in this cell type in cGKI brain-KO mice (**Figure 45**). Additionally, other cell type markers such as the fibroblast markers CRBP-1 and FSP-1, the macrophage marker Mac2, and the endothelial marker CD31 did not show any immunoreactivity in these cells (data not shown). On the other hand, βIII-tubulin, a neuronal marker, was also not detectable in these cells (data not shown). Therefore, the exact identity of the cGKI-positive cells in BAT needs to be further characterised. Nevertheless, in line with the immunohistochemical data, cGKI expression in protein lysates of BAT in SM-Iβ rescue and cGKI brain-KO mice is reduced compared to controls (**Figure 42**).

In order to study a potential physiological function of cGKI in thermoregulation, transmitters were implanted into SM-Iβ rescue and cGKI brain-KO mice to measure core body temperature telemetrically. At room temperature (19-21°C) SM-Iβ rescue mice showed a slightly, but significantly decreased core body temperature compared to controls during the light phase (**Figure 22**). This suggests a role for cGKI in thermoregulation. But cGKI function in thermoregulation under room temperature conditions seems not to be centrally regulated, because cGKI brain-KO mice had core body temperatures comparable to controls (**Figure 23**).

Surprisingly, cGKI brain-KO mice showed increased locomotor activity during the dark phase, which is in contrast to earlier findings, in which infrared monitoring of locomotor activity in male cGKI brain-KO mice was indistinguishable from controls (Lutz et al., 2011). Also Langmesser et al. (2009) detected no differences in the wheel-running activity in male cGKI brain-KO mice compared to control mice. The discrepancy could be gender-related, because only female mice were taken for the telemetric temperature measurements. In the study performed by Lutz et al. also energy expenditure was comparable to controls in cGKI brain-KO mice, but SM-Iβ rescue mice had increased energy expenditure during the light phase. The increased metabolic rate could represent a compensatory mechanism to defend core body temperature to the permanent cold stress. Under laboratory temperature conditions, which are below the thermoneutral zone of rodents, mice need to permanently produce heat to defend their core body temperature and thus the metabolic rate would also be increased (Cannon and Nedergaard, 2011).

Cold stress induced only a slight drop of ~2 °C in core body temperature in SM-Iβ rescue mice and controls, but no difference between the genotypes was observed (**Figure 24** and **Figure 25**). The results are in contrast to earlier cold stress experiments in SM-Iβ rescue mice, in which rectal temperature was significantly decreased in SM-Iβ rescue mice compared to controls (Dr. Susanne Feil, personal communication). The discrepancy is most likely due to experimental differences, because conditions for the cold stress were still in the process of optimisation during the core body temperature experiments in SM-Iβ rescue mice. Thus, temperature fluctuations during the experiment can not be excluded. Therefore, the cold stress experiments in SM-Iβ rescue mice would need to be repeated to make final conclusions. On the other hand, rectal temperature in cold-stressed SM-Iβ rescue mice could be lower without an effect in core body temperature, since peripheral temperature decreases faster than core body temperature, of course. However, cGKI brain-KO mice lost their core body temperature more rapidly than controls during cold exposure. Whether the thermoregulatory problems in cGKI brain-KO mice are due to the lack of cGKI in the brain or BAT is not clear yet and both could contribute to the observed phenotype. However, usually a 4-6 h cold stress is not sufficient to recruit the capacity of BAT-dependent non-shivering thermogenesis (Cannon and Nedergaard, 2004). On the other hand, a room temperature of 19-21 °C is far below the zone of thermoneutrality in mice (30 °C) and can be accounted as a constant cold stress (Gordon, 1990; Karp, 2012). Therefore, in mice housed below 20 °C an addtional temperature challenge, such as cold stress, leads to the recruitment of non-shivering thermogenetic capacity (Cannon and Nedergaard, 2004). This non-shivering thermogenesis in cold acclimated mice is completely dependent on BAT and induced by norepinephrine released from nerve endings of the SNS in the brown adipose tissue (Lowell and Spiegelman, 2000). The increased norepinephrine levels observed in the basal state in cGKI KO and cGKI brain-KO mice (**Figure 16**) indicate an involvement of the SNS in the thermoregulatory phenotype. In any case, further studies are needed to learn more about the mechanism how cGKI contributes to thermoregulation. Since cGKI is expressed in the hypothalamus, BAT and in peripheral nerves innervating BAT, a contribution at various levels is possible. Nonetheless, the

results from the cold stress experiments confirm the assumption that cGKI plays an important role in thermogenesis.

During the cold stress, some of the cGKI brain-KO mice actually underwent torpor, indicating an inability to keep their core body temperature. Torpor is a hypothermic and hypometabolic state that is rather known from hibernators, but also mice can undergo shallow torpor bouts in response to cold stress or caloric restriction to save energy. In contrast to hibernators which can lower their temperature to almost the same level as the ambient temperature (~4°C), mice only allow their body temperature to fall to a minimum of ~20 °C (Swoap, 2008). A rapid decrease in core body temperature and complete inactivity were taken as hints on torpor. The exact signalling pathways leading to the induction and entry into torpor are not clear yet. UCP-1 seems to be more important for the arousal than for torpor entry (Oelkrug et al., 2011), while mice lacking norepinephrine are not able to enter torpor upon fasting (Swoap and Weinshenker, 2008). Ghrelin and leptin also play an important role in torpor induction (Gavrilova et al., 1999; Swoap, 2008). Leptin is released from white fat depots during fasting and low leptin levels act as the entry signal for torpor (Gavrilova et al., 1999). Secretion of leptin from adipocytes is in direct proportion to the adipose mass (Morris and Rui, 2009). Also leptin was not measured directly in SM-Iβ rescue mice, their lower total adipose mass (Lutz et al., 2011) suggests low circulating leptin levels and might enable them to enter torpor more easily during fasting than controls. Indeed 4 out of 9 SM-Iβ rescue mice entered a torpor-like state during fasting compared to only 1 control animal. This caused significantly lower core body temperatures in SM-Iβ rescue mice than in controls. On the other hand, only 1 out of 10 cGKI brain-KO mice entered torpor during fasting, but 4 out of 10 cGKI brain-KO mice entered torpor during cold stress. Additionally, cGKI brain-KO mice have normal body weights (Lutz et al., 2011) and therefore most likely normal circulating leptin levels. Hence, low leptin levels might not be the only reason for increased torpor entry in cGKI-deficient mice. Leptin activates among others leptin receptors in the dorsomedial hypothalamus (DMH) (Elmquist et al., 1998), in which cGKI is highly expressed (Feil et al., 2005b) and which has been implicated in cold-induced thermogenesis (Dimicco and Zaretsky, 2007). Thus, the DMH could provide another site for cGKI action in thermoregulation.

In summary, cGKI-deficient mice showed deficits in thermoregulation under basal conditions and following cold and fasting stress. cGKI expression in several tissues such as the hypothalamus, BAT and SNS could contribute to the observed phenotype. Further studies are obviously needed to learn more about cGKI's role in thermoregulation (see D.3.2).

D.3. Future prospects

D.3.1. Resolving the role of cGKI in HPA axis modulation

To learn more about the mechanism causing the observed phenotype of reduced HPA axis responsiveness in cGKI-deficient mice, the identification of the cGKI-positive cells in the adrenal cortex is crucial. The performed experiments hint on a fibroblastic-/myofibroblastic nature, and thus further characterisation should focus on fibroblastic markers. As mentioned above, no general fibroblast marker is known. Also no specific marker for adrenal gland fibroblasts has been identified, because so far these cells have not aroused much interest. From the fibroblast markers tested, only vimentin co-localised with cGKI, but the staining itself was rather weak. Other fibroblast markers should therefore be used to confirm the identity of the cGKI-positive cells in the adrenal gland. Antibodies against CD34 (undifferentiated fibroblasts), fibroblast surface antigen (SFA), or prolyl-4-hydroxylase (activated fibroblasts) could be used for this purpose (Krenning et al., 2010). Additionally, the vasculature of the adrenal glands should be visualised by staining with tomato lectin to ensure an intact vascularisation in SM-Iβ rescue mice and to confirm the proximity of cGKI-positive cells to the vascular lumen.

As mentioned in D.1, the stimulation of the adrenal slices with maximal ACTH concentrations might mask paracrine effects and therefore lower doses should also be tested. The adrenal slice preparations are additionally a good model to test, if other signalling molecules are involved in the modulation of steroidogenesis (e.g. VIP, ACh, endothelin, PACAP) and the supernatant of slices from SM-Iβ rescue and control mice can be compared and screened for the paracrine factor (e.g. cytokines) potentially secreted by the cGKI-positive cells.

If no differences are observed in the adrenal slice experiments, further *in vivo* experiments can be performed to resolve the mechanism of reduced CORT levels. First of all, the ACTH stimulation experiments can be repeated with higher ACTH concentrations and with a preceding injection of dexamethasone to block endogenous ACTH secretion (Karpac et al., 2008). Since no differences were observed in basal ACTH levels between SM-Iβ rescue mice and control, preceding dexamethasone blocking should also not cause any differences in the results.

Another interesting *in vivo* experiment would be blood flow measurements in adrenal glands of SM-Iβ rescue and control mice in the basal state and after stimulation. Regional blood flow studies can be done with a microsphere technique. Regional organ perfusion can be estimated by the injection of non-radioactive microspheres (e.g. FluoSpheres® by Life Technologies) into the blood system at the desired location and counting of microspheres trapped in the capillaries of the investigated organ. If the size of the microspheres is appropriately chosen, the number of trapped microspheres is proportional to the regional blood flow (Bassingthwaighte, 1990; Heymann et al., 1977). For instance, hepatic arterial blood flow in the mouse has already been measured with this technique (Vollmar and Menger, 2009).

Even though, no differences in basal ACTH levels were found, and elevated ACTH levels after IL-1β induced stress in SM-Iβ rescues are most likely a consequence of the reduced CORT levels (drawback), analysis of pituitary gland-specific cGKI KO mice would be worthwile, since cGKI is highly expressed in the pars intermedia and a defect at the level of the pituitary gland should be excluded. These mice are generated by crossing POMC Cre mice (Akagi et al., 1997), in which expression of Cre recombinase is under the control of the proopiomelanocortin (POMC) promoter, to “floxed” cGKI mice. POMC expression is restricted to the pars intermedia and few cells in the pars distalis of the pituitary gland as well as to the arcuate nucleus in the hypothalamus (Schmidt et al., 2009). So far, only preliminary data could be obtained from this mouse line, because very few mice were available due to the bad breeding performance of these mutants.

Furthermore, an isoform specific effect can currently not be excluded, since all experiments were performed in SM-Iβ rescue mice. Due to breeding problems not enough SM-Iα rescue mice were available for the experiments. Nevertheless, analysis of SM-Iα rescue mice could provide important information about the mechanism of reduced CORT levels. cGKIα can, in contrast to cGKIβ, additionally be activated in an NO/cGMP-independent manner via hydrogenperoxide-induced dimerisation (Burgoyne et al., 2007). Therefore, NO/cGMP-independent vasorelaxation might provide another possibility for regional blood flow regulation influencing adrenocortical output. Since only SM-Iβ rescue mice, in which the cGKIβ isoform is restored in smooth muscle cells, were used in this study, the observed phenotype might be due to the lack of cGKIα in smooth muscle cells. According to the mRNA expression levels, both cGKI isoforms are present in wild type adrenal glands (C.3.1.6). cGKIα might be more important than cGKIβ in the well vascularised adrenal gland since it can additionally be activated NO/cGMP independently.

D.3.2. Deciphering the role of cGKI in thermogenesis

The obtained results represent just the beginning of this project, and numerous experiments are needed to further characterise cGKI function in thermoregulation and the underlying mechanism.

As in the adrenal gland, the cGKI-positive cells in BAT need to be further characterised. Morphologically the cells resemble mesenchymal stem cells (MSCs). Also in their study, Haas et al. (2009) isolated MSCs from cGKI KO mice and showed deficits in their differentiation potential into adipocytes. As multipotent adult stem cells, MSCs are additionally able to differentiate into cells of the osteogenic, myogenic and chondrogenic lineage (Zuk et al., 2002). Hence, it would be interesting to see, if these differentiation processes are also impaired in cGKI KO mice. One possibility are impedance measurements, since it was shown that differentiation of adipose-derived stem cells into osteoblasts and adipocytes can be distinguished using impedance sensing (Bagnaninchi and Drummond, 2011).To prove that cGKI-positive cells in BAT are indeed MSCs is rather complicated, because no marker exclusively for MSCs exists (Chamberlain et al., 2007; Docheva et al., 2008). Nestin is a potential marker shown to be expressed in bone-marrow

derived MSCs under certain culture conditions (Wislet-Gendebien et al., 2005). However, usually a combination of several surface markers, e.g. CD29, CD44, CD105, and Sca-1, is used for the identification of MSCs (Sung et al., 2008). Antibodies against these surface markers can also be used to isolate MSCs from BAT via MACS (magnetic activated cell sorting) or FACS (fluorescent activated cell sorting). The isolated cells could then be investigated in terms of cGKI expression and differentiation potential.

Further analysis of BAT from SM-Iβ rescue mice and cGKI brain-KO mice in terms of genes involved in thermogenesis and BAT differentiation like UCP-1, PPARγ (peroxisome proliferator-activated receptor γ), and PGC-1α (PPARγ coactivator-1α) would also be interesting, since protein levels of UCP-1 and PPARγ, for example, have been shown to be reduced in BAT of cGKI KO mice (Haas et al., 2009).

To learn more about the role of cGKI in the noradrenergic innervation of BAT, tissue and plasma samples have been taken after the cold stress experiments, and these can now be analysed in terms of catecholamine content. Additionally norepinephrine injections could be used to test the capacity for non-shivering thermogenesis in SM-Iβ rescue and cGKI brain-KO mice. An increase in the response to NE injections is considered to be equivalent to an increase in thermogenic capacity (Cannon and Nedergaard, 2011; Jansky, 1973).

Cold stress has also been shown to increase the accumulation of 18-Fluorodeoxyglucose (^{18}F-FDG) in BAT (Tatsumi et al., 2004) and this accumulation is associated with increased thermogenesis (Carter et al., 2011). Therefore, positron emission tomography (PET) measurements of ^{18}F-FDG uptake in BAT of cold-stressed cGKI brain-KO mice are currently performed. Furthermore, BAT temperature as an indicator of BAT thermogenesis might also be measured directly with DSI transmitters (model TA-F40 W/TP*) in parallel with core body temperature and activity. With this method, recruitment of BAT during cold stress could be distinguished from non-shivering thermogenesis.

E Summary

The cGMP-dependent protein kinase type I (cGKI) represents an important downstream component of nitric oxide/cyclic guanosine monophosphate (NO/cGMP) signalling. It mediates many physiological effects of NO such as smooth muscle relaxation and platelet inhibition. The expression of cGKI in various other tissues suggests additional functions that still need to be elucidated. In the present work, a potential role of cGKI in the stress response and in thermogenesis was investigated.

Previous work indicated that NO/cGMP signalling modulates the activity of the hypothalamic-pituitary-adrenal (HPA) axis, the main mediator of the stress response. However, it is unknown whether these effects are mediated by cGKI. Within the scope of this project, cGKI expression was demonstrated in tissues of the HPA axis including the hypothalamic paraventricular nucleus, pituitary and adrenal glands. A potential physiological function of cGKI in HPA axis regulation was investigated in two cGKI-deficient mouse models: (1) cGKI smooth muscle-specific rescue mice (SM-Iβ rescue mice), in which expression of the cGKIβ isoform has been restored selectively in smooth muscle cells of cGKI knock-out (KO) mice, and (2) neuron-specific cGKI KO mice (referred to as cGKI brain-KO mice) generated via Cre/*loxP* technology. Stimulation of the HPA axis was obtained by injection of interleukin-1β (IL-1β). IL-1β injections resulted in increased plasma concentrations of adrenocorticotropic hormone (ACTH) and corticosterone (CORT) in SM-Iβ rescue and cGKI brain-KO mice. cGKI brain-KO mice responded like control mice demonstrating that cGKI in neurons is most likely not involved in IL-1β induced activation of the HPA axis. However, SM-Iβ rescue mice showed after IL-1β stimulation significantly higher ACTH, but lower CORT levels than control littermates indicating a reduced sensitivity of their adrenal glands to ACTH. The altered stress response was not limited to an immunological challenge, because also restraint stress, a mixed physical and psychological stressor, led to a diminished rise in CORT levels in SM-Iβ rescue mice. The restraint stress experiment additionally revealed that the reduced CORT levels were independent from elevated plasma IL-6 levels in older (7-month-old) SM-Iβ rescue mice. The adrenal glands of SM-Iβ rescue mice appeared morphologically and histologically inconspicuous. Interestingly, cGKI expression was not detectable in parenchymal steroidogenic cells, but in fibroblast-like cells located between the CORT-producing cells of the zona fasciculata suggesting a paracrine effect of these cGKI-positive cells on CORT production and/or secretion. The potentially reduced sensitivity of adrenal glands of SM-Iβ rescue mice to ACTH was analysed both *in vitro* and *in vivo*. ACTH-induced CORT secretion was not significantly different in adrenal slices and primary cells derived from SM-Iβ rescue and control mice demonstrating that, *in vitro*, steroidogenic cells of SM-Iβ rescue mice respond normally to the tested concentrations of ACTH. *In vivo* stimulation of SM-Iβ rescue mice with different doses of ACTH caused controversial results. Thus, it is unclear whether the *in vivo* sensitivity to ACTH is disturbed in SM-Iβ rescue mice or whether cGKIs' influence on the plasma CORT levels is independent of ACTH.

In the second part of this work, the function of cGKI in thermogenesis, which is involved in the response to cold and fasting stress, was investigated *in vivo* in SM-Iβ rescue and cGKI brain-KO mice. Indeed, cGKI expression in brown adipose tissue (BAT), the main site of heat production during non-shivering thermogenesis, could be demonstrated. Within BAT, cGKI was detected in the vasculature, peripheral nerves and distinct cells, which need to be further characterised. The adipocytes were not stained for cGKI. Core body temperature was measured telemetrically at room temperature and during cold and fasting stress. At room temperature, SM-Iβ rescue mice showed during the light phase a significantly lower core body temperature than controls. Since cGKI brain-KO mice had core body temperatures indistinguishable from controls, the function of cGKI in thermoregulation at room temperature is probably not localised in the nervous system. However, following cold and fasting stress, core body temperature dropped more rapidly in cGKI brain-KO mice than in control mice. These data show that cGKI-dependent pathways stimulate thermogenesis *in vivo*. Whether this function is due to a role of cGKI in brain nuclei involved in thermoregulation or reflects a function of cGKI in BAT, in which cGKI is also reduced in brain-KO mice, is presently not clear.

In summary, this study demonstrates a role for cGKI in the modulation of the HPA axis as well as in thermogenesis in mice, but the underlying cellular and molecular mechanisms need to be further deciphered. In the future, cGKI might provide an interesting target for the treatment of diseases caused by HPA axis dysregulation such as depression or for BAT-dependent treatment of adipositas.

F References

Adams, M.L., Nock, B., Truong, R., and Cicero, T.J. (1992). Nitric oxide control of steroidogenesis: endocrine effects of NG-nitro-L-arginine and comparisons to alcohol. Life Sci *50*, PL35-40.

Akagi, K., Sandig, V., Vooijs, M., Van der Valk, M., Giovannini, M., Strauss, M., and Berns, A. (1997). Cre-mediated somatic site-specific recombination in mice. Nucleic Acids Res *25*, 1766-1773.

Andrews, M.H., Wood, S.A., Windle, R.J., Lightman, S.L., and Ingram, C.D. (2012). Acute glucocorticoid administration rapidly suppresses basal and stress-induced hypothalamo-pituitary-adrenal axis activity. Endocrinology *153*, 200-211.

Andric, S.A., Janjic, M.M., Stojkov, N.J., and Kostic, T.S. (2007). Protein kinase G-mediated stimulation of basal Leydig cell steroidogenesis. Am J Physiol Endocrinol Metab *293*, E1399-1408.

Andric, S.A., Janjic, M.M., Stojkov, N.J., and Kostic, T.S. (2010). Sildenafil treatment in vivo stimulates Leydig cell steroidogenesis via the cAMP/cGMP signaling pathway. Am J Physiol Endocrinol Metab *299*, E544-550.

Antoni, F.A. (1993). Vasopressinergic control of pituitary adrenocorticotropin secretion comes of age. Front Neuroendocrinol *14*, 76-122.

Arancio, O., Antonova, I., Gambaryan, S., Lohmann, S.M., Wood, J.S., Lawrence, D.S., and Hawkins, R.D. (2001). Presynaptic role of cGMP-dependent protein kinase during long-lasting potentiation. J Neurosci *21*, 143-149.

Armario, A., Valles, A., Dal-Zotto, S., Marquez, C., and Belda, X. (2004). A single exposure to severe stressors causes long-term desensitisation of the physiological response to the homotypic stressor. Stress *7*, 157-172.

Assinder, S.J., Stanton, J.A., and Prasad, P.D. (2009). Transgelin: an actin-binding protein and tumour suppressor. Int J Biochem Cell Biol *41*, 482-486.

Baez, M., and Volosin, M. (1994). Corticosterone influences forced swim-induced immobility. Pharmacol Biochem Behav *49*, 729-736.

Bagnaninchi, P.O., and Drummond, N. (2011). Real-time label-free monitoring of adipose-derived stem cell differentiation with electric cell-substrate impedance sensing. Proc Natl Acad Sci U S A *108*, 6462-6467.

Balcombe, J.P., Barnard, N.D., and Sandusky, C. (2004). Laboratory routines cause animal stress. Contemp Top Lab Anim Sci *43*, 42-51.

Bassett, J.R., and West, S.H. (1997). Vascularization of the adrenal cortex: its possible involvement in the regulation of steroid hormone release. Microsc Res Tech *36*, 546-557.

Bassingthwaighte, J.B. (1990). Microcirculatory considerations in NMR flow imaging. Magn Reson Med *14*, 172-178.

Beavo, J.A., and Brunton, L.L. (2002). Cyclic nucleotide research -- still expanding after half a century. Nat Rev Mol Cell Biol *3*, 710-718.

Bender, A.T., and Beavo, J.A. (2006). Cyclic nucleotide phosphodiesterases: molecular regulation to clinical use. Pharmacol Rev *58*, 488-520.

Berkenbosch, F., van Oers, J., del Rey, A., Tilders, F., and Besedovsky, H. (1987). Corticotropin-releasing factor-producing neurons in the rat activated by interleukin-1. Science *238*, 524-526.

Berthon, A., Sahut-Barnola, I., Lambert-Langlais, S., de Joussineau, C., Damon-Soubeyrand, C., Louiset, E., Taketo, M.M., Tissier, F., Bertherat, J., Lefrancois-Martinez, A.M., *et al.* (2010). Constitutive beta-catenin activation induces adrenal hyperplasia and promotes adrenal cancer development. Hum Mol Genet *19*, 1561-1576.

Besedovsky, H., del Rey, A., Sorkin, E., and Dinarello, C.A. (1986). Immunoregulatory feedback between interleukin-1 and glucocorticoid hormones. Science *233*, 652-654.

Bethin, K.E., Vogt, S.K., and Muglia, L.J. (2000). Interleukin-6 is an essential, corticotropin-releasing hormone-independent stimulator of the adrenal axis during immune system activation. Proc Natl Acad Sci U S A *97*, 9317-9322.

Bicknell, A.B. (2008). The tissue-specific processing of pro-opiomelanocortin. J Neuroendocrinol *20*, 692-699.

Biel, M., Zong, X., Ludwig, A., Sautter, A., and Hofmann, F. (1999). Structure and function of cyclic nucleotide-gated channels. Rev Physiol Biochem Pharmacol *135*, 151-171.

Bielohuby, M. (2007). The mouse adrenal gland : age- and gender- dependent alterations of growth and function.

Bisgaier, C.L., Chanderbhan, R., Hinds, R.W., and Vahouny, G.V. (1985). Adrenal cholesterol esters as substrate source for steroidogenesis. J Steroid Biochem *23*, 967-974.

Bornstein, S.R. (2000). Cytokines and the adrenal cortex: basic research and clinical implications. Curr Opin Endocrinol Diabetes and Obes *7*, 128-137.

Bornstein, S.R., and Chrousos, G.P. (1999). Clinical review 104: Adrenocorticotropin (ACTH)- and non-ACTH-mediated regulation of the adrenal cortex: neural and immune inputs. J Clin Endocrinol Metab *84*, 1729-1736.

Bornstein, S.R., Rutkowski, H., and Vrezas, I. (2004). Cytokines and steroidogenesis. Mol Cell Endocrinol *215*, 135-141.

Bornstein, S.R., Stratakis, C.A., and Chrousos, G.P. (1999). Adrenocortical tumors: recent advances in basic concepts and clinical management. Ann Intern Med *130*, 759-771.

Boyden, E.S., Katoh, A., and Raymond, J.L. (2004). Cerebellum-dependent learning: the role of multiple plasticity mechanisms. Annu Rev Neurosci *27*, 581-609.

Brann, D.W., Bhat, G.K., Lamar, C.A., and Mahesh, V.B. (1997). Gaseous transmitters and neuroendocrine regulation. Neuroendocrinology *65*, 385-395.

Breslow, M.J. (1992). Regulation of adrenal medullary and cortical blood flow. Am J Physiol *262*, H1317-1330.

Bressler, R.S. (1973). Myoid cells in the capsule of the adrenal gland and in monolayers derived from cultured adrenal capsules. Anat Rec *177*, 525-531.

Breuner, C.W., and Orchinik, M. (2002). Plasma binding proteins as mediators of corticosteroid action in vertebrates. J Endocrinol *175*, 99-112.

Briassoulis, G., Damjanovic, S., Xekouki, P., Lefebvre, H., and Stratakis, C.A. (2011). The glucocorticoid receptor and its expression in the anterior pituitary and the adrenal cortex: a source of variation in hypothalamic-pituitary-adrenal axis function; implications for pituitary and adrenal tumors. Endocr Pract *17*, 941-948.

Bright, G.M. (1995). Corticosteroid-binding globulin influences kinetic parameters of plasma cortisol transport and clearance. J Clin Endocrinol Metab *80*, 770-775.

Bright, G.M., and Darmaun, D. (1995). Corticosteroid-binding globulin modulates cortisol concentration responses to a given production rate. The Journal of clinical endocrinology and metabolism *80*, 764-769.

Brink, C.B., Clapton, J.D., Eagar, B.E., and Harvey, B.H. (2008). Appearance of antidepressant-like effect by sildenafil in rats after central muscarinic receptor blockade: evidence from behavioural and neuro-receptor studies. J Neural Transm *115*, 117-125.

Brunton, P.J., Sausbier, M., Wietzorrek, G., Sausbier, U., Knaus, H.G., Russell, J.A., Ruth, P., and Shipston, M.J. (2007). Hypothalamic-pituitary-adrenal axis hyporesponsiveness to restraint stress in mice deficient for large-conductance calcium- and voltage-activated potassium (BK) channels. Endocrinology *148*, 5496-5506.

Bryan, N.S., Bian, K., and Murad, F. (2009). Discovery of the nitric oxide signaling pathway and targets for drug development. Front Biosci *14*, 1-18.

Burgoyne, J.R., Madhani, M., Cuello, F., Charles, R.L., Brennan, J.P., Schroder, E., Browning, D.D., and Eaton, P. (2007). Cysteine redox sensor in PKGIa enables oxidant-induced activation. Science *317*, 1393-1397.

Cannon, B., and Nedergaard, J. (2004). Brown adipose tissue: function and physiological significance. Physiol Rev *84*, 277-359.

Cannon, B., and Nedergaard, J. (2011). Nonshivering thermogenesis and its adequate measurement in metabolic studies. J Exp Biol *214*, 242-253.

Carter, E.A., Bonab, A.A., Paul, K., Yerxa, J., Tompkins, R.G., and Fischman, A.J. (2011). Association of heat production with 18F-FDG accumulation in murine brown adipose tissue after stress. J Nucl Med *52*, 1616-1620.

Chamberlain, G., Fox, J., Ashton, B., and Middleton, J. (2007). Concise review: mesenchymal stem cells: their phenotype, differentiation capacity, immunological features, and potential for homing. Stem Cells *25*, 2739-2749.

Charmandari, E., Tsigos, C., and Chrousos, G. (2005). Endocrinology of the stress response. Annu Rev Physiol *67*, 259-284.

Chen, C., and Tonegawa, S. (1997). Molecular genetic analysis of synaptic plasticity, activity-dependent neural development, learning, and memory in the mammalian brain. Annu Rev Neurosci *20*, 157-184.

Chida, D., Nakagawa, S., Nagai, S., Sagara, H., Katsumata, H., Imaki, T., Suzuki, H., Mitani, F., Ogishima, T., Shimizu, C.*, et al.* (2007). Melanocortin 2 receptor is required for adrenal gland development, steroidogenesis, and neonatal gluconeogenesis. Proc Natl Acad Sci U S A *104*, 18205-18210.

Chrousos, G.P. (1995). The hypothalamic-pituitary-adrenal axis and immune-mediated inflammation. N Engl J Med *332*, 1351-1362.

Chrousos, G.P. (2009). Stress and disorders of the stress system. Nat Rev Endocrinol *5*, 374-381.

Cinti, S. (2007). The Adipose Organ. In, G. Fantuzzi, and T. Mazzone, eds. (Totowa, NJ: Humana Press Inc.), pp. 3-19.

Connelly, M.A. (2009). SR-BI-mediated HDL cholesteryl ester delivery in the adrenal gland. Mol Cell Endocrinol *300*, 83-88.

Conti, M., and Beavo, J. (2007). Biochemistry and physiology of cyclic nucleotide phosphodiesterases: essential components in cyclic nucleotide signaling. Annu Rev Biochem *76*, 481-511.

Costa, A., Trainer, P., Besser, M., and Grossman, A. (1993). Nitric oxide modulates the release of corticotropin-releasing hormone from the rat hypothalamus in vitro. Brain Res *605*, 187-192.

Cymeryng, C.B., Dada, L.A., and Podesta, E.J. (1998). Effect of nitric oxide on rat adrenal zona fasciculata steroidogenesis. J Endocrinol *158*, 197-203.

Dallman, M.F. (2005). Fast glucocorticoid actions on brain: back to the future. Front Neuroendocrinol *26*, 103-108.

Dallman, M.F., Engeland, W.C., Rose, J.C., Wilkinson, C.W., Shinsako, J., and Siedenburg, F. (1978). Nycthemeral rhythm in adrenal responsiveness to ACTH. Am J Physiol *235*, R210-218.

Davies, E., Omer, S., Buckingham, J.C., Morris, J.F., and Christian, H.C. (2007). Expression and externalization of annexin 1 in the adrenal gland: structure and function of the adrenal gland in annexin 1-null mutant mice. Endocrinology *148*, 1030-1038.

de Kloet, E.R., Joels, M., and Holsboer, F. (2005). Stress and the brain: from adaptation to disease. Nat Rev Neurosci *6*, 463-475.

Delarue, C., Contesse, V., Lenglet, S., Sicard, F., Perraudin, V., Lefebvre, H., Kodjo, M., Leboulenger, F., Yon, L., Gallo-Payet, N.*, et al.* (2001). Role of neurotransmitters and neuropeptides in the regulation of the adrenal cortex. Rev Endocr Metab Disord *2*, 253-267.

Denef, C. (2008). Paracrinicity: the story of 30 years of cellular pituitary crosstalk. J Neuroendocrinol *20*, 1-70.

Dickmeis, T. (2009). Glucocorticoids and the circadian clock. J Endocrinol *200*, 3-22.

Dijkstra, I., Binnekade, R., and Tilders, F.J. (1996). Diurnal variation in resting levels of corticosterone is not mediated by variation in adrenal responsiveness to adrenocorticotropin but involves splanchnic nerve integrity. Endocrinology *137*, 540-547.

Dimicco, J.A., and Zaretsky, D.V. (2007). The dorsomedial hypothalamus: a new player in thermoregulation. Am J Physiol Regul Integr Comp Physiol *292*, R47-63.

Djordjević, J., Cvijić, G., and Davidović, V. (2003). Different activation of ACTH and corticosterone release in response to various stressors in rats. Physiol Res *52*, 67-72.

Docheva, D., Haasters, F., and Schieker, M. (2008). Mesenchymal Stem Cells and Their Cell Surface Receptors. Curr Rheumatol Rev *4*, 155-160.

Draijer, R., Vaandrager, A.B., Nolte, C., de Jonge, H.R., Walter, U., and van Hinsbergh, V.W. (1995). Expression of cGMP-dependent protein kinase I and phosphorylation of its substrate, vasodilator-stimulated phosphoprotein, in human endothelial cells of different origin. Circ Res *77*, 897-905.

Ducsay, C.A., and Myers, D.A. (2011). eNOS activation and NO function: differential control of steroidogenesis by nitric oxide and its adaptation with hypoxia. J Endocrinol *210*, 259-269.

Dunn, A.J. (2000). Cytokine activation of the HPA axis. Ann N Y Acad Sci *917*, 608-617.

Edwards, A.V., Jones, C.T., and Bloom, S.R. (1986). Reduced adrenal cortical sensitivity to ACTH in lambs with cut splanchnic nerves. J Endocrinol *110*, 81-85.

Ehrhart-Bornstein, M., Hinson, J.P., Bornstein, S.R., Scherbaum, W.A., and Vinson, G.P. (1998). Intraadrenal interactions in the regulation of adrenocortical steroidogenesis. Endocr Rev *19*, 101-143.

Elmquist, J.K., Maratos-Flier, E., Saper, C.B., and Flier, J.S. (1998). Unraveling the central nervous system pathways underlying responses to leptin. Nat Neurosci *1*, 445-450.

Emptoz-Bonneton, A., Crave, J.C., LeJeune, H., Brebant, C., and Pugeat, M. (1997). Corticosteroid-binding globulin synthesis regulation by cytokines and glucocorticoids in human hepatoblastoma-derived (HepG2) cells. J Clin Endocrinol Metab *82*, 3758-3762.

Engelmann, M., Landgraf, R., and Wotjak, C.T. (2004). The hypothalamic-neurohypophysial system regulates the hypothalamic-pituitary-adrenal axis under stress: an old concept revisited. Front Neuroendocrinol *25*, 132-149.

Ericsson, A., Liu, C., Hart, R.P., and Sawchenko, P.E. (1995). Type 1 interleukin-1 receptor in the rat brain: distribution, regulation, and relationship to sites of IL-1-induced cellular activation. J Comp Neurol *361*, 681-698.

Falkenstein, E., Tillmann, H.C., Christ, M., Feuring, M., and Wehling, M. (2000). Multiple actions of steroid hormones--a focus on rapid, nongenomic effects. Pharmacol Rev *52*, 513-556.

Feil, R. (2007). Conditional somatic mutagenesis in the mouse using site-specific recombinases. Handb Exp Pharmacol, 3-28.

Feil, R., Hartmann, J., Luo, C., Wolfsgruber, W., Schilling, K., Feil, S., Barski, J.J., Meyer, M., Konnerth, A., De Zeeuw, C.I.*, et al.* (2003). Impairment of LTD and cerebellar learning by Purkinje cell-specific ablation of cGMP-dependent protein kinase I. J Cell Biol *163*, 295-302.

Feil, R., Hofmann, F., and Kleppisch, T. (2005a). Function of cGMP-dependent protein kinases in the nervous system. Rev Neurosci *16*, 23-41.

Feil, R., Holter, S.M., Weindl, K., Wurst, W., Langmesser, S., Gerling, A., Feil, S., and Albrecht, U. (2009). cGMP-dependent protein kinase I, the circadian clock, sleep and learning. Commun Integr Biol *2*, 298-301.

Feil, R., and Kleppisch, T. (2008). NO/cGMP-dependent modulation of synaptic transmission. Handb Exp Pharmacol, 529-560.

Feil, S., Zimmermann, P., Knorn, A., Brummer, S., Schlossmann, J., Hofmann, F., and Feil, R. (2005b). Distribution of cGMP-dependent protein kinase type I and its isoforms in the mouse brain and retina. Neuroscience *135*, 863-868.

Ferns, G.A., and Avades, T.Y. (2000). The mechanisms of coronary restenosis: insights from experimental models. Int J Exp Pathol *81*, 63-88.

Fiedler, J., Jara, P., Luza, S., Dorfman, M., Grouselle, D., Rage, F., Lara, H.E., and Arancibia, S. (2006). Cold stress induces metabolic activation of thyrotrophin-releasing hormone-synthesising neurones in the magnocellular division of the hypothalamic paraventricular nucleus and concomitantly changes ovarian sympathetic activity parameters. J Neuroendocrinol *18*, 367-376.

Forstermann, U., Closs, E.I., Pollock, J.S., Nakane, M., Schwarz, P., Gath, I., and Kleinert, H. (1994). Nitric oxide synthase isozymes. Characterization, purification, molecular cloning, and functions. Hypertension *23*, 1121-1131.

Foster, D.O., and Frydman, M.L. (1979). Tissue distribution of cold-induced thermogenesis in conscious warm- or cold-acclimated rats reevaluated from changes in tissue blood flow: the dominant role of brown adipose tissue in the replacement of shivering by nonshivering thermogenesis. Can J Physiol Pharmacol *57*, 257-270.

Francis, S.H., and Corbin, J.D. (1999). Cyclic nucleotide-dependent protein kinases: intracellular receptors for cAMP and cGMP action. Crit Rev Clin Lab Sci *36*, 275-328.

Friebe, A., and Koesling, D. (2003). Regulation of nitric oxide-sensitive guanylyl cyclase. Circ Res *93*, 96-105.

Gabbiani, G. (1981). The myofibroblast: a key cell for wound healing and fibrocontractive diseases. Prog Clin Biol Res *54*, 183-194.

Gabbiani, G. (1996). The cellular derivation and the life span of the myofibroblast. Pathol Res Pract *192*, 708-711.

Gaillard, R.C. (2001). Interaction between the hypothalamo-pituitary-adrenal axis and the immunological system. Ann Endocrinol (Paris) *62*, 155-163.

Gallo-Payet, N., Cote, M., Chorvatova, A., Guillon, G., and Payet, M.D. (1999). Cyclic AMP-independent effects of ACTH on glomerulosa cells of the rat adrenal cortex. J Steroid Biochem Mol Biol *69*, 335-342.

Gallo-Payet, N., and Payet, M.D. (2003). Mechanism of action of ACTH: beyond cAMP. Microsc Res Tech *61*, 275-287.

Gambaryan, S., Butt, E., Marcus, K., Glazova, M., Palmetshofer, A., Guillon, G., and Smolenski, A. (2003). cGMP-dependent protein kinase type II regulates basal level of aldosterone production by zona glomerulosa cells without increasing expression of the steroidogenic acute regulatory protein gene. J Biol Chem *278*, 29640-29648.

Gavrilova, O., Leon, L.R., Marcus-Samuels, B., Mason, M.M., Castle, A.L., Refetoff, S., Vinson, C., and Reitman, M.L. (1999). Torpor in mice is induced by both leptin-dependent and -independent mechanisms. Proc Natl Acad Sci U S A *96*, 14623-14628.

Geiselhöringer, A., Werner, M., Sigl, K., Smital, P., Wörner, R., Acheo, L., Stieber, J., Weinmeister, P., Feil, R., Feil, S.*, et al.* (2004). IRAG is essential for relaxation of receptor-triggered smooth muscle contraction by cGMP kinase. EMBO J *23*, 4222-4231.

Girotti, M., Pace, T.W., Gaylord, R.I., Rubin, B.A., Herman, J.P., and Spencer, R.L. (2006). Habituation to repeated restraint stress is associated with lack of stress-induced c-fos expression in primary sensory processing areas of the rat brain. Neuroscience *138*, 1067-1081.

Goldstein, D.S. (2010). Adrenal responses to stress. Cell Mol Neurobiol *30*, 1433-1440.

Goldstein, D.S., and Kopin, I.J. (2007). Evolution of concepts of stress. Stress *10*, 109-120.

Goldstein, D.S., and Kopin, I.J. (2008). Adrenomedullary, adrenocortical, and sympathoneural responses to stressors: a meta-analysis. Endocr Regul *42*, 111-119.

Gomez-Sanchez, C.E. (2007). Regulation of adrenal arterial tone by adrenocorticotropin: the plot thickens. Endocrinology *148*, 3566-3568.

Gomez, D., and Owens, G.K. (2012). Smooth muscle cell phenotypic switching in atherosclerosis. Cardiovasc Res *95*, 156-164.

Gordon, C.J. (1990). Thermal biology of the laboratory rat. Physiol Behav *47*, 963-991.

Gross, K.L., and Cidlowski, J.A. (2008). Tissue-specific glucocorticoid action: a family affair. Trends Endocrinol Metab *19*, 331-339.

Guild, S.B., and Cramb, G. (1999). Characterisation of the effects of natriuretic peptides upon ACTH secretion from the mouse pituitary. Mol Cell Endocrinol *152*, 11-19.

Haas, B., Mayer, P., Jennissen, K., Scholz, D., Berriel Diaz, M., Bloch, W., Herzig, S., Fassler, R., and Pfeifer, A. (2009). Protein kinase G controls brown fat cell differentiation and mitochondrial biogenesis. Sci Signal *2*, ra78.

Harkin, a.J., Bruce, K.H., Craft, B., and Paul, I.a. (1999). Nitric oxide synthase inhibitors have antidepressant-like properties in mice. 1. Acute treatments are active in the forced swim test. Eur J Pharmacol *372*, 207-213.

Hatipoglu, B.A. (2012). Cushing's syndrome. J Surg Oncol.

Heiberg, I.L., Wegener, G., and Rosenberg, R. (2002). Reduction of cGMP and nitric oxide has antidepressant-like effects in the forced swimming test in rats. Behav Brain Res *134*, 479-484.

Heisler, S., Tallerico-Melnyk, T., Yip, C., and Schimmer, B.P. (1989). Y-1 adrenocortical tumor cells contain atrial natriuretic peptide receptors which regulate cyclic nucleotide metabolism and steroidogenesis. Endocrinology *125*, 2235-2243.

Henley, D.E., and Lightman, S.L. (2011). New insights into corticosteroid-binding globulin and glucocorticoid delivery. Neuroscience *180*, 1-8.

Herman, J.P., and Cullinan, W.E. (1997). Neurocircuitry of stress: central control of the hypothalamo-pituitary-adrenocortical axis. Trends Neurosci *20*, 78-84.

Herman, J.P., Cullinan, W.E., Ziegler, D.R., and Tasker, J.G. (2002). Role of the paraventricular nucleus microenvironment in stress integration. Eur J Neurosci *16*, 381-385.

Heymann, M.A., Payne, B.D., Hoffman, J.I., and Rudolph, A.M. (1977). Blood flow measurements with radionuclide-labeled particles. Prog Cardiovasc Dis *20*, 55-79.

Hinson, J.P., Vinson, G.P., and Whitehouse, B.J. (1986). The relationship between perfusion medium flow rate and steroid secretion in the isolated perfused rat adrenal gland in situ. J Endocrinol *111*, 391-396.

Hinz, B., and Hirschelmann, R. (2000). Rapid non-genomic feedback effects of glucocorticoids on CRF-induced ACTH secretion in rats. Pharm Res *17*, 1273-1277.

Hoekstra, M., Meurs, I., Koenders, M., Out, R., Hildebrand, R.B., Kruijt, J.K., Van Eck, M., and Van Berkel, T.J. (2008). Absence of HDL cholesteryl ester uptake in mice via SR-BI impairs an adequate adrenal glucocorticoid-mediated stress response to fasting. J Lipid Res *49*, 738-745.

Hofmann, F., Bernhard, D., Lukowski, R., and Weinmeister, P. (2009). cGMP regulated protein kinases (cGK). Handb Exp Pharmacol, 137-162.

Hofmann, F., Feil, R., Kleppisch, T., and Schlossmann, J. (2006). Function of cGMP-dependent protein kinases as revealed by gene deletion. Physiol Rev *86*, 1-23.

Holgert, H., Dagerlind, A., and Hokfelt, T. (1998). Immunohistochemical characterization of the peptidergic innervation of the rat adrenal gland. Horm Metab Res *30*, 315-322.

Holmes, P.V. (2003). Rodent models of depression: reexamining validity without anthropomorphic inference. Crit Rev Neurobiol *15*, 143-174.

Ignarro, L.J. (2002). Nitric oxide as a unique signaling molecule in the vascular system: a historical overview. J Physiol Pharmacol *53*, 503-514.

Imura, H., Sparks, L.L., Grodsky, G.M., and Forsham, P.H. (1965). Immunologic studies of adrenocorticotropic hormone (ACTH): dissociation of biologic and immunologic activities. J Clin Endocrinol Metab *25*, 1361-1369.

Ising, M., and Holsboer, F. (2006). Genetics of stress response and stress-related disorders. Dialogues Clin Neurosci *8*, 433-444.

Jansky, L. (1973). Non-shivering thermogenesis and its thermoregulatory significance. Biol Rev Camb Philos Soc *48*, 85-132.

Jefcoate, C. (2002). High-flux mitochondrial cholesterol trafficking, a specialized function of the adrenal cortex. J Clin Invest *110*, 881-890.

Jefferys, D., Copolov, D., Irby, D., and Funder, J. (1983). Behavioural effect of adrenalectomy: reversal by glucocorticoids or [D-Ala2,Met5]enkephalinamide. Eur J Pharmacol *92*, 99-103.

Jessop, D.S. (1999). Stimulatory and inhibitory regulators of the hypothalamo-pituitary-adrenocortical axis. Baillieres Best Pract Res Clin Endocrinol Metab *13*, 491-501.

Johnson, E.O., Kamilaris, T.C., Chrousos, G.P., and Gold, P.W. (1992). Mechanisms of stress: a dynamic overview of hormonal and behavioral homeostasis. Neurosci Biobehav Rev *16*, 115-130.

Joseph, N.M., Mukouyama, Y.S., Mosher, J.T., Jaegle, M., Crone, S.A., Dormand, E.L., Lee, K.F., Meijer, D., Anderson, D.J., and Morrison, S.J. (2004). Neural crest stem cells undergo multilineage differentiation in developing peripheral nerves to generate endoneurial fibroblasts in addition to Schwann cells. Development *131*, 5599-5612.

Joyce, N.C., DeCamilli, P., Lohmann, S.M., and Walter, U. (1986). cGMP-dependent protein kinase is present in high concentrations in contractile cells of the kidney vasculature. J Cyclic Nucleotide Phosphor Res *11*, 191-198.

Kaneda, K., Ekataksin, W., Sogawa, M., Matsumura, A., Cho, A., and Kawada, N. (1998). Endothelin-1-induced vasoconstriction causes a significant increase in portal pressure of rat liver: localized constrictive effect on the distal segment of preterminal portal venules as revealed by light and electron microscopy and serial reconstruction. Hepatology *27*, 735-747.

Karp, C.L. (2012). Unstressing intemperate models: how cold stress undermines mouse modeling. J Exp Med *209*, 1069-1074.

Karpac, J., Czyzewska, K., Kern, A., Brush, R.S., Anderson, R.E., and Hochgeschwender, U. (2008). Failure of adrenal corticosterone production in POMC-deficient mice results from lack of integrated effects of POMC peptides on multiple factors. Am J Physiol Endocrinol Metab *295*, E446-455.

Kaupp, U.B., and Seifert, R. (2002). Cyclic nucleotide-gated ion channels. Physiol Rev *82*, 769-824.

Keegan, C.E., and Hammer, G.D. (2002). Recent insights into organogenesis of the adrenal cortex. Trends Endocrinol Metab *13*, 200-208.

Keilbach, A., Ruth, P., and Hofmann, F. (1992). Detection of cGMP dependent protein kinase isozymes by specific antibodies. Eur J Biochem *208*, 467-473.

Keller-Wood, M.E., and Dallman, M.F. (1984). Corticosteroid inhibition of ACTH secretion. Endocr Rev *5*, 1-24.

Kemp-Harper, B., and Feil, R. (2008). Meeting report: cGMP matters. Sci Signal *1*, pe12.

Kitamura, H., Konno, A., Morimatsu, M., Jung, B.D., Kimura, K., and Saito, M. (1997). Immobilization stress increases hepatic IL-6 expression in mice. Biochem Biophys Res Commun *238*, 707-711.

Kleppisch, T., Pfeifer, a., Klatt, P., Ruth, P., Montkowski, a., Fässler, R., and Hofmann, F. (1999). Long-term potentiation in the hippocampal CA1 region of mice lacking cGMP-dependent kinases is normal and susceptible to inhibition of nitric oxide synthase. J Endocrinol *19*, 48-55.

Kleppisch, T., Wolfsgruber, W., Feil, S., Allmann, R., Wotjak, C.T., Goebbels, S., Nave, K.-A., Hofmann, F., and Feil, R. (2003). Hippocampal cGMP-dependent protein kinase I supports an age- and protein synthesis-dependent component of long-term potentiation but is not essential for spatial reference and contextual memory. J Neurosci *23*, 6005-6012.

Klingenspor, M. (2003). Cold-induced recruitment of brown adipose tissue thermogenesis. Exp Physiol *88*, 141-148.

Korte, S.M., De Kloet, E.R., Buwalda, B., Bouman, S.D., and Bohus, B. (1996). Antisense to the glucocorticoid receptor in hippocampal dentate gyrus reduces immobility in forced swim test. Eur J Pharmacol *301*, 19-25.

Kovanen, P.T., Goldstein, J.L., Chappell, D.A., and Brown, M.S. (1980). Regulation of low density lipoprotein receptors by adrenocorticotropin in the adrenal gland of mice and rats in vivo. J Biol Chem *255*, 5591-5598.

Kraemer, F.B. (2007). Adrenal cholesterol utilization. Mol Cell Endocrinol *265-266*, 42-45.

Krenning, G., Zeisberg, E.M., and Kalluri, R. (2010). The origin of fibroblasts and mechanism of cardiac fibrosis. J Cell Physiol *225*, 631-637.

Kuhn, M. (2003). Structure, regulation, and function of mammalian membrane guanylyl cyclase receptors, with a focus on guanylyl cyclase-A. Circ Res *93*, 700-709.

Kvetnansky, R., Pacak, K., Fukuhara, K., Viskupic, E., Hiremagalur, B., Nankova, B., Goldstein, D.S., Sabban, E.L., and Kopin, I.J. (1995). Sympathoadrenal system in stress. Interaction with the hypothalamic-pituitary-adrenocortical system. Ann N Y Acad Sci *771*, 131-158.

Kvetnansky, R., Sabban, E.L., and Palkovits, M. (2009). Catecholaminergic systems in stress: structural and molecular genetic approaches. Physiol Rev *89*, 535-606.

Kyrou, I., and Tsigos, C. (2009). Stress hormones: physiological stress and regulation of metabolism. Curr Opin Pharmacol *9*, 787-793.

Landgraf, W., Hofmann, F., Pelton, J.T., and Huggins, J.P. (1990). Effects of cyclic GMP on the secondary structure of cyclic GMP dependent protein kinase and analysis of the enzyme's amino-terminal domain by far-ultraviolet circular dichroism. Biochemistry *29*, 9921-9928.

Langmesser, S., Franken, P., Feil, S., Emmenegger, Y., Albrecht, U., and Feil, R. (2009). cGMP-dependent protein kinase type I is implicated in the regulation of the timing and quality of sleep and wakefulness. PloS one *4*, e4238.

Lawson, D., Harrison, M., and Shapland, C. (1997). Fibroblast transgelin and smooth muscle SM22α are the same protein, the expression of which is down-regulated in many cell lines. Cell Motil Cytoskeleton *38*, 250-257.

Lehoux, J.G., Fleury, A., and Ducharme, L. (1998). The acute and chronic effects of adrenocorticotropin on the levels of messenger ribonucleic acid and protein of steroidogenic enzymes in rat adrenal in vivo. Endocrinology *139*, 3913-3922.

Liang, F., Kapoun, A.M., Lam, A., Damm, D.L., Quan, D., O'Connell, M., and Protter, A.A. (2007). B-Type natriuretic peptide inhibited angiotensin II-stimulated cholesterol biosynthesis, cholesterol transfer, and steroidogenesis in primary human adrenocortical cells. Endocrinology *148*, 3722-3729.

Liebenberg, N., Muller, H.K., Fischer, C.W., Harvey, B.H., Brink, C.B., Elfving, B., and Wegener, G. (2011). An inhibitor of cAMP-dependent protein kinase induces behavioural and neurological antidepressant-like effects in rats. Neurosci Lett *498*, 158-161.

Lohmann, S.M., Walter, U., Miller, P.E., Greengard, P., and De Camilli, P. (1981). Immunohistochemical localization of cyclic GMP-dependent protein kinase in mammalian brain. Proc Natl Acad Sci U S A *78*, 653-657.

Lowell, B.B., and Spiegelman, B.M. (2000). Towards a molecular understanding of adaptive thermogenesis. Nature *404*, 652-660.

Lucas, K.A., Pitari, G.M., Kazerounian, S., Ruiz-Stewart, I., Park, J., Schulz, S., Chepenik, K.P., and Waldman, S.A. (2000). Guanylyl cyclases and signaling by cyclic GMP. Pharmacol Rev *52*, 375-414.

Lukowski, R., Weinmeister, P., Bernhard, D., Feil, S., Gotthardt, M., Herz, J., Massberg, S., Zernecke, A., Weber, C., Hofmann, F.*, et al.* (2008). Role of smooth muscle cGMP/cGKI signaling in murine vascular restenosis. Arterioscler Thromb Vasc Biol *28*, 1244-1250.

Lutz, S.Z., Hennige, A.M., Feil, S., Peter, A., Gerling, A., Machann, J., Krober, S.M., Rath, M., Schurmann, A., Weigert, C.*, et al.* (2011). Genetic ablation of cGMP-dependent protein kinase type I causes liver inflammation and fasting hyperglycemia. Diabetes *60*, 1566-1576.

MacFarland, R.T., Zelus, B.D., and Beavo, J.A. (1991). High concentrations of a cGMP-stimulated phosphodiesterase mediate ANP-induced decreases in cAMP and steroidogenesis in adrenal glomerulosa cells. J Biol Chem *266*, 136-142.

Madetoja, J., and Madetoja, M. (2009). Blood sampling from the tail vein, in comparison with two other techniques, causes less stress to mice. Scand J Lab Anim … *36*, 215-221.

Maletic, V., Robinson, M., Oakes, T., Iyengar, S., Ball, S.G., and Russell, J. (2007). Neurobiology of depression: an integrated view of key findings. Int J Clin Pract *61*, 2030-2040.

Malisch, J.L., Breuner, C.W., Gomes, F.R., Chappell, M.A., and Garland, T., Jr. (2008). Circadian pattern of total and free corticosterone concentrations, corticosteroid-binding globulin, and physical activity in mice selectively bred for high voluntary wheel-running behavior. Gen Comp Endocrinol *156*, 210-217.

Mallet, C., Feraud, O., Ouengue-Mbele, G., Gaillard, I., Sappay, N., Vittet, D., and Vilgrain, I. (2003). Differential expression of VEGF receptors in adrenal atrophy induced by dexamethasone: a protective role of ACTH. Am J Physiol Endocrinol Metab *284*, E156-167.

Martin, S.J., and Morris, R.G. (2002). New life in an old idea: the synaptic plasticity and memory hypothesis revisited. Hippocampus *12*, 609-636.

Massberg, S., Sausbier, M., Klatt, P., Bauer, M., Pfeifer, A., Siess, W., Fassler, R., Ruth, P., Krombach, F., and Hofmann, F. (1999). Increased adhesion and aggregation of platelets lacking cyclic guanosine 3',5'-monophosphate kinase I. J Exp Med *189*, 1255-1264.

Mastorakos, G., and Ilias, I. (2006). Interleukin-6: a cytokine and/or a major modulator of the response to somatic stress. Ann N Y Acad Sci *1088*, 373-381.

Matsushita, H., Matsuzaki, M., Han, X.J., Nishiki, T.I., Ohmori, I., Michiue, H., Matsui, H., and Tomizawa, K. (2012). Antidepressant-like effect of sildenafil through oxytocin-dependent cyclic AMP response element-binding protein phosphorylation. Neuroscience *200*, 13-18.

McCann, S.M., Kimura, M., Karanth, S., Yu, W.H., and Rettori, V. (1998). Role of nitric oxide in the neuroendocrine responses to cytokines. Ann N Y Acad Sci *840*, 174-184.

Metzger, D., and Feil, R. (1999). Engineering the mouse genome by site-specific recombination. Curr Opin Biotechnol *10*, 470-476.

Miyazawa, T., Ogawa, Y., Chusho, H., Yasoda, A., Tamura, N., Komatsu, Y., and Pfeifer, A. (2002). Cyclic GMP-Dependent Protein Kinase II Plays a Critical Role in C-Type Natriuretic Peptide-Mediated Endochondral Ossification. In Endocrinology, pp. 3604-3610.

Mohn, C.E., Fernandez-Solari, J., De Laurentiis, A., Prestifilippo, J.P., de la Cal, C., Funk, R., Bornstein, S.R., McCann, S.M., and Rettori, V. (2005). The rapid release of corticosterone from the adrenal induced by ACTH is mediated by nitric oxide acting by prostaglandin E2. Proc Natl Acad Sci U S A *102*, 6213-6218.

Morris, D.L., and Rui, L. (2009). Recent advances in understanding leptin signaling and leptin resistance. Am J Physiol Endocrinol Metab *297*, E1247-1259.

Morrison, S.F., Nakamura, K., and Madden, C.J. (2008). Central control of thermogenesis in mammals. Exp Physiol *93*, 773-797.

Munzel, T., Feil, R., Mulsch, A., Lohmann, S.M., Hofmann, F., and Walter, U. (2003). Physiology and pathophysiology of vascular signaling controlled by guanosine 3',5'-cyclic monophosphate-dependent protein kinase [corrected]. Circulation *108*, 2172-2183.

Nakamura, K. (2011). Central circuitries for body temperature regulation and fever. Am J Physiol Regul Integr Comp Physiol *301*, R1207-1228.

Nikolaev, V.O., Gambaryan, S., Engelhardt, S., Walter, U., and Lohse, M.J. (2005). Real-time monitoring of the PDE2 activity of live cells: hormone-stimulated cAMP hydrolysis is faster than hormone-stimulated cAMP synthesis. J Biol Chem *280*, 1716-1719.

Nisoli, E., Clementi, E., Paolucci, C., Cozzi, V., Tonello, C., Sciorati, C., Bracale, R., Valerio, A., Francolini, M., Moncada, S.*, et al.* (2003). Mitochondrial biogenesis in mammals: the role of endogenous nitric oxide. Science *299*, 896-899.

Nisoli, E., Clementi, E., Tonello, C., Sciorati, C., Briscini, L., and Carruba, M.O. (1998). Effects of nitric oxide on proliferation and differentiation of rat brown adipocytes in primary cultures. Br J Pharmacol *125*, 888-894.

Nukina, H., Sudo, N., Aiba, Y., Oyama, N., Koga, Y., and Kubo, C. (2001). Restraint stress elevates the plasma interleukin-6 levels in germ-free mice. J Neuroimmunol *115*, 46-52.

Nussdorfer, G.G., Rossi, G.P., Malendowicz, L.K., and Mazzocchi, G. (1999). Autocrine-paracrine endothelin system in the physiology and pathology of steroid-secreting tissues. Pharmacol Rev *51*, 403-438.

Oelkrug, R., Heldmaier, G., and Meyer, C.W. (2011). Torpor patterns, arousal rates, and temporal organization of torpor entry in wildtype and UCP1-ablated mice. J Comp Physiol B *181*, 137-145.

Omori, K., and Kotera, J. (2007). Overview of PDEs and their regulation. Circ Res *100*, 309-327.

Oster, H., Werner, C., Magnone, M.C., Mayser, H., Feil, R., Seeliger, M.W., Hofmann, F., and Albrecht, U. (2003). cGMP-dependent protein kinase II modulates mPer1 and mPer2 gene induction and influences phase shifts of the circadian clock. Curr Biol *13*, 725-733.

Overton, J.M., and Williams, T.D. (2004). Behavioral and physiologic responses to caloric restriction in mice. Physiol Behav *81*, 749-754.

Owens, G.K., Kumar, M.S., and Wamhoff, B.R. (2004). Molecular regulation of vascular smooth muscle cell differentiation in development and disease. Physiol Rev *84*, 767-801.

Pacak, K. (2000). Stressor-specific activation of the hypothalamic-pituitary-adrenocortical axis. Physiol Res *49 Suppl 1*, S11-17.

Pacak, K., and Palkovits, M. (2001). Stressor specificity of central neuroendocrine responses: implications for stress-related disorders. Endocr Rev *22*, 502-548.

Papadimitriou, A., and Priftis, K.N. (2009). Regulation of the hypothalamic-pituitary-adrenal axis. Neuroimmunomodulation *16*, 265-271.

Paul, C., Schoberl, F., Weinmeister, P., Micale, V., Wotjak, C.T., Hofmann, F., and Kleppisch, T. (2008). Signaling through cGMP-dependent protein kinase I in the amygdala is critical for auditory-cued fear memory and long-term potentiation. J Neurosci *28*, 14202-14212.

Perlman, R.L., and Chalfie, M. (1977). Catecholamine release from the adrenal medulla. Clin Endocrinol Metab *6*, 551-576.

Perlstein, R.S., Mougey, E.H., Jackson, W.E., and Neta, R. (1991). Interleukin-1 and interleukin-6 act synergistically to stimulate the release of adrenocorticotropic hormone in vivo. Lymphokine Cytokine Res *10*, 141-146.

Perras, B., Schultes, B., Behn, B., Dodt, C., Born, J., and Fehm, H.L. (2004). Intranasal atrial natriuretic peptide acts as central nervous inhibitor of the hypothalamo-pituitary-adrenal stress system in humans. J Clin Endocrinol Metab *89*, 4642-4648.

Petit-Demouliere, B., Chenu, F., and Bourin, M. (2005). Forced swimming test in mice: a review of antidepressant activity. Psychopharmacology *177*, 245-255.

Pfeifer, A., Aszodi, A., Seidler, U., Ruth, P., Hofmann, F., and Fassler, R. (1996). Intestinal secretory defects and dwarfism in mice lacking cGMP-dependent protein kinase II. Science *274*, 2082-2086.

Pfeifer, A., Klatt, P., Massberg, S., Ny, L., Sausbier, M., Hirneiss, C., Wang, G.X., Korth, M., Aszodi, A., Andersson, K.E.*, et al.* (1998). Defective smooth muscle regulation in cGMP kinase I-deficient mice. EMBO J *17*, 3045-3051.

Pfeifer, A., Ruth, P., Dostmann, W., Sausbier, M., Klatt, P., and Hofmann, F. (1999). Structure and function of cGMP-dependent protein kinases. Rev Physiol Biochem Pharmacol *135*, 105-149.

Pignatelli, D., Magalhaes, M.M., and Magalhaes, M.C. (1998). Direct effects of stress on adrenocortical function. Horm Metab Res *30*, 464-474.

Porsolt, R.D., Anton, G., Blavet, N., and Jalfre, M. (1978). Behavioural despair in rats: a new model sensitive to antidepressant treatments. Eur J Pharmacol *47*, 379-391.

Porsolt, R.D., Le Pichon, M., and Jalfre, M. (1977). Depression: a new animal model sensitive to antidepressant treatments. Nature *266*, 730-732.

Powell, D.W., Mifflin, R.C., Valentich, J.D., Crowe, S.E., Saada, J.I., and West, A.B. (1999). Myofibroblasts. I. Paracrine cells important in health and disease. Am J Physiol *277*, C1-9.

Qiao, S., Okret, S., and Jondal, M. (2009). Thymocyte-synthesized glucocorticoids play a role in thymocyte homeostasis and are down-regulated by adrenocorticotropic hormone. Endocrinology *150*, 4163-4169.

Rainey, W.E., Saner, K., and Schimmer, B.P. (2004). Adrenocortical cell lines. Mol Cell Endocrinol *228*, 23-38.

Ravussin, E., and Galgani, J.E. (2011). The implication of brown adipose tissue for humans. Annu Rev Nutr *31*, 33-47.

Renner, U., Gloddek, J., Pereda, M.P., Arzt, E., and Stalla, G.K. (1998). Regulation and role of intrapituitary IL-6 production by folliculostellate cells. Domest Anim Endocrinol *15*, 353-362.

Rensen, S.S., Doevendans, P.A., and van Eys, G.J. (2007). Regulation and characteristics of vascular smooth muscle cell phenotypic diversity. Neth Heart J *15*, 100-108.

Rigotti, A., Edelman, E.R., Seifert, P., Iqbal, S.N., DeMattos, R.B., Temel, R.E., Krieger, M., and Williams, D.L. (1996). Regulation by adrenocorticotropic hormone of the in vivo expression of scavenger receptor class B type I (SR-BI), a high density lipoprotein receptor, in steroidogenic cells of the murine adrenal gland. J Biol Chem *271*, 33545-33549.

Rivier, C. (2001). Does IL-6 release ACTH by exerting a direct effect in the rat anterior pituitary. Stress *4*, 39-55.

Rothwell, N.J., and Stock, M.J. (1987). Stimulation of thermogenesis and brown fat activity in rats fed medium chain triglyceride. Metabolism *36*, 128-130.

Rousset, S., Alves-Guerra, M.C., Mozo, J., Miroux, B., Cassard-Doulcier, A.M., Bouillaud, F., and Ricquier, D. (2004). The biology of mitochondrial uncoupling proteins. Diabetes *53 Suppl 1*, S130-135.

Ruth, P., Landgraf, W., Keilbach, A., May, B., Egleme, C., and Hofmann, F. (1991). The activation of expressed cGMP-dependent protein kinase isozymes I alpha and I beta is determined by the different amino-termini. Eur J Biochem *202*, 1339-1344.

Rybalkin, S.D., Yan, C., Bornfeldt, K.E., and Beavo, J.A. (2003). Cyclic GMP phosphodiesterases and regulation of smooth muscle function. Circ Res *93*, 280-291.

Sainz, J.M., Reche, C., Rabano, M.A., Mondillo, C., Patrignani, Z.J., Macarulla, J.M., Pignataro, O.P., and Trueba, M. (2004). Effects of nitric oxide on aldosterone synthesis and nitric oxide synthase activity in glomerulosa cells from bovine adrenal gland. Endocrine *24*, 61-71.

Sapolsky, R., Rivier, C., Yamamoto, G., Plotsky, P., and Vale, W. (1987). Interleukin-1 stimulates the secretion of hypothalamic corticotropin-releasing factor. Science *238*, 522-524.

Sausbier, M., Hu, H., Arntz, C., Feil, S., Kamm, S., Adelsberger, H., Sausbier, U., Sailer, C.A., Feil, R., Hofmann, F.*, et al.* (2004). Cerebellar ataxia and Purkinje cell dysfunction caused by Ca2+-activated K+ channel deficiency. Proc Natl Acad Sci U S A *101*, 9474-9478.

Sausbier, M., Schubert, R., Voigt, V., Hirneiss, C., Pfeifer, A., Korth, M., Kleppisch, T., Ruth, P., and Hofmann, F. (2000). Mechanisms of NO/cGMP-dependent vasorelaxation. Circ Res *87*, 825-830.

Schinner, S., and Bornstein, S.R. (2005). Cortical-chromaffin cell interactions in the adrenal gland. Endocr Pathol *16*, 91-98.

Schlossmann, J., Ammendola, A., Ashman, K., Zong, X., Huber, A., Neubauer, G., Wang, G.-X., Allescher, H.-D., Korth, M., Wilm, M.*, et al.* (2000). Regulation of intracellular calcium by a signalling complex of IRAG, IP3 receptor and cGMP kinase I[beta]. Nature *404*, 197-201.

Schmid, J., Ludwig, B., Schally, A.V., Steffen, A., Ziegler, C.G., Block, N.L., Koutmani, Y., Brendel, M.D., Karalis, K.P., Simeonovic, C.J.*, et al.* (2011). Modulation of pancreatic islets-stress axis by hypothalamic releasing hormones and 11beta-hydroxysteroid dehydrogenase. Proc Natl Acad Sci U S A *108*, 13722-13727.

Schmidt, H., Werner, M., Heppenstall, P.A., Henning, M., More, M.I., Kuhbandner, S., Lewin, G.R., Hofmann, F., Feil, R., and Rathjen, F.G. (2002). cGMP-mediated signaling via cGKIalpha is required for the guidance and connectivity of sensory axons. J Cell Biol *159*, 489-498.

Schmidt, M.V., Enthoven, L., van der Mark, M., Levine, S., de Kloet, E.R., and Oitzl, M.S. (2003). The postnatal development of the hypothalamic-pituitary-adrenal axis in the mouse. Int J Dev Neurosci *21*, 125-132.

Schmidt, M.V., Sterlemann, V., Wagner, K., Niederleitner, B., Ganea, K., Liebl, C., Deussing, J.M., Berger, S., Schutz, G., Holsboer, F.*, et al.* (2009). Postnatal glucocorticoid excess due to pituitary glucocorticoid receptor deficiency: differential short- and long-term consequences. Endocrinology *150*, 2709-2716.

Schwartz, J. (1990). Evidence for intrapituitary intercellular control of adrenocorticotropin secretion. Mol Cell Endocrinol *68*, 77-83.

Selye, H. (1950). Stress and the general adaptation syndrome. Br Med J *1*, 1383-1392.

Serini, G., and Gabbiani, G. (1999). Mechanisms of myofibroblast activity and phenotypic modulation. Exp Cell Res *250*, 273-283.

Sewer, M.B., and Waterman, M.R. (2003). ACTH modulation of transcription factors responsible for steroid hydroxylase gene expression in the adrenal cortex. Microsc Res Tech *61*, 300-307.

Shipston, M.J. (1995). Mechanism(s) of early glucocorticoid inhibition of adrenocorticotropin secretion from anterior pituitary corticotropes. Trends Endocrinol Metab *6*, 261-266.

Siiteri, P.K., Murai, J.T., Hammond, G.L., Nisker, J.A., Raymoure, W.J., and Kuhn, R.W. (1982). The serum transport of steroid hormones. Recent Prog Horm Res *38*, 457-510.

Silva, J.E. (2006). Thermogenic mechanisms and their hormonal regulation. Physiol Rev *86*, 435-464.

Singh, A.K., Spiessberger, B., Zheng, W., Xiao, F., Lukowski, R., Wegener, J.W., Weinmeister, P., Saur, D., Klein, S., Schemann, M.*, et al.* (2012). Neuronal cGMP kinase I is essential for stimulation of duodenal bicarbonate secretion by luminal acid. FASEB journal : official publication of the Federation of American Societies for Experimental Biology *26*, 1745-1754.

Smolenski, A., Poller, W., Walter, U., and Lohmann, S.M. (2000). Regulation of human endothelial cell focal adhesion sites and migration by cGMP-dependent protein kinase I. J Biol Chem *275*, 25723-25732.

Sonnenburg, W.K., and Beavo, J.A. (1994). Cyclic GMP and regulation of cyclic nucleotide hydrolysis. Adv Pharmacol *26*, 87-114.

Soriano, P. (1999). Generalized lacZ expression with the ROSA26 Cre reporter strain. Nat Genet *21*, 70-71.

Sorrell, J.M., and Caplan, A.I. (2009). Fibroblasts-a diverse population at the center of it all. Int Rev Cell Mol Biol *276*, 161-214.

Spencer, R.L., Miller, A.H., Moday, H., McEwen, B.S., Blanchard, R.J., Blanchard, D.C., and Sakai, R.R. (1996). Chronic social stress produces reductions in available splenic type II corticosteroid receptor binding and plasma corticosteroid binding globulin levels. Psychoneuroendocrinology *21*, 95-109.

Spiessberger, B., Bernhard, D., Herrmann, S., Feil, S., Werner, C., Luppa, P.B., and Hofmann, F. (2009). cGMP-dependent protein kinase II and aldosterone secretion. FEBS J *276*, 1007-1013.

Stocco, D.M. (2001). StAR protein and the regulation of steroid hormone biosynthesis. Annu Rev Physiol *63*, 193-213.

Sung, J.H., Yang, H.M., Park, J.B., Choi, G.S., Joh, J.W., Kwon, C.H., Chun, J.M., Lee, S.K., and Kim, S.J. (2008). Isolation and characterization of mouse mesenchymal stem cells. Transplant Proc *40*, 2649-2654.

Surks, H.K. (2007). cGMP-dependent protein kinase I and smooth muscle relaxation: a tale of two isoforms. Circ Res *101*, 1078-1080.

Surks, H.K., Richards, C.T., and Mendelsohn, M.E. (2003). Myosin phosphatase-Rho interacting protein. A new member of the myosin phosphatase complex that directly binds RhoA. J Biol Chem *278*, 51484-51493.

Swaab, D.F., Bao, A.M., and Lucassen, P.J. (2005). The stress system in the human brain in depression and neurodegeneration. Ageing Res Rev *4*, 141-194.

Swanson, L.W., and Sawchenko, P.E. (1980). Paraventricular nucleus: a site for the integration of neuroendocrine and autonomic mechanisms. Neuroendocrinology *31*, 410-417.

Swoap, S.J. (2008). The pharmacology and molecular mechanisms underlying temperature regulation and torpor. Biochem Pharmacol *76*, 817-824.

Swoap, S.J., and Weinshenker, D. (2008). Norepinephrine controls both torpor initiation and emergence via distinct mechanisms in the mouse. PloS one *3*, e4038.

Tasker, J.G., Di, S., and Malcher-Lopes, R. (2006). Minireview: rapid glucocorticoid signaling via membrane-associated receptors. Endocrinology *147*, 5549-5556.

Tatsumi, M., Engles, J.M., Ishimori, T., Nicely, O.B., Cohade, C., and Wahl, R.L. (2004). Intense (18)F-FDG uptake in brown fat can be reduced pharmacologically. J Nucl Med *45*, 1189-1193.

Temel, R.E., Trigatti, B., DeMattos, R.B., Azhar, S., Krieger, M., and Williams, D.L. (1997). Scavenger receptor class B, type I (SR-BI) is the major route for the delivery of high density lipoprotein cholesterol to the steroidogenic pathway in cultured mouse adrenocortical cells. Proc Natl Acad Sci U S A *94*, 13600-13605.

Ten, S., New, M., and Maclaren, N. (2001). Clinical review 130: Addison's disease 2001. J Clin Endocrinol Metab *86*, 2909-2922.

Thomas, M., Keramidas, M., Monchaux, E., and Feige, J.J. (2003). Role of adrenocorticotropic hormone in the development and maintenance of the adrenal cortical vasculature. Microsc Res Tech *61*, 247-251.

Thomson, M. (1998). Molecular and cellular mechanisms used in the acute phase of stimulated steroidogenesis. Horm Metab Res *30*, 16-28.

Tomlinson, J.W., Walker, E.A., Bujalska, I.J., Draper, N., Lavery, G.G., Cooper, M.S., Hewison, M., and Stewart, P.M. (2004). 11beta-hydroxysteroid dehydrogenase type 1: a tissue-specific regulator of glucocorticoid response. Endocr Rev *25*, 831-866.

Tronche, F., Kellendonk, C., Kretz, O., Gass, P., Anlag, K., Orban, P.C., Bock, R., Klein, R., and Schutz, G. (1999). Disruption of the glucocorticoid receptor gene in the nervous system results in reduced anxiety. Nat Genet *23*, 99-103.

Tsai, L.C., and Beavo, J.A. (2011). The roles of cyclic nucleotide phosphodiesterases (PDEs) in steroidogenesis. Curr Opin Pharmacol *11*, 670-675.

Tuli, J.S., Smith, J.A., and Morton, D.B. (1995). Stress measurements in mice after transportation. Lab Anim *29*, 132-138.

Turnbull, A.V., and Rivier, C.L. (1999). Regulation of the hypothalamic-pituitary-adrenal axis by cytokines: actions and mechanisms of action. Physiol Rev *79*, 1-71.

Ulrich-Lai, Y.M., Arnhold, M.M., and Engeland, W.C. (2006a). Adrenal splanchnic innervation contributes to the diurnal rhythm of plasma corticosterone in rats by modulating adrenal sensitivity to ACTH. Am J Physiol Regul Integr Comp Physiol *290*, R1128-1135.

Ulrich-Lai, Y.M., Figueiredo, H.F., Ostrander, M.M., Choi, D.C., Engeland, W.C., and Herman, J.P. (2006b). Chronic stress induces adrenal hyperplasia and hypertrophy in a subregion-specific manner. Am J Physiol Endocrinol Metab *291*, E965-973.

Ulrich-Lai, Y.M., and Herman, J.P. (2009). Neural regulation of endocrine and autonomic stress responses. Nat Rev Neurosci *10*, 397-409.

Vaandrager, A.B., Hogema, B.M., and de Jonge, H.R. (2005). Molecular properties and biological functions of cGMP-dependent protein kinase II. Front Biosci *10*, 2150-2164.

Vaandrager, A.B., Smolenski, A., Tilly, B.C., Houtsmuller, A.B., Ehlert, E.M., Bot, A.G., Edixhoven, M., Boomaars, W.E., Lohmann, S.M., and de Jonge, H.R. (1998). Membrane targeting of cGMP-dependent protein kinase is required for cystic fibrosis transmembrane conductance regulator Cl-channel activation. Proc Natl Acad Sci U S A *95*, 1466-1471.

Vahl, T.P., Ulrich-Lai, Y.M., Ostrander, M.M., Dolgas, C.M., Elfers, E.E., Seeley, R.J., D'Alessio, D.A., and Herman, J.P. (2005). Comparative analysis of ACTH and corticosterone sampling methods in rats. Am J Physiol Endocrinol Metab *289*, E823-828.

Valtcheva, N., Nestorov, P., Beck, A., Russwurm, M., Hillenbrand, M., Weinmeister, P., and Feil, R. (2009). The commonly used cGMP-dependent protein kinase type I (cGKI) inhibitor Rp-8-Br-PET-cGMPS can activate cGKI in vitro and in intact cells. J Biol Chem *284*, 556-562.

van Herck, H., Baumans, V., de Boer, S.F., van der Gugten, J., van Woerkom, A.B., and Beynen, A.C. (1991). Endocrine stress response in rats subjected to singular orbital puncture while under diethyl-ether anaesthesia. Lab Anim *25*, 325-329.

Van Loo, P.L., Van Zutphen, L.F., and Baumans, V. (2003). Male management: Coping with aggression problems in male laboratory mice. Lab Anim *37*, 300-313.

Van Rossen, E., Vander Borght, S., van Grunsven, L.A., Reynaert, H., Bruggeman, V., Blomhoff, R., Roskams, T., and Geerts, A. (2009). Vinculin and cellular retinol-binding protein-1 are markers for quiescent and activated hepatic stellate cells in formalin-fixed paraffin embedded human liver. Histochem Cell Biol *131*, 313-325.

Vankelecom, H., Carmeliet, P., Van Damme, J., Billiau, A., and Denef, C. (1989). Production of interleukin-6 by folliculo-stellate cells of the anterior pituitary gland in a histiotypic cell aggregate culture system. Neuroendocrinology *49*, 102-106.

Veldhuis, H.D., De Korte, C.C., and De Kloet, E.R. (1985). Glucocorticoids facilitate the retention of acquired immobility during forced swimming. Eur J Pharmacol *115*, 211-217.

Venihaki, M., Dikkes, P., Carrigan, A., and Karalis, K.P. (2001). Corticotropin-releasing hormone regulates IL-6 expression during inflammation. J Clin Invest *108*, 1159-1166.

Vinson, G.P., Hinson, J.P., and Toth, I.E. (1994). The neuroendocrinology of the adrenal cortex. J Neuroendocrinol *6*, 235-246.

Vollmar, B., and Menger, M.D. (2009). The hepatic microcirculation: mechanistic contributions and therapeutic targets in liver injury and repair. Physiol Rev *89*, 1269-1339.

Walker, J.J., Terry, J.R., and Lightman, S.L. (2010). Origin of ultradian pulsatility in the hypothalamic-pituitary-adrenal axis. Proc Biol Sci *277*, 1627-1633.

Weber, S., Bernhard, D., Lukowski, R., Weinmeister, P., Worner, R., Wegener, J.W., Valtcheva, N., Feil, S., Schlossmann, J., Hofmann, F.*, et al.* (2007). Rescue of cGMP kinase I knockout mice by smooth muscle specific expression of either isozyme. Circ Res *101*, 1096-1103.

Wegener, J.W., Nawrath, H., Wolfsgruber, W., Kuhbandner, S., Werner, C., Hofmann, F., and Feil, R. (2002). cGMP-dependent protein kinase I mediates the negative inotropic effect of cGMP in the murine myocardium. Circ Res *90*, 18-20.

Werner, C., Raivich, G., Cowen, M., Strekalova, T., Sillaber, I., Buters, J.T., Spanagel, R., and Hofmann, F. (2004). Importance of NO/cGMP signalling via cGMP-dependent protein kinase II for controlling emotionality and neurobehavioural effects of alcohol. Eur J Neurosci *20*, 3498-3506.

Wernet, W., Flockerzi, V., and Hofmann, F. (1989). The cDNA of the two isoforms of bovine cGMP-dependent protein kinase. FEBS Lett *251*, 191-196.

West, A.P. (1990). Neurobehavioral studies of forced swimming: the role of learning and memory in the forced swim test. Prog Neuropsychopharmacol Biol Psychiatry *14*, 863-877.

Whitnall, M.H. (1993). Regulation of the hypothalamic corticotropin-releasing hormone neurosecretory system. Prog Neurobiol *40*, 573-629.

Whitworth, E.J., Kosti, O., Renshaw, D., and Hinson, J.P. (2003). Adrenal neuropeptides: regulation and interaction with ACTH and other adrenal regulators. Microsc Res Tech *61*, 259-267.

Willenberg, H.S., Path, G., Vogeli, T.A., Scherbaum, W.A., and Bornstein, S.R. (2002). Role of interleukin-6 in stress response in normal and tumorous adrenal cells and during chronic inflammation. Ann N Y Acad Sci *966*, 304-314.

Wislet-Gendebien, S., Hans, G., Leprince, P., Rigo, J.M., Moonen, G., and Rogister, B. (2005). Plasticity of cultured mesenchymal stem cells: switch from nestin-positive to excitable neuron-like phenotype. Stem Cells *23*, 392-402.

Wolfsgruber, W., Feil, S., Brummer, S., Kuppinger, O., Hofmann, F., and Feil, R. (2003). A proatherogenic role for cGMP-dependent protein kinase in vascular smooth muscle cells. Proc Natl Acad Sci U S A *100*, 13519-13524.

Wurtman, R.J. (2002). Stress and the adrenocortical control of epinephrine synthesis. Metabolism *51*, 11-14.

Yasin, S., Costa, A., Trainer, P., Windle, R., Forsling, M.L., and Grossman, A. (1993). Nitric oxide modulates the release of vasopressin from rat hypothalamic explants. Endocrinology *133*, 1466-1469.

Yoshimura, S., Sakamoto, S., Kudo, H., Sassa, S., Kumai, A., and Okamoto, R. (2003). Sex-differences in adrenocortical responsiveness during development in rats. Steroids *68*, 439-445.

Zhang, J., and Rivest, S. (1999). Distribution, regulation and colocalization of the genes encoding the EP2- and EP4-PGE2 receptors in the rat brain and neuronal responses to systemic inflammation. Eur J Neurosci *11*, 2651-2668.

Zhang, X., Ji, J., Yan, G., Wu, J., Sun, X., Shen, J., Jiang, H., and Wang, H. (2010). Sildenafil promotes adipogenesis through a PKG pathway. Biochem Biophys Res Commun *396*, 1054-1059.

Zhou, D., Kusnecov, A.W., Shurin, M.R., DePaoli, M., and Rabin, B.S. (1993). Exposure to physical and psychological stressors elevates plasma interleukin 6: relationship to the activation of hypothalamic-pituitary-adrenal axis. Endocrinology *133*, 2523-2530.

Zhuo, M., Hu, Y., Schultz, C., Kandel, E.R., and Hawkins, R.D. (1994). Role of guanylyl cyclase and cGMP-dependent protein kinase in long-term potentiation. Nature *368*, 635-639.

Zimmerman, L., Parr, B., Lendahl, U., Cunningham, M., McKay, R., Gavin, B., Mann, J., Vassileva, G., and McMahon, A. (1994). Independent regulatory elements in the nestin gene direct transgene expression to neural stem cells or muscle precursors. Neuron *12*, 11-24.

Zoeller, R.T., Kabeer, N., and Albers, H.E. (1990). Cold exposure elevates cellular levels of messenger ribonucleic acid encoding thyrotropin-releasing hormone in paraventricular nucleus despite elevated levels of thyroid hormones. Endocrinology *127*, 2955-2962.

Zuk, P.A., Zhu, M., Ashjian, P., De Ugarte, D.A., Huang, J.I., Mizuno, H., Alfonso, Z.C., Fraser, J.K., Benhaim, P., and Hedrick, M.H. (2002). Human adipose tissue is a source of multipotent stem cells. Mol Biol Cell *13*, 4279-4295.

G Publications

Journal articles

GERLING A., FEIL S., LUTZ SZ., SHIPSTON MJ., FEIL R. Reduced hypothalamic-pituitary-adrenal axis responsiveness in mice lacking cGMP-dependent protein kinase I. (*in preparation*)

JAUMANN M., DETTLING J., GRUBELT M., ZIMMERMANN U., **GERLING A.**, PAQUET-DURAND F., FEIL S., WOLPERT S., FRANZ C., VARAKINA K., XIONG H., BRANDT N., KUHN S., GEISLER HS., ROHBOCK K., RUTH P., SCHLOSSMANN J., HÜTTER J., SANDNER P., FEIL R., ENGEL J., KNIPPER M., RÜTTIGER L. 2012. cGMP-Prkg1 sinaling and Pde5 inhibition shelter chochlear hair cells and hearing function. *Nature Medicine*, 18, 252-9.

LUTZ SZ., HENNIGE AM., FEIL S., PETER A., **GERLING A.**, MACHANN J., KRÖBER SM., RATH M., SCHÜRMANN A., WEIGERT C., HÄRING HU., FEIL R. 2011. Genetic ablation of cGMP-dependent protein kinase type I causes liver inflammation and fasting hyperglycemia. *Diabetes*, 60, 1566-76.

PALCHYKOVA S., WINSKY-SOMMERER R., SHEN HY., BOISON D., **GERLING A.**, TOBLER I. 2010. Manipulation of adenosine kinase affects sleep regulation in mice. *Journal of Neuroscience*, 30, 13157-65.

KLAIBER M., KRUSE M., VÖLKER K., SCHRÖTER J., FEIL R., FREICHEL M., **GERLING A.**, FEIL S, DIETRICH A., LONDONO JE., BABA HA., ABRAMOWITZ J., BIRNBAUMER L., PENNINGER JM., PONGS O., KUHN M. 2010. Novel insights into the mechanisms mediating the local antihypertrophic effects of cardiac atrial natriuretic peptide: role of cGMP-dependent protein kinase and RGS2. *Basic Research in Cardiology*, 105, 298-301.

FEIL R., HÖLTER SM., WEINDL K., WURST W., LANGMESSER S., **GERLING A.**, FEIL S., ALBRECHT U. 2009. cGMP-dependent protein kinase I, the circadian clock, sleep and learning. *Communicative & Integrative Biology*, 2, 298-301.

FÖLLER M., FEIL S., GHORESCHI K., KOKA S., **GERLING A.**, THUNEMANN M., HOFMANN F., SCHULER B., VOGEL J., PICHLER B., KASINATHAN RS., NICOLAY JP., HUBER SM., LANG F., FEIL R. 2008. Anemia and splenomegaly in cGKI-deficient mice. *Proceedings of the National Academy of Sciences of the United States of America*, 105, 6771-6.

Conference contributions

GERLING A., BIRK B., FEIL S., SHIPSTON MJ., FEIL R. 2010 Analysis of the hypothalamic-pituitary-adrenal axis in cGKI-deficient mouse models. *Naunyn-Schmiedebergs Archives of Pharmacology*, *381:20*. 51th Annual Meeting Deutsche Gesellschaft für Experimentelle und Klinische Pharmakologie und Toxikologie, Mainz, Germany, March 23-25, 2010. **Oral presentation**

GNUEGGE R., JESSEN S., VALTCHEVA N., HILLENBRAND M., **GERLING A.**, FEIL S., RUTH P., FEIL R. 2009 Influence of oxidative stress on the structure and function of the cGMP-dependent protein kinase I. *Naunyn-Schmiedebergs Archives of Pharmacology, 379:27*. 50th Annual Meeting Deutsche Gesellschaft für Experimentelle und Klinische Pharmakologie und Toxikologie, Mainz, Germany, March 10-12, 2009. **Poster**

GERLING A., BECKER C., SCHÖNEGGE A., FEIL S., WEINDL K., HÖLTER SM., WURST W., FEIL R. *In vivo* analysis of cGMP/cGKI signalling in learning and cognition. *Naunyn-Schmiedebergs Archives of Pharmacology, 379:27*. 50th Annual Meeting Deutsche Gesellschaft für Experimentelle und Klinische Pharmakologie und Toxikologie, Mainz, Germany, March 10-12, 2009. **Poster**

FEIL S., FÖLLER M., KOKA S., GHORESCHI K., **GERLING A.**, THUNEMANN M., PICHLER B., HOFMANN F., SCHULER B., VOGEL J., KASINATHAN RS., NICOLAY JP., HUBER SM., LANG F., FEIL R. Anemia and splenomegaly in cGKI knockout mice. *Naunyn-Schmiedebergs Archives of Pharmacology, 377:23*. 49th Annual Meeting Deutsche Gesellschaft für Experimentelle und Klinische Pharmakologie und Toxikologie, Mainz, Germany, March 11-13, 2008. **Poster**

GERLING A., WINSKY-SOMMERER R., TOBLER I. Effect of sleep deprivation on the activity-rest behaviour in mice with reduced adenosine kinase activity. Joint meeting of the Swiss Society for Neuroscience, NCCR “Neural Pasticity and Repair”, Swiss Multiple Sclerosis Society. Bern, Switzerland. March 9-10, 2007. **Poster**

H Curriculum vitae

Personal background

Date of birth	October 25, 1978
Place of birth	Heidelberg
Nationality	German
Martial status	Married

Education

1985-1989	Grundschule Sinsheim-Dühren (primary school), Germany
1989-1998	Wilhelmi-Gymnasium Sinsheim (grammar school), Germany
Oktober 1998	Abitur (A-levels, mark: 1.6)
1998-1999	University of Veterinary Medicine Hannover, Germany
	Studies of veterinary medicine
1999-2006	University of Stuttgart, Germany
	Studies of technical biology
May 2006	Diploma in Technical Biology (mark: 1.0)
2006-2007	University of Zuerich, Switzerland
	EU Marie Curie Early Stage Researcher
2007-2012	University of Tuebingen (PhD student), Germany
	PhD Thesis: “Role of cGMP-dependent protein kinase type I in the regulation of stress response and thermogenesis”

I Appendix

I.1. Chemical, equipment and consumables

Reagent name, company and order number are given in alphabetical order. Substances not listed here were purchased from Roth.

Chemicals and reagents

$ACTH_{1-24}$	Bachem	H1150
AffiniPure Fab Fragment Goat Anti-Rabbit IgG (H+L)	dianova	#111-007-003
Agarose LE	Biozym	#840001
3,3'-Diaminobenzidine (DAB)	Sigma	D8001
DMEM GlutaMAX™	Gibco®/LifeTechnologies	#10566-032
1 Kb DNA ladder	Invitrogen/LifeTechnologies	#15615016
FCS, heat-inactivated	Gibco®/LifeTechnologies	#10500-064
Gentamicin	Gibco®/LifeTechnologies	#15750-037
Hoechst 33258	Sigma	#861405
Na-L-Glutamat Monohydrat	Merck	#1.06445.1000
Normal Rabbit Serum	dianova	#011-000-001
Oil Red O	Sigma	O0625
PageRuler™ Prestained Protein Ladder	Fermentas/ThermoScientific	#26616
Penicillin-Streptomycin, liquid	Gibco®/LifeTechnologies	#15140-122
Pure Taq DNA Polymerase	Peqlab	#01-9130
Recombinant murine IL-6	PreproTech	#216-16
Recombinant mouse IL-1β	R&D Systems	401-ML-005
Toluidine Blue O	Sigma	T3260
Trypan Blue Stain	Gibco®/LifeTechnologies	#15250061

8-Br-cGMP	Biolog	#B004E

*Enzyme*s

Collagenase	Sigma	#C7926
Papain	Sigma	P5762
Proteinase K	Roth	#7528.1
Taq-Polymerase	Peqlab	#01-1040

Commercially available kits

ECL Advance Western Blotting Detection Kit	GE Healthcare	#RPN2135
ImmuChem™ double antibody corticosterone RIA	MP Biomedicals	#07120102
Quantikine® ELISA mouse IL-6 immunoassay	R&D systems	#M6000B
Nucleospin® RNA XS Kit	Macherey-Nagel	#740902.10
Total Protein Kit, Micro Lowry, Peterson's Modification	Sigma	#TP0300
Vectastain® ABC-AP Kit	Vectorlabs	#AK5000
Vectastain® Elite® ABC Kit	Vectorlabs	#PK6100
Vector Blue Alkaline Phosphatase Substrate Kit	Vectorlabs	#SK5300

Equipment is listed in alphabetical order. Device designation, manufacturer and unique type reference is given.

Equipment

Autoclave	SANOclav	La-Va
	MMM GmbH	Ventilab S3000
Balance	Sartorius	Excellence
	Mettler	AM50
Binocular light	Schott	KL 1500 LCD
Camera	Allied Vision Technologies GmbH	Marlin F-046C
	Cybertech	CS1
	SONY	Cyber-shot VX DSC-W17
	Logitech	WebcamPro9000
Centrifuge (cell culture room)	Eppendorf	Centrifuge 5804R (A-4-44)
Centrifuge (lab)	Eppendorf	Centrifuge 5417C(F35-40-11)
Clean bench	Thermo Scientific	HERA safe
Cryostat	MicromInternational	HM525
Digital imaging system	Biozym Scientific GmbH	FluorChem® FC3
Gel preparing system	BioRad	Mini-Protean® 3
Freezer (−20 °C)	Liebherr	Premium No Frost
Freezer (−80 °C)	Revco Technologies	Model # ULT2186-3-V35
Fridge-Freezer	Liebherr	Comfort No Frost
Fluorescence microscope	ZEISS	Axioskop 20
Heating block	Eppendorf	Thermomixer compact
	Neolab	neoBlock Duo 2-2504
Homogeniser	MP Biomedicals	FastPrep®-24
Incubator	New Brunswick Scientific	Innova® CO-170

Infrared light	Philips	InfraPhil100W, HP1511
Light microscope	ZEISS	Axiovert 40C
Manual cell counter	Neolab	_
Microplate photometer	Thermo Scientific	Multiskan EX
Microtome	MicromInternational	HM335E
Power supply	Biometra	Standard Power Pack P25
	BioRad	200/2.0 Power Supply
Scanner	Epson	Epson Perfection 4990 Photo
Shaker	Biometra	WT12
Stereoscopic microscope	ZEISS	Stemi 2000-CS
Telemetry device	Data Sciences International (DSI)	PhysioTel®TA-F20 transmitter
		RPC-1 receiver
		Data Exchange Matrix
		C10T temperature converter
		C10I light converter
Thermocycler	Peqlab	Primus 96 advanced
	Peqlab	peqSTAR 2X
UV-Transilluminator	Vilber-Lourmat	TFX-20M
Vibratome	MicromInternational	HM650V
Vortex-Mixer	neolab	Vortex Mixer
Water bath	Memmert	_
	Medax	_
Western blotting device	Roth	MAXI-Semi-Dry-Blotter
γ-counter	Berthold technologies	Multi Crystal LB 2111

All consumables (pipette tips, cell culture flasks, reaction tubes, falcons) used in this project were purchased from one of the following companies: Corning, Sarstedt and Roth.

I.2. Buffers and solutions

I.2.(a) Buffers and solutions for PCR-based genotyping:

Reagent (stock concentration)	*final concentration*	*volume*
DNA lysis buffer:		
10x reaction buffer S (Peqlab)		3 µl
Proteinase K (50 mg/ml)	10 mg/ml	1 µl
ddH_20		ad 50 µl
10x PCR buffer (store at –20 °C):		
KCl (1 M)		5 ml
Tris-HCl (1 M)	100 mM	1 ml
$MgCl_2$ (1 M)	15 mM	150 µl
dNTPs (100 mM)	2 mM	200 µl
ddH_2O		ad 10 ml
6x DNA loading dye (store at 4 °C):		
Bromophenol blue	0.125%	5 ml
Xylene cyanol	0.125%	6 mg
Sucrose	40%	2 g
1x TBE		ad 5 ml

I.2.(b) Solutions for cell and organ culture:

Cell culture medium (store at 4 °C):

DMEM with GlutaMAX™ (Dulbecco's modified eagle medium, *LifeTechnologies*)		500 ml
FCS (fetal calf serum) (LifeTechnologies, heat-inactivated)	~10%	50 ml
100x Penicillin/Streptomycin (10,000 U/ml/10,000 µg/ml)	100 U/ml/100 µg/ml	5 ml

Ca^{2+}-free medium, pH 7.4 (store at 4 °C)

Na-L-Glutamat Monohydrat (*Merck*)	85 mM	15.91 g
NaCl	60 mM	3.5 g
HEPES	10 mM	2.38 g
KCl	5.6 mM	0.42 g
$MgCl_2 \bullet 6\ H_20$	1 mM	0.20 g
ddH_2O		ad 1 l
→ autoclave		

BSA (bovine serum albumin) (store at –20 °C)

BSA	100 mg/ml	500 mg
Ca^{2+}-free medium, pH 7.4		ad 5 ml

DTT (Dithiothreitol) (store at -20 °C)

DTT	100 mg/ml	500 mg
Ca^{2+}-free medium, pH 7.4		ad 5 ml

Enzyme working solution A (prepare freshly; warm to 37 °C before use)

Collagenase (10 mg/ml, *Sigma*)	0.5 mg/ml	50 µl
BSA (100 mg/ml)	1 mg/ml	10 µl
Ca^{2+}-free medium, pH 7.4		Ad 1 ml

Enzyme working solution B (prepare freshly; warm to 37 °C before use)

Papain (7 mg/ml, *Sigma*)	0.7 mg/ml	100 µl
BSA (100 mg/ml)	1 mg/ml	10 µl
DTT (100 mg/ml)	1 mg/ml	10 µl
Ca^{2+}-free medium, pH 7.4		Ad 1 ml

1x Trypsin/EDTA (store at 4 °C)

10x Trypsin/EDTA (5 g/l/2 g/l, *LifeTechnologies*)	3 ml
PBS, pH 7.4	ad 30 ml

ACTH stock solution (10 µM; store at -80 °C)

$ACTH_{1-24}$ (*Bachem*)	10 µM	1 mg
ddH_20		34.1 ml

1% BSA-PBS (store at -20 °C)

Bovine serum albumin (BSA; *Roth*)		0.1 g
PBS, pH 7.4		10 ml

4% low melt agarose

Agarose low melt (#6351.1; *Roth*)	4%	0.8 g
PBS, pH 7.4		ad 20 ml

Organ culture medium (store at 4 °C)

DMEM with GlutaMAX™ (*LifeTechnologies*)		50 ml
FCS (LifeTechnologies, heat-inactivated)	~2%	1 ml
100x Pen/Strep (10,000 U/ml/100 µg/ml)	(200 U/ml/2 µg/ml)	1 ml
Gentamicin (*LifeTechnologies*) (50 mg/ml)	0.1%	50 µl
β-Mercaptoethanol (50 mM)	50 µM	50 µl

8-Br-cGMP stock solution (100 mM; store at -20 °C)

8-Br-cGMP (#B004E; *Biolog*)	100 mM	50 mg
ddH_20		1.12 ml

I.2.(c) Solutions for IL-1β and ACTH injections:

5% EDTA solution, pH 7.4 (store at 4 °C)

EDTA (Ethylenediaminetetraacetic acid)	171 µM	10 g
PBS, pH 7.4		200 ml
→ adjust pH to 7.4 with NaOH		

IL-1β stock solution (0.5 µg/ml; 30 nM; store at -20 °C)

recombinant mouse IL-1β (401-ML-005; *R&D Systems*)	5 µg
0.1% BSA-PBS	10 ml

ACTH stock solution, 0.5 mg/ml (store at -80 °C)

$ACTH_{1-24}$ (#H-1150, *Bachem*)	5 mg
ddH_20	10 ml

→ dilute 1:500 (1:50) in 0.1% BSA-PBS for injection of 10 µg/kg (100 µg/kg)

I.2.(d) Solutions for transmitter implantation:

Anesthesia mixture (3 components anesthesia) (store at 4 °C)

Fentanyl citrate (Fentanyl-ratiopharm®) (50 µg/ml)	50 µg /ml	200 µl
Midazolam hydrochloride (Midazolam-ratiopharm®) (5 mg/ml)	0.5 mg/ml	200 µl
Medetomidine hydrochloride (Domitor®, *Pfizer*) (1 mg/ml)	0.05 mg/ml	100 µl
0.9% NaCl		ad 2 ml

→ inject 0.1 ml/10 g body weight i.p.

Antidote mixture (store at 4 °C)

Naloxon hydrochloride (*Curamed*) (0.4 mg/ml)	0.12 mg/ml	670 µl
Flumazenil (Anexate®, *Roche*) (0.1 mg/ml)	0.05 mg/ml	1000 µl
Atipamezole hydrochloride (Antisedan®, *Pfizer*) (5 mg/ml)	50 µg/ml	100 µl
0.9% NaCl		ad 2 ml

→ inject subcutaneously 0.1 ml/10 g body weight to reverse anesthesia

Carprofen dilution (store at 4 °C)

Carprofen (Rimadyl®, *Pfizer*) (50 mg/ml)	16 mg/ml	0.1 ml
0.9% NaCl		2.9 ml

→ inject subcutaneously 0.1 ml/per mouse ~20 min. before anesthesia reversal

I.2.(e) Solutions for protein analysis:

SDS protein lysis buffer (prepare freshly before use)

Tris-HCl, pH 8.0 (1M)	21 mM	210 µl
SDS (10%)	~0.7%	670 µl
β-Mercaptoethanol	1.7%	170 µl
PMSF (100 mM)	0.2 mM	20 µl
ddH_20		ad 10 ml

5x Lämmli sample buffer (store at -20°C)

Tris, pH 6.8 (1M)	32%	3.2 ml
Glycerol	40%	4 ml
SDS	15%	1.5 g
Bromphenol blue	0.1%	10 mg
β-Mercaptoethanol	25%	2.5 ml
ddH_20		ad 10 ml

4x Tris/SDS (pH 8.8)(store at 4 °C)

Tris	1.5 M	18.2 g
SDS	0.4%	0.4 g
ddH_20		ad 100 ml

→ adjust pH with 10 M NaOH

4x Tris/SDS (pH 6.8)(store at 4 °C)

Tris	0.5 M	3.02 g
SDS	0.4%	0.2 g
ddH_20		ad 50 ml
→ adjust pH with 10 M NaOH		

10x SDS running buffer (store at room temperature)

Tris	0.25 M	15.1 g
Glycine	2 M	72.0 g
SDS	1%	5 g
ddH_20		ad 500 ml

Coomassie stainer (store at room temperature)

Coomassie Brilliant Blue R-250	2.5g/l	2.5 g
Methanol	50%	500 ml
Acetic acid	10%	100 ml
ddH_20		ad 1 l

Coomassie destainer (store at room temperature)

Methanol	20%	200 ml
Acetic acid	20%	200 ml
Isopropanol	20%	200 ml
ddH_20		ad 1 l

Anode buffer I (pH 10.4, store at room temperature)

Tris	0.3 M	36.3 g
Methanol	20%	200 ml
ddH_20		ad 1 l
→ adjust pH to 10.4, if necessary		

Anode buffer II (pH 10.4, store at room temperature)

Tris	0.025 M	3.03 g
Methanol	20%	200 ml
ddH_20		ad 1 l
→ adjust pH to 10.4, if necessary		

Cathode buffer (pH 7.6, store at room temperature)

Tris	0.025 M	3.03 g
6-amino-hexanoic-acid	40 mM	5.2 g
Methanol	20%	200 ml
ddH_20		ad 1 l
→ adjust pH to 7.6		

5% milk powder in TBS-T (store at 4 °C)

Milk powder (blotting grade)	5%	25 g
TBS-T		ad 500 ml

I.2.(f) Solutions for cryosectioning:

Cell fix (store at 4 °C)

Formaldehyde (37%)	2%	27 ml
Glutaraldehyde (25%)	0.2%	4 ml
PBS, pH 7.4		ad 500 ml

Heparin solution (store at 4 °C)

Heparin Natriumsalz (≥180 U/mg)	40,000 U/l	26 mg
PBS, pH 7.4		ad 100 ml

4% Paraformaldehyde (PFA, prepare freshly)

Paraformaldehyde (reinst)	4%	12 g
PBS, pH 7.4		ad 300 ml

→ solve by heating to 57-59 °C with constant stirring until solution becomes clear

→ filter and store at 4 °C until usage

30% sucrose solution

D-Sucrose	30%	150 g
PBS, pH 7.4		ad 500 ml

I.2.(g) Solutions for Cresyl violet stain:

Cresyl violet acetate (*Sigma*)	0.1%	0.1 g
ddH_2O		100 ml

I.2.(h) Solutions for X-gal staining:

X-gal stock solution (store at -20 °C in aliquots à 1 ml)

X-gal (5-bromo-4-chloro-3-indolyl-β-D-galactopyranoside)	40 mg/ml	400 mg
DMSO (Dimethylsulfoxide)		10 ml

X-gal staining solution (store in the dark at RT)

$K_4Fe(CN)_6$	2,5 mM	0.83 g
$K_3Fe(CN)_6$	2,5 mM	1.07 g
$MgCl_2$ (1M)	2 mM	1 ml
PBS, pH 7.4		ad 500 ml

→ right before usage: add X-gal stock solution(final concentration: 1 mg/ml) to the staining solution

I.2.(i) Solutions for Oil Red O staining:

0.5% Oil Red O solution (store at RT)

Oil Red O	0.5%	0.5 g
100% Propylene glycol (1,2-Propanediol)		ad 100 ml

→ heat under constant stirring carefully to 95-100 °C

→ do not allow to go over 110 °C (high background staining)

→ filter solution

I.2.(j) Solutions for immunohistochemistry:

Peroxidase blocking solution

H_2O_2 (30%)	~10%	300 µl
10% methanol in PBS	~1%	130 µl
PBS, pH 7.4		1 ml

Citrate buffer, pH 6.0 (store at RT)

Citric acid monohydrate ($C_6H_8O_7 \bullet H_20$)	10 mM	2.1 g
ddH_20		ad 1 l
→ adjust pH to 6.0 with NaOH		

ABC reagent (VECTASTAIN® Elite ABC Kit, Vectorlabs)

Solution A		12 µl
Solution B		12 µl
PBS, pH 7.4		ad 600 µl
→ add 600 µl TBS-T right before use		

ABC reagent (VECTASTAIN® Standard ABC-AP Kit, Vectorlabs)

Solution A		50 µl
Solution B		50 µl
PBS, pH 7.4		ad 5 ml

DAB (3,3'-Diaminobenzidine) staining solution

DAB stock solution 0.1%	0.05%	800 µl
PBS, pH 7.4		800 µl
→ add 1 µl H_2O_2 right before use		

Vector Blue Alkaline Phosphatase substrate kit

Substrate 1	2 drops
Substrate 2	2 drops
Substrate 3	2 drops
100 mM Tris-HCl, pH 8.2	ad 5 ml

→ mix well after adding each substrate

I.2.(k) Solutions for immunofluorescence:

Permeablization buffer (store at 4 °C)

Triton-X-100	0.5%	200 µl
PBS, pH 7.4		ad 40 ml

Reaction buffer (store at 4 °C)

NaCl	2%	800 µl
Triton-X-100	0.1%	40 µl
PBS, pH 7.4		ad 40 ml
normal serum (from the host species of the secondary antibody)	1%	400 µl

→ prepare reaction buffer without serum, and add serum just before use

Fab fragment solution (prepare fresh; stock solution stored at 4 °C)

AffiniPure Fab Fragment Goat Anti-Rabbit IgG (H+L) (*Dianova*) (1.3 mg/ml)	13 µg/ml	20 µl
PBS, pH 7.4		2 ml

Hoechst stock solution (store in small aliquots at -20 °C, in the dark)

Hoechst 33258 (*Sigma*)	1 mg/ml	100 mg
ddH_20		100 ml

I.2.(l) Solutions for RT-PCR:

DEPC-treated water (store at RT)

DEPC (Diethylpyrocarbonate)	0.1%	1 ml
ddH_20		1 l

→ stir overnight at RT

→ autoclave to inactivate DEPC

3 M Sodium acetate, pH 5.2 (store at RT)

Sodium acetate (NaOAc)	3 M	40.8 g
ddH_20		ad 100 ml

→ dissolve NaOAc first in 70 ml ddH_20 and adjust pH to 5.2 with glacial acetic acid

→ add ddH_20 to bring to a total volume of 100 ml

I.3. Primer sequences

I.3.1. Genotyping

Primer sequences

Table 9: Primer sequences for genotyping PCRs

primer	sequence 5'-3'	gene
RF53	CCT GGC TGT GAT TTC ACT CCA	cGKI_forward
RF118	AAA TTA TAA CTT GTC AAA TTC TTG	cGKI_reverse
RF125	GTC AAG TGA CCA CTA TG	cGKI_reverse
Cre800	GCT GCC ACG ACC AAG TGA CAG CAA	Cre_forward
Cre1200	GTA GTT ATT CGG ATC ATC AGC TAC AC	Cre_reverse
RF67	CTC AGA GTG GAA GGC CTG CTT	SMIα/β/WT_forward
RF90	CAC ACC ATT CTT CAG CCA CA	WT_reverse
SW8	AAC TCC AGC TCC AGC TCG	SMIβ_reverse
SW12	CCT CCT TGA GCA TGA GAA TCT TG	SMIα_reverse

I.3.2. RT-PCR

Table 10: Primer concentrations and conditions for RT-PCR

gene	conc. [pmol/µl]	GAPDH/HPRT [pmol/µl]	annealing temp. touch-down [°C]	annealing temp. [°C]	amplicon size
MC2R	0.08	0.1 HPRT	61	55	580
Cyp11A1	0.1	0.1 HPRT	61	55	224
StAR	0.25	0.125 GAPDH	66	60	188
SR-BI	0.1	0.2 HPRT	61	55	121
CBG	0.125	0.05 GAPDH	61	55	182
LDLR	0.25	0.125 GAPDH	66	60	68
11β -HSD1	0.25	0.25 HPRT	61	55	133
cGKIα	0.25	0.125/0.25	61	55	533
cGKIβ	0.25	0.125/0.25	61	55	574

Primer sequences

Table 11: Sequences of RT-PCR primers

primer	sequence 5'-3'	gene	Tm [°C]	source
AG1_fwd	CAT CTT GCC GAG AAA GAT CCT A	MC2R	58.4	Chida et al., 2007
AG1_rev	AGG ATG AAC ATG CAG TCA ATG AT		57.1	pga.mgh.harvard.edu/cgi-bin/primerbank primerID:31560668b2
AG2_fwd	GAC CTG GAA GGA CCA TGC A	Cyp11A1	58.8	Qiao et al., 2009
AG2_rev	ACT GCA GGG TCA TGG AGG T		58.8	Chida et al., 2007
AG3_fwd	CGG GTG GAT GGG TCA AGT TC	StAR	61.4	http://pga.mgh.harvard.edu/cgi-bin/primerbank/primerID:118130138b1
AG3_rev	GCA CTT CGT CCC CGT TCT C		61.0	
AG4_fwd	AGC GTG GAC CCT ATG TCT ACA	SR-BI	59.8	http://pga.mgh.harvard.edu/cgi-bin/primerbank/primerID:14389422b3
AG4_rev	CCA TGC GAC TTG TCA GGC T		58.8	
AG5_fwd	AGA CCT GGA TAG TTC AGC CAC	CBG	59.8	http://pga.mgh.harvard.edu/cgi-bin/primerbank/primerID:118131216b2
AG5_rev	TCG CCG AAT CAC GAA AGT AAC		57.9	
AG6_fwd	CTG TGG GCT CCA TAG GCT ATC T	LDLR	62.1	Hoekstra et al., 2009
AG6_rev	GCG GTC CAG GGT CAT CTT C		61.0	
AG7_fwd	GAA GAG TCA TGG AGG TCA AC	11β- HSD1	57.3	Schmid et al., 2011 (adapted for mouse)
AG7_rev	GCA ATC ATA GGC TGG GTC AT		57.3	
GAPDH_fwd	ACT CAC GGC AAA TTC AAC GGC ACA G	GAPDH	64.6	Davies et al., 2007
GAPDH_rev	TGG TCA TGA GCC CTT CCA CAA TGC C		66.3	
QG197	GTA ATG ATC AGT CAA CGG GGG AC	HPRT	62.4	Diploma thesis Ruth Ferstl 2005

QG198	CCA GCA AGC TTG CAA CCT TAA CCA		62.7	
RM50	CGC CAG GCG TTC CGG AAG T	cGKIα	70.0	Diploma thesis Ruth Ferstl 2005
RM44	TCC TCT TGC ACC CTG CCT GAT		66.6	
RM52	CTC CGC GGA AGC CCA CCG CCT	cGKIβ	76.9	Diploma thesis Ruth Ferstl 2005
RM44	TCC TCT TGC ACC CTG CCT GAT		66.6	

I.4. Antibody dilutions

Primary antibodies

Table 12: Dilutions of pimary antibodies

antibody	origin	application/dilution	company
βIII-tubulin	monoclonal mouse	IF/1:500	Promega (#G7121)
		IHC/1:2,000	
CD31 (Pecam-1) (V-16)	polyclonal goat	IF/1:100	Santa Cruz (#sc-31045)
cGKIα (N-16)	polyclonal goat	WB/1:500	Santa Cruz (#sc-10335)
cGKIβ (E-20)	polyclonal goat	WB/1:500	Santa Cruz (#sc-10342)
cGKIc	polyclonal rabbit	WB/1:5,000	Valtcheva et al., 2009
		IF/1:1,500	
		IHC/1:1,500	
GAPDH (14C10)	monoclonal rabbit	WB/1:5,000	Cell signaling (#2118)
Mac2	monoclonal rat	WB/1:3,000	Cedarlan (#CL8942AP)
		IF/1:200	
Phospho-Akt (Ser^{473})	polyclonal rabbit	WB/1:1,000	Cell signaling (#9271)
SMα-actin	monoclonal mouse	IF/1:800	Sigma (#A-2547)
SM22α	polyclonal rabbit	IF/1:200	abcam (#ab14106)
SOCS3 (L210)	polyclonal rabbit	WB/1:1,000	Cell signaling (#2932)
Vimentin	polyclonal chicken	IF/1:2,000	LS Biosciences (#LS-B291)

Secondary antibodies

Table 13: Dilutions of secondary antibodies

antibody	origin	application/dilution	company
anti-goat-HRP	donkey	WB/1:5,000	Santa Cruz (#2056)
anti-rabbit-HRP	goat	WB/1:5,000	Cell signaling (#7074)
anti-rat-HRP	goat	WB/1:5,000	Santa Cruz (#2065)
biotinylated anti-mouse	horse	IHC/1:250	Vectorlabs (#BA-2000)
biotinylated anti-rabbit	goat	IHC/1:200	Vectorlabs (#BA-1000)
anti-chicken-AlexaFluor555	goat	IF/1:500	LifeTechnologies (#A21437)
anti-goat-AlexaFluor594	donkey	IF/1:500	LifeTechnologies (#A11058)
anti-mouse-AlexaFluor555	goat	IF/1:500	LifeTechnologies (#A21127)
anti-rabbit-AlexaFluor488	goat	IF/1:500	LifeTechnologies (#A11008)
anti-rabbit-AlexaFluor595	goat	IF/1:500	LifeTechnologies (#A11012)
anti-rat-AlexaFluor594	rabbit	IF/1:500	LifeTechnologies (#A21211)

I.5. Raw data

I.5.1. Temperature

I.5.1.1.Core body temperature during normal conditions

Table 14: Core body temperature and lococmotor activity in cGKI-deficient mice and controls. Statistically significant differences are marked with asterisks. *, p<0.05; **, p<0.01; ***, p<0.001.

	SM-Iβ rescues	controls	SM-Iβ rescues	controls
Time ZT [h]	Temperature [°C]	Temperature [°C]	activity [counts/min]	activity [counts/min]
6	36.56 ± 0.06**	36.95 ± 0.12	2.5 ± 0.26	2.65±0.67
9	36.41 ± 0.06*	36.72 ± 0.12	1.86 ± 0.24	1.17±0.18
12	36.37 ± 0.05**	36.74± 0.10	1.62 ±0.21	1.3±0.08
15	36.6 ± 0.05**	36.95 ± 0.10	2.01 ±0.26	1.6±0.26
18	37.35 ± 0.06	37.56 ± 0.03	3.81 ±0.55	3.8±0.62
21	37.41 ± 0.05	37.54 ± 0.03	3.41 ±0.45	3.05±0.23
24	37.39 ± 0.05	37.53 ± 0.06	3.6 ±0.5	3.35±0.53
3	37.23 ± 0.06	37.52 ± 0.10	4.17 ±0.55	4.57±0.52
	cGKI brain-KO	controls	cGKI brain-KO	controls
Time ZT [h]	Temperature [°C]	Temperature [°C]	activity [counts/min]	activity [counts/min]
6	36.44 ± 0.10	36.6 ± 0.05	2.41 ± 0.27	1.86±0.28
9	36.36 ± 0.10	36.29 ± 0.05	2.24 ± 0.22	1.48±0.19
12	36.37 ± 0.11	36.33± 0.04	2.19 ±0,22	1.41±0.19
15	36.75 ± 0.09	36.62 ± 0.03	3.28 ±0,32	1.7±0.23
18	38.03 ± 0.16	37.73 ± 0.04	24.19 ±4.83***	8.86±1.37
21	37.71 ± 0.14	37.61 ± 0.07	14.65 ±2.53	7.79±1.66
24	37.70 ± 0.12	37.41 ± 0.04	14.17 ±2.75	6.17±0.79
3	37.14 ± 0.08	37.1 ± 0.04	7.49 ±0.68	5.19±0.64

I.5.1.2.Core body temperature under cold stress

Table 15: Temperature and activity during cold stress (starting at ZT 14 h) in cGKI-deficient mice and controls. Statistically significant differences are marked with asterisks. *, p<0.05; **, p<0.01; ***, p<0.001.

	SM-Iβ rescues	controls	SM-Iβ rescues	controls
Time ZT [h]	Temperature [°C]	Temperature [°C]	activity [counts/min]	activity [counts/min]
14	37.1 ± 0.26	37.40 ± 0.38	14.7 ± 0.25	13.14±1.01
14.5	36.87 ± 0.40	36.96 ± 0.43	9.23 ± 0.90	9.18±1.63
15	37.01 ± 0.25	37.07± 0.33	7.08 ±1.53	8.59±2.75
15.5	36.40 ± 0.26	36.74 ± 0.36	3.89 ±0.83	5.12±1.77
16	36.49 ± 0.10	36.55 ± 0.31	4.07 ±0.69	3.48±0.79
16.5	36.09 ± 0.16	36.32 ± 0.23	1.7 ±0.33	1.74±0.42
17	35.77 ± 0.16	36.02 ± 0.24	1.23 ±0.4	1.36±0.59
17.5	35.52 ± 0.23	35.75 ± 0.32	0.93 ±0.21	0.91±0.27
18	35.93± 0.27	36.40± 0.26	6.01 ±1.97	6.34±0.02
18.5	36.08± 0.23	36.74± 0.15	6.33 ±2.6	7.15±2.49
19	35.79± 0.29	36.34± 0.34	1.81 ±0.43	2.71±0.51
19.5	36.42± 0.38	36.24± 0.95	1.91 ±0.28	1.22±0.46
	cGKI brain-KO	controls	cGKI brain-KO	controls
Time ZT [h]	Temperature [°C]	Temperature [°C]	activity [counts/min]	activity [counts/min]
14	37.13± 0.30	37.39 ± 0.15	10.06 ± 2.99	7.26±0.91
14.5	36.96 ± 0.36	37.47 ± 0.19	11.53 ± 2.44	8.31±1.36
15	36.63± 0.43	37.42± 0.20	12.22 ±2.36	12.13±2.89
15.5	35.89± 0.79	37.23 ± 0.29	11.42 ±2.07	8.89±1.55
16	34.91± 1.13	37.04 ± 0.33	12.39 ±2.41	7.86±1.61
16.5	33.67± 1.77	36.91 ± 0.37	11.91 ±3.10	5.97±1.88
17	32.62± 2.19	36.61 ± 0.44	7.77 ±2.84	6.57±2.21
17.5	32.07± 2.15	35.99 ± 0.64	5.50±1.78	3.79±1.46
18	31.32± 2.15*	35.67 ± 0.84	9.74±5.79	6.28±1.69
18.5	30.71± 2.20*	35.21 ± 1.24	7.09±2.62	4.79±1.77

I.5.1.3.Core body temperature under fasting stress

Table 16: Temperature and activity during fasting stress (starting at ZT 17 h) in cGKI-deficient mice and controls. Statistically significant differences are marked with asterisks. *, p<0.05; **, p<0.01; ***, p<0.001.

	SM-Iβ rescues	controls	SM-Iβ rescues	controls
Time ZT [h]	Temperature [°C]	Temperature [°C]	activity [counts/min]	activity [counts/min]
17	37.59 ± 0.13	37.96 ± 018	7.82 ± 1.53	8.89±1.14
19	37.16 ± 0.27	37.72 ± 0.24	6.73 ± 2.01	6.85±1.60
21	36.77 ± 0.23	37.38± 0.28	5.32 ±1.17	5.77±1.03
23	35.52 ± 0.51	36.18± 0.50	3.88±0.87	4.49±1.22
01	33.35 ± 0.98	34.31 ± 0.57	2.94 ±1.04	1.59±0.46
03	31.72 ± 0.97*	34.68 ± 0.58	1.39 ±0.46	3.21±0.84
05	29.14 ± 1.08*	32.19 ± 1.19	0.47 ±0.24	0.62±0.33
07	31.07 ± 1.53***	35.35 ± 0.28	0.88 ±0.33	1.48±0.77
09	36.74± 0.12	37.22± 0.09	2.37 ±1.04	2.86±0.87
11	36.44± 0.09	36.89± 0.09	1.29 ±0.39	2.07±0.22
	cGKI brain-KO	controls	cGKI brain-KO	controls
Time ZT [h]	Temperature [°C]	Temperature [°C]	activity [counts/min]	activity [counts/min]
19	38.13± 0.10	38.27 ± 0.24	42.71 ± 7.01	23.90±2.71
21	37.84 ± 0.14	38.27 ± 0.24	56.11 ± 13.38*	29.85±4.01
23	37.60± 0.19	38.26± 0.24	52.71 ±5.74	31.94±4.32
01	37.48± 0.22	38.23 ± 0.25	49.54 ±3.40	31.81±4.91
03	37.27± 0.24	37.91 ± 0.22	48.96 ±5.42	28.66±5.30
05	36.34± 0.70	37.15 ± 0.28	35.76 ±5.61	20.31±5.55
07	34.91± 1.31*	36.87± 0.34	17.16 ±5.93	12.76±4.26

I.5.2. Weight of adrenal glands

Controls				
Mouse #	Age [months]	Body weight [g]	Adrenal gland weight [mg]	AG [µg]/BW[g]
1	7	28.5	7.8	273.7
2	7	25.3	5.8	229.6
3	7	25.7	6.7	261.1
4	7	24.1	7.9	328.5
5	7	25.1	6.5	259.5
6	7	25.5	7.4	290.2
7	9	26.3	5.5	209.5
8	9	26.5	6.2	234.4
9	9	29.8	4.8	161.3
10	9	30.1	4.6	189.5
SM-Iβ rescues				
Mouse #	Age [months]	Body weight [g]	Adrenal gland weight [mg]	AG [µg]/BW[g]
1	7	19.4	6.5	335.1
2	7	21.0	4.0	190.2
3	7	21.4	3.9	182.2
4	7	23.9	5.0	209.2
5	7	23.9	5.2	217.6
6	7	21.0	5.7	271.6
7	9	25.3	5.4	213.4
8	9	23.9	3.8	159.0
9	9	25.1	4.2	167.3
10	9	26.5	5	188.7